SCALE AND STABILITY ANALYSIS OF SELECTED ATMOSPHERIC BLOCKING EVENTS

A Dissertation

presented to

the Faculty of the Graduate School

University of Missouri

In Partial Fulfillment

Of the Requirement for the Degree

Doctor of Philosophy

---

by

ATHAR HUSSAIN

Dr. Anthony Lupo, Dissertation Supervisor

DECEMBER 2008

The undersigned, appointed by the Dean of the Graduate School, have examined the dissertation entitled

SCALE AND STABILITY ANALYSIS OF SELECTED ATMOSPHERIC BLOCKING EVENTS

Presented by Athar Hussain

A candidate for the degree of Doctor of Philosophy of Atmospheric Science

And hereby certify that in their opinion it is worthy of acceptance.

Associate Professor Anthony Lupo

Associate Professor Sergei Kopeikin

Associate Professor Patrick Market

Associate Professor Neil Fox

Dedicated to my beloved late father and mother

ACKNOWLEDGEMENTS

I am very grateful to my academic advisor, Dr. Anthony Lupo, Associate Professor of Atmospheric Science, for inviting and guiding me in all steps of my study of Atmospheric Science. Indeed, his continuous and tireless support has helped me to complete this Ph.D.

I would like to thank Dr. Sergei Kopeikin, Associate Professor of Physics for being my committee member and for his ideas and discussions on aspects related to Physics of Atmospheric Blocking.

I would like to express my appreciation to Dr. Patrick Market, Associate Professor of Atmospheric Science for being my committee member, for helping me with the Climatological Data acquisition and for discussions on the synoptic aspects of Atmospheric Blocking.

I would also like to thank Dr. Neil Fox, Associate Professor of Atmospheric Science for being my committee member and for discussions on the Radiative Forcings of Atmospheric Blocking as well as the operational aspects of it.

Discussions with Dr. Courtenay Strong, Dr. Steven Lack, Dr. Christopher Melick, Dr. Brain Pettegrew, Mr. Larry Smith, and Mr. George Limpert are gratefully acknowledged. I also thank Ms. Linda Little, Ms. Jessie Becker, Ms. Karen Decker and Ms. Leslie Palmer for their support.

I would also like to express my gratitude to Dr. Stephen Colucci, Professor of Atmospheric Science, Cornell University, for his continued and enlightening discussions on the various aspects of Atmospheric Blocking onsets and for providing me important insight to my work. Last, but not least, I would like to thank Dr. Walter Robinson, Professor of Atmospheric Science, University of Illinois at Urbana-Champaign, for providing me a general context of the Scale Analysis of Atmospheric Blocking relative to other large-scale climate variability modes.

Finally, I would like to express my deep appreciation for the tireless support and encouragement of my wife, Sara, and her family, without their support I could not have completed this Ph.D.

TABLE OF CONTENTS

LIST OF FIGURES

Figure **Page**

LIST OF TABLES

Table **Page**

SCALE AND STABILITY ANALYSIS OF SELECTED ATMOSPHERIC BLOCKING EVENTS

Athar Hussain

Dr. Anthony Lupo, Dissertation Supervisor

ABSTRACT

Global six year climatology of mid latitude atmospheric blocking events, during the period 1999-2004, is presented based on the scale and stability analysis, using the NCEP/NCAR re-analysis data. A total of 278 blocking events over the Northern as well as the Southern Hemispheres are analyzed.

The 500 mb geopotential height is decomposed into the planetary- and the synoptic-scale geopotential heights. The heights are then averaged over a $40^{o} \times 60^{o}$ latitude longitude box D, harboring the blocking event. The averaged heights are compared with their corresponding monthly mean values during the month in which the blocking event has occurred. A positive planetary-scale geopotential height dominance behavior for a given blocking event is defined as a positive planetary-scale height anomaly above its monthly mean value. Similar procedure is adopted to define synoptic-scale dominance behavior.

It is pointed out that globally, over the six year period, 83% of the blocking events have single-scale dominance, whereas remaining 17% of the blocking events have an alternating-scale dominance behavior. In the Northern Hemisphere, during the later half of the six year period, a 28% rise in the planetary-scale dominance behavior blocking events is noticed over the synoptic-scale dominance behavior blocking events.

Stability analysis of the blocking events over the six year period is performed, under the assumption of barotropic flow, using the following three stability indicators: i) max $|\nabla\psi|$, ii) max$|\nabla\Omega_a|$, and iii) $\int_D |\Omega|^2(y)dxdy$. Here, ψ is geosptrophic stream function, Ω_a is the absolute vorticity and $\Omega = -\partial u/\partial y$, in usual meteorological notation.

A comparison of the time variability of the three stability indicators over the entire life cycle of the selected blocking events with earlier works performing the synoptic and dynamics studies shows that the three stability indicators can be used as climatologically reliable stability indicators giving useful insight into the stability of the flow attending the blocking event. It is noticed that in the scale dependent flow, the scale that dominates during the mature stage of the blocking event determines the stability of the flow during the blocking, and that the blocking is relatively more stable state than the more frequent zonal flow, irrespective of which scale dominates the flow during blocking.

For the selected blocking events, the calculations for both the scale height dominance as well as for the stability of the flow attending the blocking are extended to include the stratospheric signals as well, for operational relevance.

CHAPTER 1

BACKGROUND, DATA AND METHODOLOGY

The development of a mainly meridional circulation pattern in the midtroposphere is commonly referred to as blocking. This stagnation of the zonal atmospheric flow gives rise to difficulties in obtaining a confident regional weather forecast. For an overview, see, Benzi et al. (1986). It is thus of interest to develop understanding of the processes that lead to the formation of such circulation patterns.

1.1 Background and Motivation of Present Work

Considerable theoretical efforts have been made to explain the phenomenon of atmospheric blocking, particularly those emanating from the model solutions of the quasi-geostrophic potential vorticity equation. For a review, see De Swart (1988).

The Charney and De Vore model provides a framework to incorporate the low frequency (planetary-scale) dynamics into the quasi-geostrophic barotropic vorticity equation to obtain the blocking pattern for the given forcings using the concept of stable equilibria (Charney and De Vore 1979). An example of the *y*-amplitude of the interacting wave function having a single maximum in the interior, from this model, is shown in Fig. 1.1. The resulting wave function describing the projected geopotential height/stream function onto the *xy*-plane is shown in Fig. 1.2 for various choices of forcing parameters. Note that blocking events in this model are reproducible for a certain range of the forcing parameters.

The Shutts model on the other hand provides a framework to incorporate the high frequency (synoptic-scale) dynamics into the quasi-geostropic barotropic vorticity equation to obtain the blocking events for prescribed forcings (Shutts 1983). Both models offer solutions of the non-linear barotropic vorticity equation numerically.

From the synoptic-dynamic point of view, making use of more consistent surface and upper air data (Kalnay et al. 1996; Kistler et al. 2001), numerous studies have been carried out leading to valuable insight into the forcing mechanisms that may be operative at various stages of atmospheric blocking in specific case studies (Tracton 1990; Nakamura and Wallace 1990; Lupo and Smith 1995b; Nakamua et al. 1997; Dong and Colucci 2005, 2007). This class of studies is usually referred to as the diagnostic studies.

In several of the recent case studies, the question of the role of planetary-scale versus synoptic-scale processes during various stages of the blocking anticyclones is

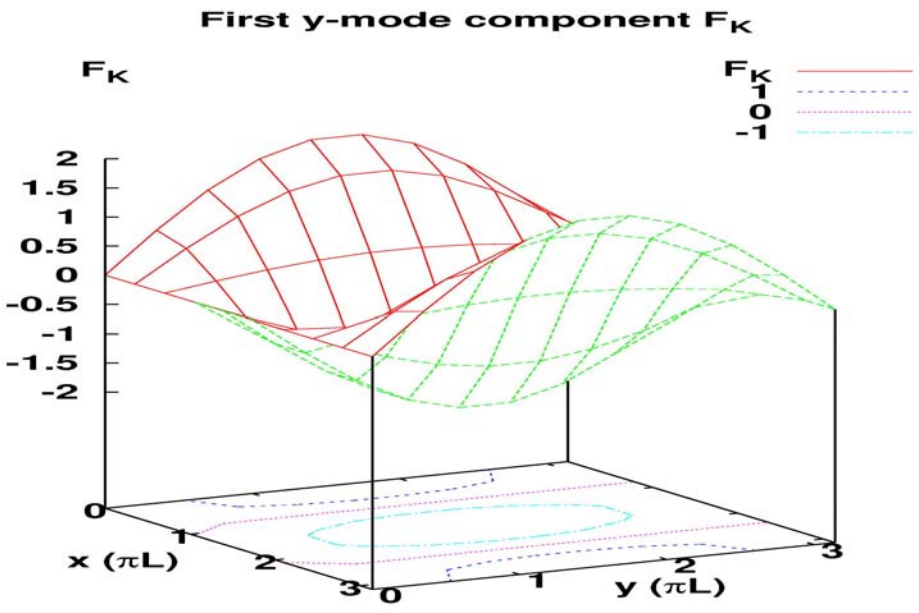

Fig. 1.1. The first y-mode component F_K as a function of x and y for n = 2 in the Charney and De Vore (1979) model. Three equi F_K contours are also shown.

addressed. In this dissertation, we continue along these lines and discuss the relative stability of the flow in terms of the scales of motion.

We shall adopt here an empirically oriented approach to quantify the stability of various regimes of the atmospheric flow. In this context, blocking may be viewed as a stable but stationary regime (steady in time) in barotropic atmospheric circulation. A diagnostic/stability study of atmospheric blocking may thus be performed by partitioning the atmospheric flow into planetary- and synoptic-scale components.

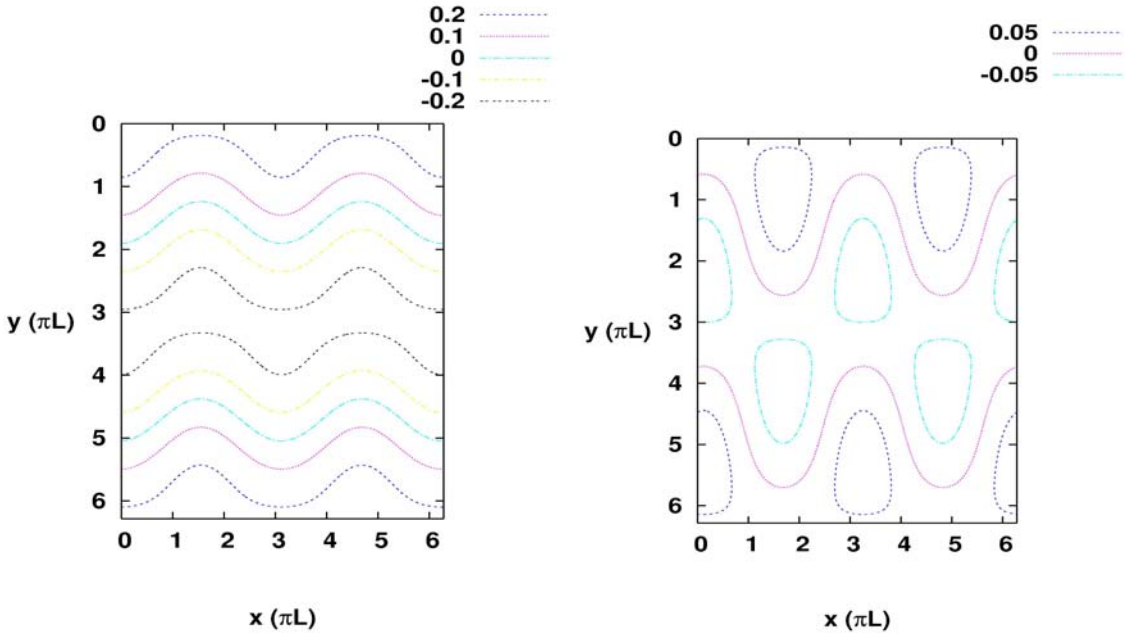

Fig. 1.2. Stream function fields for the stable first mode equilibria of a topologically forced flow for $k=10^{-2}$, L/a=1/4, n=2, $\psi^*_A=0.2$, and $h_0/H=0.2$ for the low index state in the Charney and De Vore (1979) model. Left Panel: Slightly above resonance. Right Panel: Slightly below resonance.

In recent years, several studies have examined the relative role of each scale and their interactions as well as the nature of the interactions themselves (e.g., Tracton 1990; Marques and Rao 1999; Lupo et al. 2007 and references cited therein). In addition to these studies, and from those of earlier pioneers (e.g., Kalnay-Rivas and Merkine 1981; Frederiksen 1982; Mullen 1986, 1987), a consistent picture emerges that the synoptic-scale plays an important role in the life cycle of blocking events. Many of the

studies represented above show that the magnitude of the synoptic-scale forcing is large compared to that of the planetary-scale forcing.

However, others have shown that the planetary-scale is very influential in the life cycle of the blocking events (e.g., Haines and Holland 1998; Colucci and Baumhefner 1998). While the studies referenced in the above paragraph do not downplay the role of the planetary-scale, they do focus more on the role of synoptic-scale contributions. For instance, in their model study, Haines and Holland suggest that blocking regimes will break down when there is a substantial change in the planetary-scale flow regime. Colucci and Baumhefner (1998) focus on the role of planetary-scale deformation as a pre-conditioned environment for the formation of blocking events (see also Colucci 2001). These two studies together support the notion that while the planetary-scale may not itself lead to block formation and maintenance, nevertheless this scale may provide a favorable environment in the interaction with the synoptic-scale environment. Thus, a substantial change in the planetary-scale flow regime would not support blocking and these events would decay fairly quickly.

Historically, the planetary-scale flow in both hemispheres has been assumed to behave as, or treated like, an oscillating pendulum (e.g., Lorenz 1963; Hansen 1986; Nese et al. 1987; Hansen and Sutera 1988). More recently, this type of physical behavior has been discussed by Lynch (2003) who also extended the analogy to describe the planetary-scale flow as a swinging “spring” in describing the behavior of Rossby wave triads.

1.2 Objectives and Statement of Present Work

The main goal of this work is to demonstrate that abrupt changes in the planetary-scale environment can lead to the onset of blocking whereas the abrupt changes in the synoptic-scale environment leads to rapid decay of blocking. Statement of objectives of present work is as follows.

- This work will also look at the utility of characteristic exponents, defined as the eigenvalues of the linearization operator of the barotropic vorticity equation, as a diagnostic tool in blocking studies, which are calculated using both components of the flow. In this context, the time variability of the planetary/synoptic-scale geopotential height and of the stability indices (derivable from the gradients of stream function and the absolute vorticity) will be studied. We also elaborate the stratified role of planetary/synoptic-scale wavelengths over the entire troposphere in various stages of the block life cycle. In contrast to all the previous studies mentioned in this section, *we concentrate on the relative role of both the planetary- and synoptic- scales in the context of stability of the flow*.

- We evaluate the scale and stability characteristics of all the mid latitude blocking events occurring over both hemispheres during the six year period (1999-2004), lasting for 5 days or more, to assess the relative role

of the two contributions in the scale dynamics and stability of the flow. The Southern Hemisphere (SH) blocking events differ in several respects from the Northern Hemisphere (NH) blocking event as summarized in the next paragraph. Motivated from these observational facts, we attempted to answer the question that how these characteristics are reflected in the scale and stability dynamics over an extended period of time for a relatively large number of blocking events. We present detailed characterization of the blocking events during the above six year period based on the relative role of planetary-scale and/or synoptic-scale dynamics.

Climatologically, SH blocking events have several characteristic features that are absent in their NH counter parts. These include the geographic location of frequent occurrences of the blocking events as well as their relative frequency of occurrence. A recent 30 year (January 1970 – December 1999) comparative climatological study of midtropospheric SH blocking events indicates that Pacific region is the location of frequent occurrence of blocking events and that the SH blocking events are less frequent than their NH counterparts (Wiedenmann et al. 2002). Another characteristic feature of SH blocking events is their relative isolated occurrence as compared to more frequent episodic occurrence of NH blocking events. As indicated in the above cited study, this difference is attributable to the relative role of the

synoptic-scale and planetary-scale wavelengths during the life cycle of the blocking event. It is thus of some significance to study the relative role of the scales that may lead to the formation of the blocking events in SH as compared to NH blocking events to obtain a global perspective.

- Our findings include the observation that although the number of blocking events in which the planetary-scale dominates the stability of the flow is different in the two hemispheres, however a common feature is that if it is the dominating scale then the planetary scale flow is more stable during the mature stage of the blocking events irrespective of the hemisphere. The same conclusions hold for synoptic-scale dominance.

- Our global six year climatology of scale dynamics indicates that the single scale dominance (83%) is more frequent than the alternating height scale dominance (17%). Chapter 2 presents details of these two scale dominances.

It is thus of relevance to perform detailed case studies of selected blocking events in which single wavelength dominance occurs. For the selected blocking events in both hemispheres in our study, cases studies were performed earlier using a different set of diagnostic tools for the same blocking events so that a context of comparison is also available, as far as it is permissible.

- For the NH, we study a blocking event that was studied earlier by Glisan (2007) as a representative example. For the SH, we study a blocking event that was studied by Dong and Colucci (2005, 2007) as a representative example but use a different set of diagnostic tools, including that by Dymnikov et al. (1992), to analyze both the synoptic as well as the stability features of the blocking in order to get a more general and broader dynamic perspective in terms of stability of the main mechanisms operative in the onset, maintenance and decay of the selected blocking events.

1.3 A Stability Indicator

It is suggested that a meridional perturbation destabilizes/weakens the zonal flow and leads to blocking of it (Dymnikov et al. 1992). Starting from the barotropic vorticity equation, the (blocking) area integrated enstrophy is suggested as a measure of change in the zonal flow that may lead to blocking.

Here, we make use of the Dymnikov et al. (1992) conjecture which suggests a strong correlation between the sum of the positive eigenvalues of the linearization operator of barotropic flow and the blocking domain integrated regional enstrophy, i.e.,

$$\sum_i \lambda_i^+ \approx \int_D |\Omega|^2(y)\,dxdy, \tag{1.1}$$

where $\Omega = -\partial u / \partial y$ and D is the blocking domain. In Eq. (1), a term proportional to the magnitude of the gradient of the vorticity, Ω, is neglected as this contribution is small relative to the considered term, in our situation. The blocking domain D is defined as a latitude and longitude box. The latitude span is taken as 40^o between 20^o and 60^o (the midlatitude), whereas the longitude span varies depending upon the size of blocking. Typically, it is 60^o. We call the right hand side of Eq. (1.1) as the blocking area integrated regional enstrophy (IRE). We regard the IRE as a stability indicator. Higher positive values of the IRE correspond to more unstable flow and vice versa.

The time variability of right hand side of Eq. (1.1) may thus represent the relative stability of the barotropic flow. Development of a mainly meridional perturbation signifies relative stability of the flow which we interpret as the blocking following Dymnikov et al. (1992) conjecture. Note that the right hand side of Eq. (1.1) refers to the blocking area averaged (relative) vorticity squared as mentioned earlier.

We shall discuss in some detail the time variability of the mean planetary- and the synoptic-scale eddy height and of the IRE for selected isolated blocking events to assess the usefulness of the stability indicator at various isobaric levels under the assumption that, at each isobaric level, the flow is barotropic.

We shall thus make use of the relationship given by Eq. (1.1) between the IRE and the sum of positive eigenvalues to study the relative stability of the region of the barotropic flow harboring the selected blocking events. Next, we first present the brief details of the gridded climatological data that will be used in our analysis and then the methodologies used to analyze the data.

1.4 Description of Gridded Climatological Data

The data set used here was the National Center for Environmental Prediction (NCEP) and National Center for Atmospheric Research (NCAR) gridded re-analyses data (Kalnay et al. 1996; Kistler et al. 2001). This data was archived at NCAR and was obtained from the mass-storage facility in Boulder, CO in the netCDF format. This re-analyzed data was the 2.5^{o} by 2.5^{o} latitude-longitude analyses available on 17 mandatory levels from 1000 mb to 10 mb at 6-h intervals on daily basis. These analyses include the standard atmospheric variables relevant for determination of physical properties of the atmosphere such as the global geopotential height Z in (m), temperature (K), relative humidity (%), vertical motion (ω) in (μb s^{-1}), u and v wind components (ms^{-1}) and the surface information. The mandatory level data were interpolated quadratically in ln(p) to 50 mb level-increments (where p is the pressure), and these more closely resemble raw sounding information (Lupo and Bosart 1999).

The stratospheric signal of geopotential height is hydrostatically calculated from the temperature field (Kalnay et al. 1996). The re-analysis data at the top of the atmosphere is also a combination of model predictions and observations, including the satellite data such as from Operational Vertical Sounder (TVOS). For the NH (20^{o}-80^{o}N), the internal differences in the NCEP re-analysis are about 6 m at 200 mb. These internal differences are 30 m at 200 mb in SH. The internal differences reflect the sensitivity to the first guess used in the analysis and are estimate of the uncertainty in the monthly mean analysis of NCEP system.

1.5 Methodology

The blocking criterion of Lupo and Smith (1995a) will be used to determine the onset and termination times for the blocking events studied here. Details regarding this criterion and its application can be found in Tractron (1990) and Lupo and Smith (1995b). Basically, these studies employ an extended set of conditions set forth earlier by Rex (1950a, b) where a climatological study of 16 year data (1933–1949) was performed under that set of conditions.

As mentioned before, this study will demonstrate that changes in the planetary-scale and synoptic-scale flow regimes can be related to the onset and, more importantly, to the decay of the blocking events. The techniques used here to extract planetary- and synoptic- scale variability have been used to extract interannual variability from a one-dimensional time series recently by Mokhov et al. (2000, 2004, and references therein) or Federov et al. (2003) and will be only briefly presented here with modifications.

The techniques used in these references are based on standard dynamic analysis techniques for physical systems (see, e.g., Lorenz 1963). In particular, the planetary-scale height fields were averaged over 40^{o} latitude by 60^{o} longitude box within the blocking sector to produce one number for each time period. This process is analogous to the procedure used by Hansen (1986) in deriving the wave amplitude index, with the exception that we filtered the fields first and then averaged them within a box. They averaged the entire mid-latitude height field into a band and then filtered to obtain a single number for the time period.

1.5.1 Wavelength Filtering Procedure

A second-order, two-dimensional Shapiro (1970) filter was used on the variables in the data set in order to separate the planetary-scale wavelengths (Z_p) from the observed geopotential height (Z). A Shapiro filter performs a center weighted symmetric finite element calculation. The synoptic-scale wavelengths (Z_s) are obtained using

$$Z_s = Z - Z_p. \tag{1.2}$$

Applying this filter results in a response function, which retains 2%, 44%, 80% of the signal for waves having a wavelength of 3000 km, 4500 km, and 6000 km at 45^o N (or S) latitude, respectively. See appendix A.2 for the description of the MATLAB code used to filter the Z_p from Z. More details regarding the use of the filtering procedure can be found in Lupo and Smith (1995b).

1.5.2 Effect of Integration Domain Size Variation

The domain D used in Eq. (1.1) is defined as the 40^o latitude by 60^o longitude box as mentioned in Section 1.5. The latitude is between 20^o and 60^o (N or S) harboring the latitude extent of the blocking event in mid latitude. The longitude is centered at the blocking center and depends on the longitude extent of the selected blocking event.

Table 1.1. Assessment of the blocking domain size variation for the 500 mb monthly mean planetary-scale geopotential height during January 1999.

D (latitude × longitude)	Monthly mean planetary-scale geopotential height averaged over blocking domain D (m)
$40^o \times 60^o$	5483
$50^o \times 70^o$	5424
$60^o \times 80^o$	5370
$70^o \times 90^o$	5380

Enlarging the blocking area domain D from $40^o \times 60^o$ does not lead to any significant deviation in the parameters that are being averaged over it. A representative example is displayed in Table 1.1, where the impact of enlarging the blocking area domain D is assessed for the 500 mb monthly mean planetary-scale geopotential height for a selected blocking event. The Shapiro filter is used to separate the planetary-scale heights from the observed geopotential heights (see Section 1.5.1). The blocking event occurred during 12-18 January 1999 over 40^o N and 180^o (Event No. 1 from Table 2.2a). The Table indicates that the maximum variation in the monthly mean planetary-scale geopotential height value is of the order of 2% relative to $40^o \times 60^o$ box averaging value. Similar magnitude of variation relative to $40^o \times 60^o$ box averaging value was found when we varied the latitude only, the longitude only, the selected blocking event, the hemisphere and the parameter that is being averaged over the blocking domain D.

We may thus conclude that the blocking domain averaged results presented in this study are not sensitive to the choice of the size of the blocking domain D within the range of latitude and longitude values specified in Table 1.1.

1.5.3 The Blocking Intensity Criterion

Following Wiedenmann et al. (2002), the blocking intensity (BI) is defined as

$$BI = 100.0\ [(MZ/RC) - 1.0)], \tag{1.3}$$

where MZ is the maximum 500 mb geopotential height in the closed anticyclone region or on a line associated with the ridge axis, and RC is the subjectively chosen representative contour such that

$$RC = \frac{\frac{(Z_u + MZ)}{2} + \frac{(Z_d + MZ)}{2}}{2}, \tag{1.4}$$

where Z_u (Z_d) represents the lowest height value in the trough axis upstream (downstream) of the block center at the same latitude.

The Chapter wise plan is as follows. In Chapter 2, using the methodology presented here we elaborate the results of the synoptic and the scale analysis performed for all the blocking events occurring during the six year period (1999-2004). As a representative example in the NH, the details of the synoptic and the stability analyses of a selected blocking event are presented in Chapter 3. The details of the synoptic and the stability analyses for a selected blocking event in the SH are presented in Chapter 4. The emphasis in both case studies is on the relative role of the planetary- and synoptic-scales to quantify the flow stability. Summary of the six year climatology and the results for both case studies are presented in Chapter 5.

CHAPTER 2

DETAILS OF GLOBAL SIX YEAR CLIMATOLOGY

In this Chapter, we first present the synoptic description of the blocking events for the six year duration 1999-2004 and then the scale dynamics characteristics of these events using the methodology presented in Chapter 1.

2.1 The Blocking Events During 1999-2004

We present the synoptic details of the blocking events during the six year period in tabular form. The blocking events details include the start date, the end date, the duration, the BI as well as the geographic location. Table 2.1 summarizes the yearly count of the blocking events in Northern as well as Southern Hemispheres.

2.1.1 Analysis Procedure

The initial blocking data was retrieved from the updated online archive of blocking events available at http://solberg.snr.missouri.edu/gcc/. The BI is defined by Eq. (1.3) and Eq. (1.4) in Chapter 1 following Wiedenmann et al. (2002).

In case of a blocking event falling over two months, in line with the on-line archive criterion of blocking month credit, the blocking month was credited to the blocking for the month for which the blocking stayed for maximum number of days. For instance, if the blocking was during 25 July through 15 August then the month of August was credited to the blocking event.

The latitude and longitude of the three geographic locations displayed in the last columns of Table 2.2 and 2.3 are defined as follows: Pacific (130^{o}E - 70^{o}W), Atlantic (70^{o}W - 30^{o}E) and Continental (NH) or Indian (SH) with 30^{o}E - 130^{o}E. Note that in each Table, the year runs from January through December, which is different as compared to what is present in the initial data set. All calculations are done at 500 mb for 1200 UTC unless otherwise stated.

The synoptic description of the blocking events from the following three years were chosen for display in this Chapter: 1999, 2002 and 2004, because the selected blocking events from these three years represent the main types of scale dynamics dominance behavior found in the data set. The synoptic description of the remaining three years (2000, 2001 and 2003) is presented in appendix B in similar format.

2.1.2 Summary of the Analysis

From Table 2.1, we note that 69% of the total detected blocking events occurred in the NH, whereas the remaining 31% of the blocking events occurred in the SH. A similar hemispheric distribution of blocking events occurrence was noticed in earlier long term climatological studies, see, Wiedenmann et al. (2002).

Table 2.1. Number of blocking events lasting 5 days or more for the 6 year period (1999 – 2004) under study. In both the hemispheres, the year is defined between January and December. During this 6 year period, the number of blocking events in NH is 213 (69% of 278) and in SH is 65 (31% of 278). The total number of events is 278.

YEAR	NH	SH	TOTAL
1999	28	9	37
2000	28	8	36
2001	31	10	41
2002	41	8	49
2003	48	18	66
2004	37	12	49

2.1.3 Event by Event Details

Table 2.2 (a-c) and Table 2.3 (a-c) display the details of the blocking events on yearly basis in the Northern Hemisphere and Southern Hemispheres, respectively. The event details from these tables are used in the subsequent sections in this Chapter to assess the climatological behavior of the scale dynamics and to perform the detailed stability analysis of two of the selected blocking events in the next two chapters.

In Table 2.2b and 2.3a, the blocking event numbers in Italic represent the selected NH and SH cases, respectively, that are diagnosed in some detail in the next two Chapters.

Table 2.2a. Blocking event details for NH 1999. For each blocking event, the start date is displayed in column 2, the end date in column 3, the event duration in column 4, the BI averaged over the entire life cycle of the blocking event in column 5, and the geographic location in column 6. For further details, see text.

EVENT NO.	START DATE	END DATE	DURATION (DAYS)	BI	GEOGRAPHIC LOCATION
1	12 Jan.	18 Jan.	6	1.62	Pacific
2	13 Jan.	25 Jan.	12	4.46	Atlantic
3	19 Jan.	26 Jan.	7	5.14	Pacific
4	21 Jan.	26 Jan.	5	4.17	Continental
5	02 Feb.	20 Feb.	18	2.53	Pacific
6	20 Feb.	29 Feb.	9	1.04	Atlantic
7	05 Mar.	15 Mar.	10	2.27	Continental
8	16 Mar.	21 Mar.	5	1.53	Pacific
9	07 Apr.	15 Apr.	8	2.54	Pacific
10	10 Apr.	24 Apr.	14	2.64	Atlantic

11	28 Mar.	03 Apr.	5	2.32	Continental
12	10 May	21 May	11	2.40	Atlantic
13	12 May	18 May	6	2.17	Continental
14	29 Apr.	03 May	5	1.63	Continental
15	04 Jun.	10 Jun.	6	2.29	Continental
16	26 Jun.	02 Jul.	6	1.68	Atlantic
17	24 Jun.	03 Jul.	9	1.50	Pacific
18	25 May	07 Jun.	12	1.24	Continental
19	13 Jul.	18 Jul.	5	2.24	Atlantic
20	15 Aug.	20 Aug.	5	1.49	Atlantic
21	22 Aug.	29 Aug.	7	2.06	Continental
22	12 Sep.	25 Sep.	13	2.15	Atlantic
23	13 Sep.	19 Sep.	6	2.37	Continental
24	14 Oct.	24 Oct.	10	3.32	Atlantic
25	04 Nov.	10 Nov.	6	1.65	Atlantic
26	09 Nov.	14 Nov.	5	3.48	Atlantic
27	15 Nov.	21 Nov.	6	2.70	Pacific
28	19 Dec.	29 Dec.	10	4.56	Pacific

Table 2.2b. Same as Table 2.2a except for NH 2002.

EVENT NO.	START DATE	END DATE	DURATION (DAYS)	BI	GEOGRAPHIC LOCATION
1	02 Jan.	11 Jan.	9.5	3.62	Atlantic
2	03 Jan.	08 Jan.	5	2.19	Pacific
3	07 Jan.	28 Jan.	21	4.50	Pacific
4	13 Jan.	27 Jan.	14	2.09	Atlantic
5	25 Jan.	30 Jan.	5	4.89	Atlantic
6	30 Jan.	05 Feb.	6	1.34	Pacific
7	31 Jan.	06 Feb.	5.5	3.75	Atlantic
8	06 Feb.	11 Feb.	5	3.15	Continental
9	02 Feb.	12 Feb.	10	4.64	Pacific
10	12 Feb.	17 Feb.	5	3.50	Pacific
11	11 Feb.	28 Feb.	17	4.79	Atlantic
12	01 Mar.	07 Mar.	6	2.50	Pacific
13	04 Mar.	21 Mar.	17	4.10	Pacific
14	06 Mar.	21 Mar.	15	1.88	Atlantic
15	09 Mar.	28 Mar.	19	3.83	Atlantic
16	01 Apr.	18 Apr.	17	4.13	Atlantic

17	02 Apr.	07 Apr.	5	3.14	Continental
18	15 Apr.	24 Apr.	9	4.22	Atlantic
19	19 Apr.	04 May	13.5	2.54	Pacific
20	23 Apr.	03 May	8.5	2.81	Atlantic
21	10 May	19 May	9	2.45	Pacific
22	09 May	29 May	20	2.41	Continental
23	01 Jun.	10 Jun.	9	2.27	Atlantic
24	04 Jun.	09 Jul.	35	1.99	Continental
25	22 Jun.	30 Jun.	8	1.65	Pacific
26	30 Jun.	08 Jul.	9	2.56	Continental
27	06 Jul.	17 Jul.	9	1.52	Atlantic
28	30 Jul.	07 Aug.	8	2.43	Pacific
29	01 Aug.	11 Aug.	10	1.75	Atlantic
30	*15 Aug.*	*28 Aug.*	*13*	*2.37*	*Atlantic*
31	07 Sep.	18 Sep.	11	3.49	Atlantic
32	23 Sep.	28 Sep.	5	2.95	Pacific
33	20 Sep.	02 Oct.	12	2.05	Atlantic
34	06 Oct.	15 Oct.	9	2.87	Atlantic
35	13 Oct.	18 Oct.	5	4.30	Pacific
36	22 Oct.	03 Nov.	12	3.72	Pacific
37	25 Oct.	30 Oct.	5	2.34	Continental
38	01 Nov.	06 Nov.	5.5	2.97	Atlantic
39	18 Nov.	25 Nov.	7	3.24	Atlantic
40	20 Oct.	11 Nov.	21	3.77	Pacific
41	26 Nov.	28 Dec.	32.5	4.30	Atlantic

Table 2.2c. Same as Table 2.2a except for NH 2004.

EVENT NO.	START DATE	END DATE	DURATION (DAYS)	BI	GEOGRAPHIC LOCATION
1	27 Dec.	09 Jan.	13	2.58	Atlantic
2	02 Jan.	11 Jan.	9.5	4.51	Pacific
3	23 Jan.	05 Feb.	13	4.60	Atlantic
4	18 Jan.	18 Feb.	31	3.46	Atlantic
5	10 Feb.	14 Feb.	31.5	5.15	Atlantic
6	14 Feb.	28 Feb.	14	3.44	Pacific
7	28 Feb.	05 Mar.	5	2.01	Pacific
8	15 Mar.	20 Mar.	5	4.62	Atlantic

9	17 Mar.	22 Mar.	5	4.28	Pacific
10	22 Mar.	29 Mar.	7.5	3.40	Continental
11	26 Mar.	12 Apr.	17	3.63	Atlantic
12	11 Apr.	16 Apr.	5	2.97	Continental
13	14 Apr.	22 Apr.	7.5	1.44	Pacific
14	16 Apr.	26 Apr.	10	2.72	Atlantic
15	20 Apr.	13 May.	23	3.81	Pacific
16	06 May	13 May	7.5	2.48	Pacific
17	10 May	25 May	15.5	2.96	Continental
18	12 May	01 Jun.	20	2.58	Atlantic
19	05 Jun.	10 Jun.	5	2.38	Pacific
20	26 Jun.	10 Jul.	14	2.47	Continental
21	02 Jul.	13 Jul.	10.5	2.13	Pacific
22	06 Jul.	11 Jul.	5	1.52	Pacific
23	12 Jul.	24 Jul.	11.5	2.31	Continental
24	27 Jul.	01 Aug.	5	1.49	Pacific
25	27 Jul.	15 Aug.	18.5	2.91	Atlantic
26	*05 Aug.*	*28 Aug.*	*23.5*	*2.44*	*Pacific*
27	09 Aug.	15 Aug.	6.5	2.14	Continental
28	06 Sep.	11 Sep.	5	2.09	Continental
29	08 Oct.	15 Oct.	7	3.26	Atlantic
30	12 Oct.	26 Oct.	14	2.98	Pacific
31	18 Oct.	28 Oct.	10	3.22	Atlantic
32	02 Nov.	13 Nov.	11	2.24	Atlantic
33	04 Nov.	26 Nov.	22	3.02	Atlantic
34	21 Nov.	26 Nov.	5	3.56	Continental
35	09 Dec.	14 Dec.	5	3.16	Atlantic
36	19 Dec.	25 Dec.	6	3.53	Pacific
37	19 Dec.	26 Dec.	7	3.25	Continental

Table 2.3a. Same as Table 2.2a except for SH 1999.

EVENT NO.	START DATE	END DATE	DURATION (DAYS)	BI	GEOGRAPHIC LOCATION
1	10 Feb.	17 Feb.	7.5	3.06	Pacific
2	23 Mar.	29 Mar.	6	3.25	Pacific
3	19 May	24 May	5	2.46	Pacific

4	26 Jun.	02 Jul.	6	3.47	Pacific
5	*24 Jul.*	*31 Jul.*	*7*	*2.70*	*Pacific*
6	04 Aug.	11 Aug.	7	1.97	Pacific
7	24 Aug.	06 Sep.	13	1.73	Pacific
8	28 Sep.	06 Oct.	8.5	2.45	Pacific
9	26 Nov.	02 Dec.	6	2.96	Pacific

Table 2.3b. Same as Table 2.3a except for SH 2002.

EVENT NO.	START DATE	END DATE	DURATION (DAYS)	BI	GEOGRAPHIC LOCATION
1	10 Jan.	15 Jan.	5	4.24	Pacific
2	05 May	16 May	11	4.22	Pacific
3	21 May	29 May	8	3.99	Indian
4	11 Jun.	16 Jun.	5	4.16	Pacific
5	18 Jul.	25 Jul.	5.5	3.96	Pacific
6	25 Aug.	30 Aug.	6.5	4.13	Pacific
7	26 Oct.	03 Oct.	5.5	2.98	Pacific
8	08 Nov.	13 Nov.	7	1.80	Pacific

Table 2.3c. Same as Table 2.3a except for SH 2004.

EVENT NO.	START DATE	END DATE	DURATION (DAYS)	BI	GEOGRAPHIC LOCATION
1	20 Apr.	26 Apr.	6	2.82	Pacific
2	30 Jun.	17 Jul.	17	3.05	Pacific
3	09 Jul.	14 Jul.	5.5	2.45	Atlantic
4	14 Jul.	23 Jul.	9	1.51	Pacific
5	19 Jul.	24 Jul.	5.5	2.75	Atlantic
6	23 Jul.	01 Aug.	9	2.04	Pacific
7	31 Jul.	20 Aug.	20.5	2.40	Pacific

8	15 Aug.	25 Aug.	10.5	1.94	Pacific
9	30 Aug.	06 Sep.	7.5	3.14	Pacific
10	05 Sep.	13 Sep.	8	2.54	Pacific
11	31 Oct.	05 Nov.	5	2.70	Pacific
12	23 Nov.	04 Dec.	11	3.40	Pacific

2.2 Scale Dynamics Comparison for the Blocking Events During 1999-2004

The longitude at the block onset was obtained from the online blocking event archive; see section 2.1 for more details. The latitude span was taken as 40^o centered at the mid latitude in accordance with discussion in section 1.5 of Chapter 1. The longitude span was varied according to the size of blocking event.

The following procedure was used throughout the entire data analysis to determine the scale dominance. The latitude was taken to be 40^o between 20^o and 60^o in both hemispheres. The longitude span was varied relative to the blocking center location by 30^o in east and west directions. The filtered planetary-scale geopotential height was averaged over this latitude and longitude box and was stored. Next, the blocking area averaged synoptic-scale eddy height was calculated following the procedure outlined in section 1.5.1 and was stored. The monthly mean reference value for each height scale was calculated numerically. The entry labeled positive in the planetary-scale height dominance column occurs if this height dominates over its corresponding monthly mean reference height value. Similarly, if the synoptic-scale height dominates over its monthly mean reference value then the blocking event was characterized as a positive entry in the synoptic-scale dominance column. If the

blocking event falls in two months such as from 25 July through 15 August, the scale dominance is determined by comparing the behavior of the heights relative to two month mean reference value.

Based on our above criterion for comparison of heights, we categorize the blocking events into the following three types:

i) Planetary-scale height dominance events,

ii) Synoptic-scale height dominance events,

iii) Alternating height dominance events.

In Chapter 3, we shall discuss in detail a representative example of a blocking event with planetary-scale height dominance behavior (category i)). In Chapter 4, we shall discuss a representative example for a positive entry for synoptic-scale height dominance behavior (category ii)). An example of category iii) is described next in some detail in this Chapter.

For the two case studies presented in the next two Chapters mentioned above, we have used different latitude longitude window to compare our findings with the earlier works on these cases. Our results for averaging remain the same when we enlarge the blocking domain size (see Table 1.1).

Fig. 2.1 (a and b) displays an alternating scale dynamics behavior for a selected blocking event. It corresponds to event number 30 in Table 2.4b (NH 2002). The blocking longitude at the onset was 20^{o}E. According to Table 2.2b (event 30), this event occurred over Atlantic with BI = 2.37.

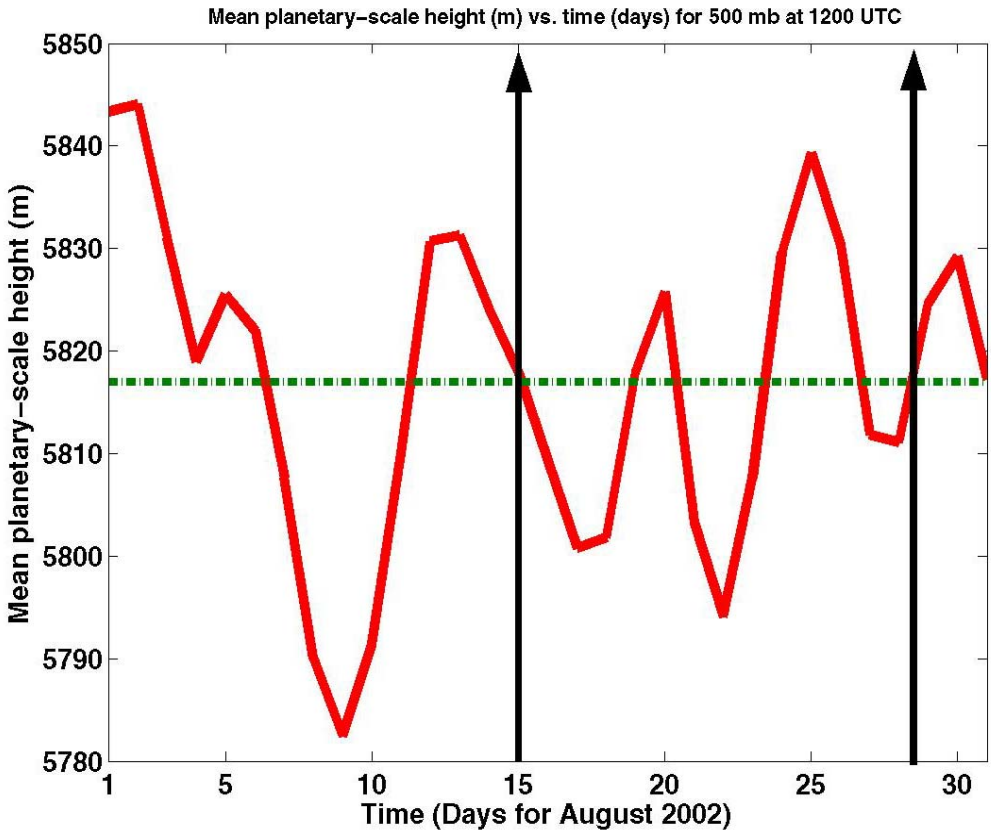

Fig. 2.1a. A diagram of the mean planetary-scale 500 mb geopotential height (m) along abscissa versus time (days) along ordinate for a stationary box (20^{o}N to 60^{o}N and 350^{o}E to 50^{o}E) in the mid-latitude Northern Hemisphere flow. The dashed dotted horizontal line defines the monthly mean reference value for the planetary-scale geopotential height.

Fig. 2.1a displays the time variability of the blocking area averaged planetary-scale geopotential height for the entire month of August 2002. We note that in contrast to Fig. 3.7, there is no single wavelength dominance during the life cycle of the selected

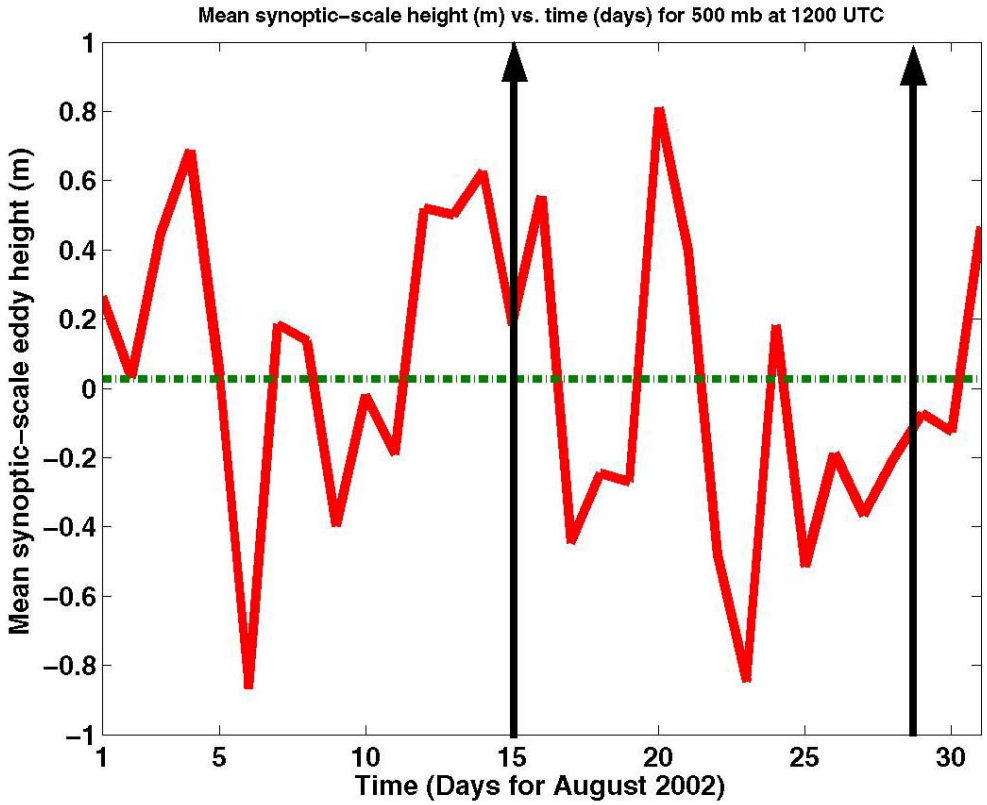

Fig. 2.1b. Same as Fig. 2.1a except for mean synoptic–scale eddy height (m).

blocking event. Similar conclusion can be drawn by comparing Fig. 2.1b and Fig. 4.7 for synoptic-scale. Both the planetary- and synoptic- scale heights rise and fall occur during the life cycle of the blocking event relative to their respective monthly mean reference value. We categorize the blocking events displaying this type of height/wavelength time variability as alternating wavelength dominance behavior blocking events. However, this category of blocking events consists of only 17% of the total detected blocking events.

Table 2.4a. Planetary-scale and synoptic-scale dominance results for all the blocking events during NH 1999. See text for details.

EVENT NO.	START DATE	END DATE	DURATION (DAYS)	PLANETARY SCALE DOMINANCE	SYNOPTIC SCALE DOMINANCE
1	12 Jan.	18 Jan.	6	Negative	Positive
2	13 Jan.	25 Jan.	12	Positive	Negative
3	19 Jan.	26 Jan.	7	Positive	Negative
4	21 Jan.	26 Jan.	5	Negative	Positive
5	02 Feb.	20 Feb.	18	Alternating	Alternating
6	20 Feb.	29 Feb.	9	Positive	Negative
7	05 Mar.	15 Mar.	10	Negative	Positive
8	16 Mar.	21 Mar.	5	Negative	Positive
9	07 Apr.	15 Apr.	8	Negative	Positive
10	10 Apr.	24 Apr.	14	Positive	Negative
11	28 Mar.	03 Apr.	5	Positive	Negative
12	10 May	21 May	11	Alternating	Alternating
13	12 May	18 May	6	Alternating	Alternating
14	29 Apr.	03 May	5	Alternating	Alternating
15	04 Jun.	10 Jun.	6	Positive	Negative
16	26 Jun.	02 Jul.	6	Alternating	Alternating
17	24 Jun.	03 Jul.	9	Positive	Negative
18	25 May	07 Jun.	12	Positive	Negative
19	13 Jul.	18 Jul.	5	Negative	Positive
20	15 Aug.	20 Aug.	5	Negative	Positive
21	22 Aug.	29 Aug.	7	Negative	Positive
22	12 Sep.	25 Sep.	13	Negative	Positive
23	13 Sep.	19 Sep.	6	Positive	Negative
24	14 Oct.	24 Oct.	10	Alternating	Alternating
25	04 Nov.	10 Nov.	6	Positive	Negative
26	09 Nov.	14 Nov.	5	Negative	Positive
27	15 Nov.	21 Nov.	6	Positive	Negative
28	19 Dec.	29 Dec.	10	Positive	Negative

Table 2.4b. Same as Table 2.4a except for NH 2002.

EVENT NO.	START DATE	END DATE	DURATION (DAYS)	PLANETARY SCALE DOMINENCE	SYNOPTIC SCALE DOMINENCE
1	02 Jan.	11 Jan.	9.5	Positive	Negative

2	03 Jan.	08 Jan.	5	Positive	Negative
3	07 Jan.	28 Jan.	21	Alternating	Alternating
4	13 Jan.	27 Jan.	14	Negative	Positive
5	25 Jan.	30 Jan.	5	Negative	Positive
6	30 Jan.	05 Feb.	6	Negative	Positive
7	31 Jan.	06 Feb.	5.5	Negative	Positive
8	06 Feb.	11 Feb.	5	Alternating	Alternating
9	02 Feb.	12 Feb.	10	Negative	Positive
10	12 Feb.	17 Feb.	5	Negative	Positive
11	11 Feb.	28 Feb.	17	Alternating	Alternating
12	01 Mar.	07 Mar.	6	Positive	Negative
13	04 Mar.	21 Mar.	17	Negative	Positive
14	06 Mar.	21 Mar.	15	Positive	Negative
15	09 Mar.	28 Mar.	19	Negative	Positive
16	01 Apr.	18 Apr.	17	Positive	Negative
17	02 Apr.	07 Apr.	5	Negative	Positive
18	15 Apr.	24 Apr.	9	Positive	Negative
19	19 Apr.	04 May	13.5	Negative	Positive
20	23 Apr.	03 May	8.5	Negative	Positive
21	10 May	19 May	9	Positive	Negative
22	09 May	29 May	20	Positive	Negative
23	01 Jun.	10 Jun.	9	Alternating	Alternating
24	04 Jun.	09 Jul.	35	Alternating	Alternating
25	22 Jun.	30 Jun.	8	Negative	Positive
26	30 Jun.	08 Jul.	9	Positive	Negative
27	06 Jul.	17 Jul.	9	Negative	Positive
28	30 Jul.	07 Aug.	8	Positive	Negative
29	01 Aug.	11 Aug.	10	Positive	Negative
30	*15 Aug.*	*28 Aug.*	*13*	*Alternating*	*Alternating*
31	07 Sep.	18 Sep.	11	Alternating	Alternating
32	23 Sep.	28 Sep.	5	Positive	Negative
33	20 Sep.	02 Oct.	12	Positive	Negative
34	06 Oct.	15 Oct.	9	Positive	Negative
35	13 Oct.	18 Oct.	5	Alternating	Alternating
36	22 Oct.	03 Nov.	12	Negative	Positive
37	25 Oct.	30 Oct.	5	Negative	Positive
38	01 Nov.	06 Nov.	5.5	Alternating	Alternating
39	18 Nov.	25 Nov.	7	Positive	Negative
40	20 Oct.	11 Nov.	21	Negative	Positive
41	26 Nov.	28 Dec.	32.5	Alternating	Alternating

Table 2.4c Same as Table 2.4a except for NH 2004.

EVENT NO.	START DATE	END DATE	DURATION (DAYS)	PLANETARY SCALE DOMINENCE	SYNOPTIC SCALE DOMINENCE
1	27 Dec.	09 Jan.	13	Positive	Negative
2	02 Jan.	11 Jan.	9.5	Negative	Positive
3	23 Jan.	05 Feb.	13	Negative	Positive
4	18 Jan.	18 Feb.	31	Positive	Negative
5	10 Feb.	14 Mar.	31.5	Alternating	Alternating
6	14 Feb.	28 Feb.	14	Negative	Positive
7	28 Feb.	05 Mar.	5	Alternating	Alternating
8	15 Mar.	20 Mar.	5	Positive	Negative
9	17 Mar.	22 Mar.	5	Negative	Positive
10	22 Mar.	29 Mar.	7.5	Negative	Positive
11	26 Mar.	12 Apr.	17	Negative	Positive
12	11 Apr.	16 Apr.	5	Negative	Positive
13	14 Apr.	22 Apr.	7.5	Positive	Negative
14	16 Apr.	26 Apr.	10	Positive	Negative
15	20 Apr.	13 May	23	Alternating	Alternating
16	06 May	13 May	7.5	Negative	Positive
17	10 May	25 May	15.5	Positive	Negative
18	12 May	01 Jun.	20	Negative	Positive
19	05 Jun.	10 Jun.	5	Negative	Positive
20	26 Jun.	10 Jul.	14	Positive	Negative
21	02 Jul.	13 Jul.	10.5	Negative	Positive
22	06 Jul.	11 Jul.	5	Negative	Positive
23	12 Jul.	24 Jul.	11.5	Positive	Negative
24	27 Jul.	01 Aug.	5	Positive	Negative
25	27 Jul.	15 Aug.	18.5	Positive	Negative
26	*05 Aug.*	*28 Aug.*	*23.5*	*Positive*	*Negative*
27	09 Aug.	15 Aug.	6.5	Positive	Negative
28	06 Sep.	11 Sep.	5	Negative	Positive
29	08 Oct.	15 Oct.	7	Positive	Negative
30	12 Oct.	26 Oct.	14	Negative	Positive
31	18 Oct.	28 Oct.	10	Negative	Positive
32	02 Nov.	13 Nov.	11	Positive	Negative
33	04 Nov.	26 Nov.	22	Positive	Negative
34	21 Nov.	26 Nov.	5	Positive	Negative
35	09 Dec.	14 Dec.	5	Positive	Negative
36	19 Dec.	25 Dec.	6	Positive	Negative
37	19 Dec.	26 Dec.	7	Negative	Positive

Table 2.5a. Same as Table 2.4a except for SH 1999.

EVENT NO.	START DATE	END DATE	DURATION (DAYS)	PLANETARY SCALE DOMINENCE	SYNOPTIC SCALE DOMINENCE
1	10 Feb.	17 Feb.	7.5	Positive	Negative
2	23 Mar.	29 Mar.	6	Positive	Negative
3	19 May	24 May	5	Positive	Negative
4	26 Jun.	02 Jul.	6	Negative	Positive
5	*24 Jul.*	*31 Jul.*	*7*	*Negative*	*Positive*
6	04 Aug.	11 Aug.	7	Negative	Positive
7	24 Aug.	06 Sep.	13	Positive	Negative
8	28 Sep.	06 Oct.	8.5	Negative	Positive
9	26 Nov.	02 Dec.	6	Positive	Negative

Table 2.5b. Same as Table 2.5a except for SH 2002.

EVENT NO.	START DATE	END DATE	DURATION (DAYS)	PLANETARY SCALE DOMINENCE	SYNOPTIC SCALE DOMINENCE
1	10 Jan.	15 Jan.	5	Positive	Negative
2	05 May	16 May	11	Negative	Positive
3	21 May	29 May	8	Positive	Negative
4	11 Jun.	16 Jun.	5	Negative	Positive
5	18 Jul.	25 Jul.	5.5	Negative	Positive
6	25 Aug.	30 Aug.	6.5	Negative	Positive
7	26 Oct.	03 Nov.	5.5	Negative	Positive
8	08 Nov.	13 Nov.	7	Positive	Negative

Table 2.5c Same as Table 2.5a except for SH 2004.

EVENT NO.	START DATE	END DATE	DURATION (DAYS)	PLANETARY SCALE DOMINENCE	SYNOPTIC SCALE DOMINENCE
1	20 Apr.	26 Apr.	6	Positive	Negative

2	30 Jun.	17 Jul.	17	Alternating	Alternating
3	09 Jul.	14 Jul.	5.5	Positive	Negative
4	14 Jul.	23 Jul.	9	Negative	Positive
5	19 Jul.	24 Jul.	5.5	Positive	Negative
6	23 Jul.	01 Aug.	9	Alternating	Alternating
7	31 Jul.	20 Aug.	20.5	Negative	Positive
8	15 Aug.	25 Aug.	10.5	Alternating	Alternating
9	30 Aug.	06 Sep.	7.5	Negative	Positive
10	05 Sep.	13 Sep.	8	Positive	Negative
11	31 Oct.	05 Nov.	5	Positive	Negative
12	23 Nov.	04 Dec.	11	Positive	Negative

2.3 Summary and Discussion

During the six year period (1999-2004), the longest duration (35 days) blocking event occurred over the Continental area during 4 June through 9 July, 2002, with BI = 1.99. It is event number 24 in Table 2.2b. During the same six year period, the highest BI blocking event occurred over the Pacific area, with BI = 5.39 with a duration of 6 days (19 March through 25 March, 2003). It is event number 11 in Table B.1a.

Table 2.6a summarizes our findings for the blocking events with single scale dominance. Yearly and hemispheric breakup is provided. Maximum (Minimum) number of blocking event having planetary-scale dominance occurs during 2003 (1999)

Table 2.6a. Planetary- and synoptic-scale dominance results for the six year period (1999-2004) global climatological analysis performed in this study. Hemispheric distribution of single scale dominance events is shown. See Table 2.1 also.

	NH		**SH**	
YEAR	**Planetary**	**Synoptic**	**Planetary**	**Synoptic**
1999	12/28	10/28	5/9	4/9
2000	15/28	10/28	5/6	1/6
2001	13/31	15/31	6/10	1/10
2002	15/41	16/41	3/8	5/8
2003	22/48	11/48	11/16	3/16
2004	18/37	16/37	6/12	3/12

in NH. Minimum (Maximum) number of blocking events having synoptic-scale dominance occurs during 1999 and 2000 (2002 and 2004) in NH.

Table 2.6b summarizes the results for the alternating height dominance for the six year period under study with hemispheric breakup. The total count for the analyzed blocking events for scale dynamics is 274 instead of 278 (see Table 2.1), since 4 blocking events were not analyzed because of discrepancy in the initial blocking data set. These are marked with asterisk (*) in Table B.2a and Table B.4a in appendix B.

Table 2.6b. Same as Table 2.6a except for the alternating height dominance results.

	Alternating Height Dominance	
YEAR	**NH**	**SH**
1999	6/28	0/28
2000	3/28	0/28
2001	3/31	3/31
2002	10/41	0/41
2003	15/48	2/48
2004	3/37	3/37

Fig. 2.2 displays the height scale dominance for all the blocking event cases studied in the six year climatology. In both hemispheres, a sharp rise in the blocking events with planetary-scale dominance is evident during the later half of the six year period. The blocking events having synoptic-scale dominance are out of phase with the blocking events having the planetary-scale dominance in both hemispheres for the entire six year duration. The blocking events with alternating height dependence are in phase with the blocking events with planetary-scale dominance for both the hemispheres for the entire six year duration. A rising trend in the number of blocking events with planetary-scale dominance is more noticeable in NH. All three dominance scales of blocking events are indicative of oscillatory nature of mid tropospheric atmospheric flow in the mid latitudes.

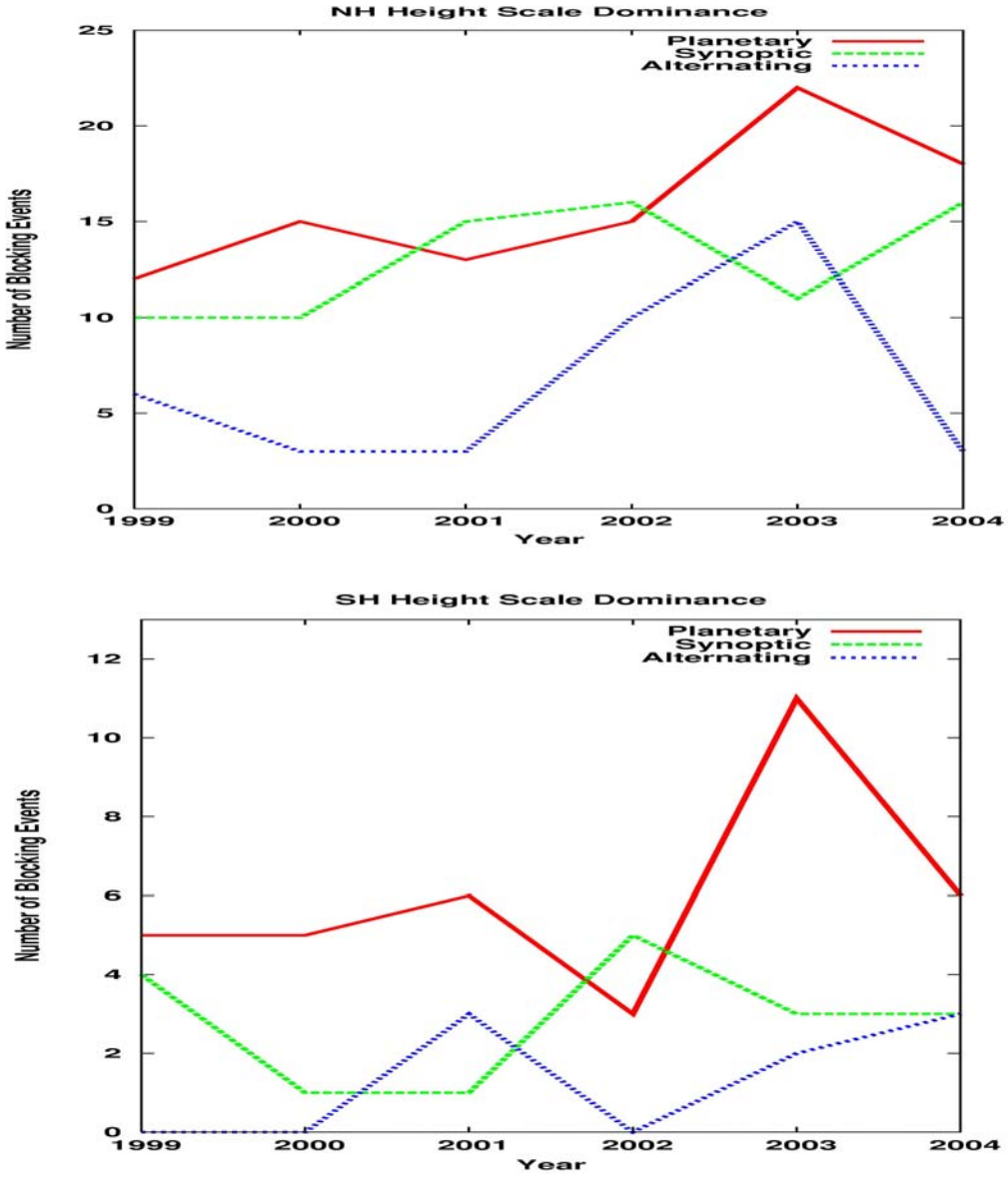

Fig. 2.2. Scale dominance distribution for the analyzed blocking events lasting for 5 days or more over the six year period (1999-2004) under study. Upper panel: NH. Lower panel: SH.

Globally, 83% (226/274) of the total analyzed blocking events have a dominance of one scale only, over a six year period under study. 48% of these events (131/274) have planetary-scale dominance. 35% of these events (95/274) have synoptic-scale dominance.

When stratified over hemispheres, over the six year period in NH, a total of 63% of the detected blocking events have single height scale dominance, whereas 15% have alternating height scale dominance. Over the same six year period in SH, a total of 19% of the detected blocking events have single height scale dominance, whereas 3% have alternating height scale dominance.

A prominent feature of our study is the finding that the scale dynamics of a vast majority of blocking events is governed by the dominance of single height scale. This category of blocking events thus constitutes a representative category of all the blocking events occurring during the six year period. It is thus of relevance to perform a detailed case study for dominance of each wavelength as a representative case study in both the hemispheres.

We shall discuss in detail a representative case from each scale dominance in next two chapters. We then present overall summary of our global six year climatology in Chapter 5. In the next two chapters, we discuss in detail a representative blocking event in NH and in SH respectively. The NH blocking events was studied earlier by Glisan (2007) and SH blocking event was studied by Dong and Colucci (2005, 2007). We use a different set of diagnostic tools to study these cases than those were used in the above studies.

CHAPTER 3

CASE STUDY I: NORTHERN HEMISPHERE

In this chapter, we discuss in detail the synoptic aspects as well as the scale and the stability analysis of barotropic flow in an unusually prolonged and moderately extreme blocking event that led to heat wave in Gulf of Alaska during August 2004. We shall first perform synoptic and then a scale and stability analysis of the NH region of the atmospheric flow where the selected blocking event occurred.

3.1 Synoptic Analysis

The selected blocking event occurred during 02 August through 28 August 2004. The block onset stage was during 02–05 August, its mature stage was during 05–20 August and its decay stage was during 20–28 August. The blocking ridge lasted for

23.5 days. This is event number 26 in Table 2.2c and Table 2.4c in Chapter 2. The above normal surface temperatures and below normal precipitation was reported during the month of August over the entire Alaska region (Alaska NWS 2004). This blocking event was earlier studied by Glisan (2007).

The geopotential height formation pattern (taken at 500 mb) that leads to identification of blocking anticyclones on an upper air chart can conveniently be quantified in terms of BI. The BI gives the combined effect of planetary-scale as well as the synoptic-scale height pattern formations simultaneously. According to Wiedenmann et al. (2002) definition of BI, the BI for the considered blocking event averaged over its entire life cycle is 2.44 which implies a moderate strength blocking on a scale of 1 to 10 (see Eq. (1.3) and Eq. (1.4) in Chapter 1). The blocking flow was located in the region encompassing 80^{o}N to 5^{o}N and 260^{o}E to 160^{o}E.

The midtropospheric synoptic features of the blocking event are displayed in Fig. 3.1, Fig. 3.2 and Fig. 3.3. Figure 3.1 displays a Hovmöller diagram generated using MATLAB for the entire month of August 2004 for the Lejenäs Øakland 1983 (LO) blocking index, which is defined as follows

$$\mathrm{LO} = Z(60^{o}) - Z(40^{o}). \qquad (3.1)$$

The 6 hourly observed geopotential height field data was used to calculate the LO index. A negative value for LO signifies a blocked zonal flow (hatched region in Fig. 3.1).

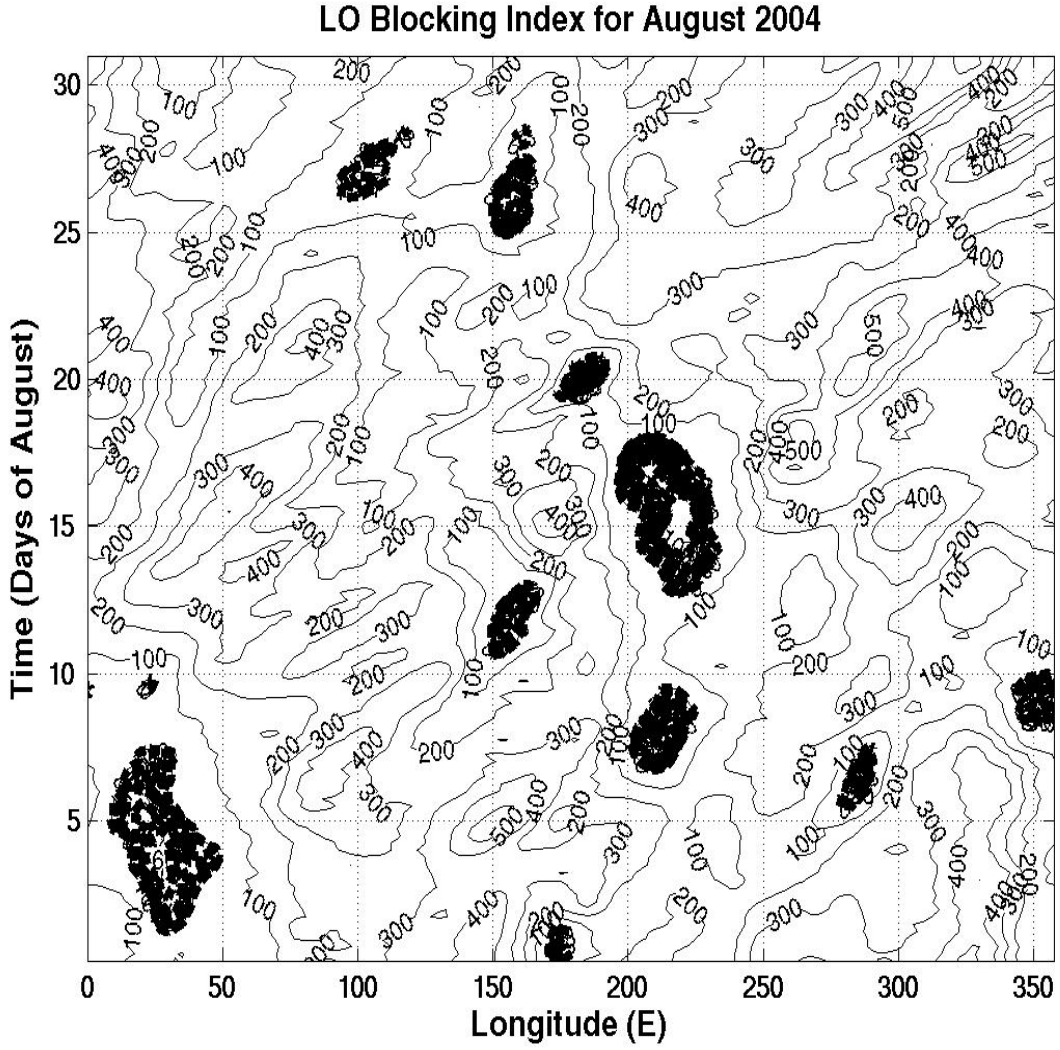

Fig. 3.1. The Hovmöller diagram depicting the LO blocking index for the entire month of August 2004. The 6 hourly geopotential height data at 500 mb is used. The hatched regions indicate the negative values for LO blocking index depicting the presence of blocking. The presence of almost continuous hatched island regions between 160^{o}E to 260^{o}E indicates the unusually prolonged blocking event under study.

Figure 3.2a displays the NH 500 mb analyzed geopotential height after the block onset stage (10 August) at 1200 UTC. Fig. 3.2b displays the region between 180^{o} and 240^{o}E that encompasses the blocking over the Gulf of Alaska.

Figure 3.3a displays the NH 500 mb analyzed geopotential height during the mature stage (18 August) at 1200 UTC. The Rex shaped block formation occurs over the Gulf of Alaska with maximum geopotential height of 5976 m. Fig. 3.3b displays the region between 180^{o} and 240^{o}E for 18 August. During the mature stage, the geopotential height is 18 m higher than during the onset stage.

Figure 3.4a displays the NH 500 mb analyzed geopotential height during the decay stage (26 August) at 1200 UTC. Fig. 3.4b displays the region between 180^{o} and 240^{o}E for 26 August. During the decay stage, the maximum geopotential height is 19 m lower than during the mature stage; where as the lower height is 160 m smaller than the corresponding mature stage lower height.

Figure 3.5 displays the analyzed 500 mb temperature field distribution for the entire blocking life cycle indicating below normal temperature in North of blocking.

Using Eq. (1.3) and Eq. (1.4), we have computed the BI for the entire life cycle of the selected blocking event and it is displayed in Fig. 3.6. Note a resemblance in the features during the peak activity stage (15–20 August) between the BI and the negative LO index values depicted in Fig. 3.1 confirming the deepening of the blocking anticyclone. A comparison of the two different block detection schemes displayed in Fig. 3.1 and Fig. 3.6 indicates that the two schemes are in gross agreement with each other. In Fig. 3.6, the oscillating behavior of the BI peaks during the maximum activity

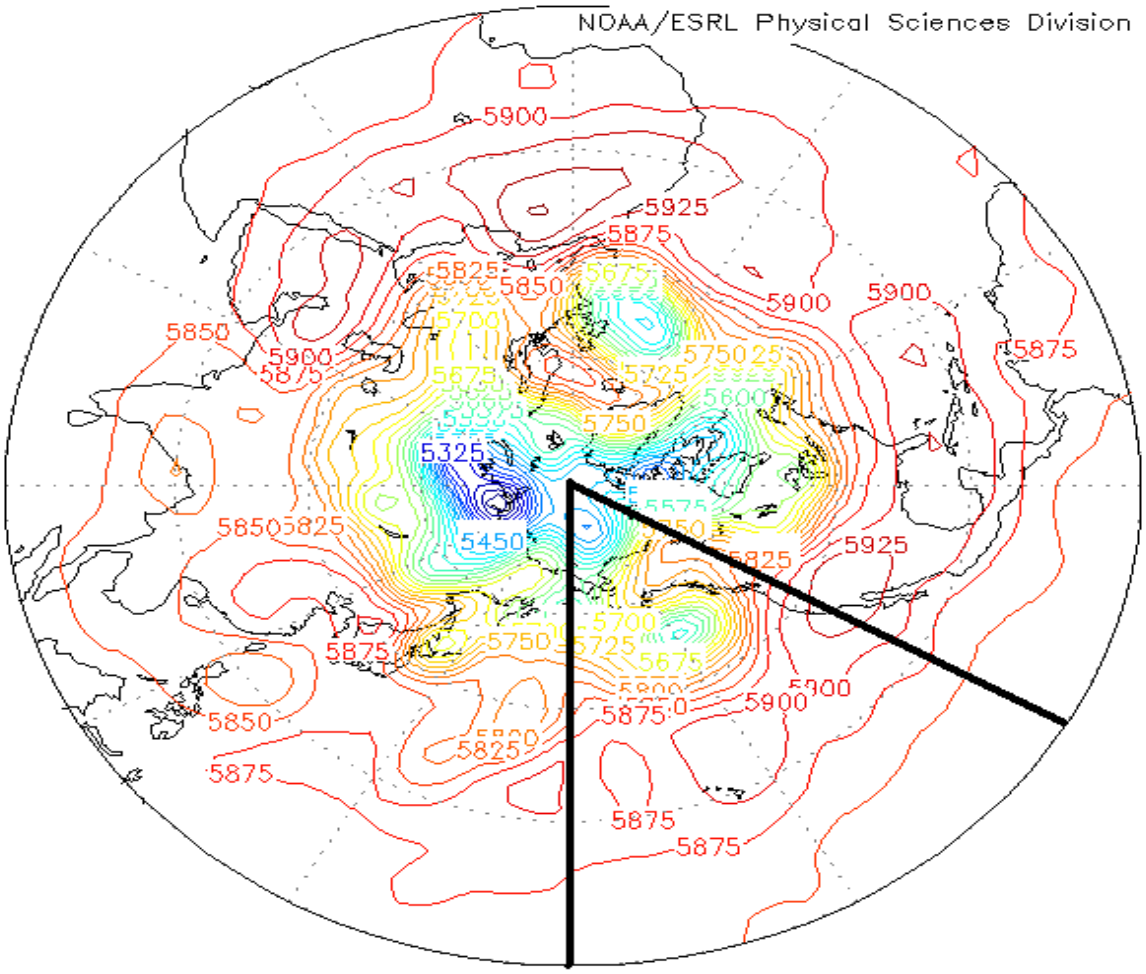

Fig. 3.2a. The 500 mb analyzed height for 1200 UTC 10 August 2004 for the blocking event over the North Pacific Ocean which lasted from 2 August 2004 through 28 August 2004. The analyzed 500 mb height is plotted every 25 m. The region of the atmospheric flow encompassing the blocking lies between 160°E to 260°E. The NH maximum geopotential height is 5977 m, whereas the minimum geopotential height is 5233 m (obtained from http://www.cdc.noaa.gov/).

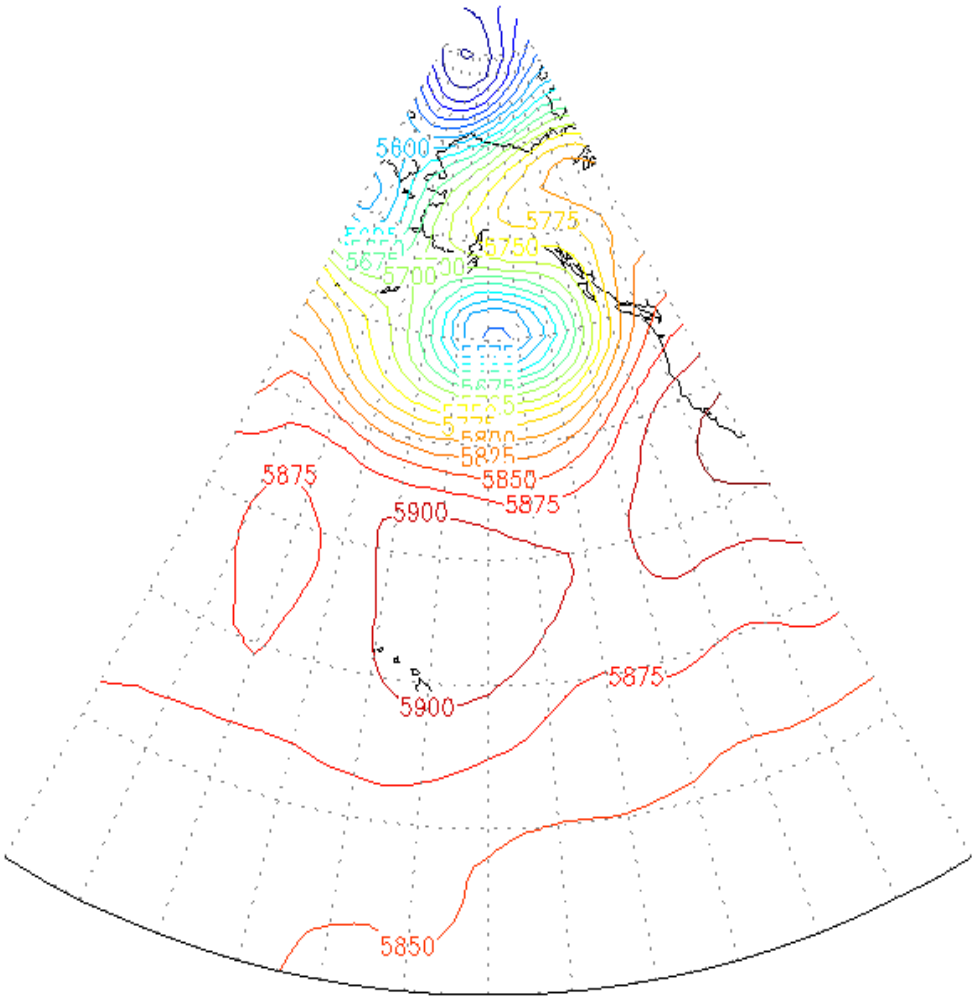

Fig. 3.2b. The 500 mb analyzed height for 1200 UTC 10 August 2004 for the blocking event over the North Pacific Ocean for 180^{o} through 240^{o}E. The analyzed 500 mb height is plotted every 25 m. The lower heights are towards the North of the high pressure ridge over the continental Alaska. The maximum geopotential height is 5941 m, whereas the minimum geopotential height is 5423 m (obtained from http://www.cdc.noaa.gov/).

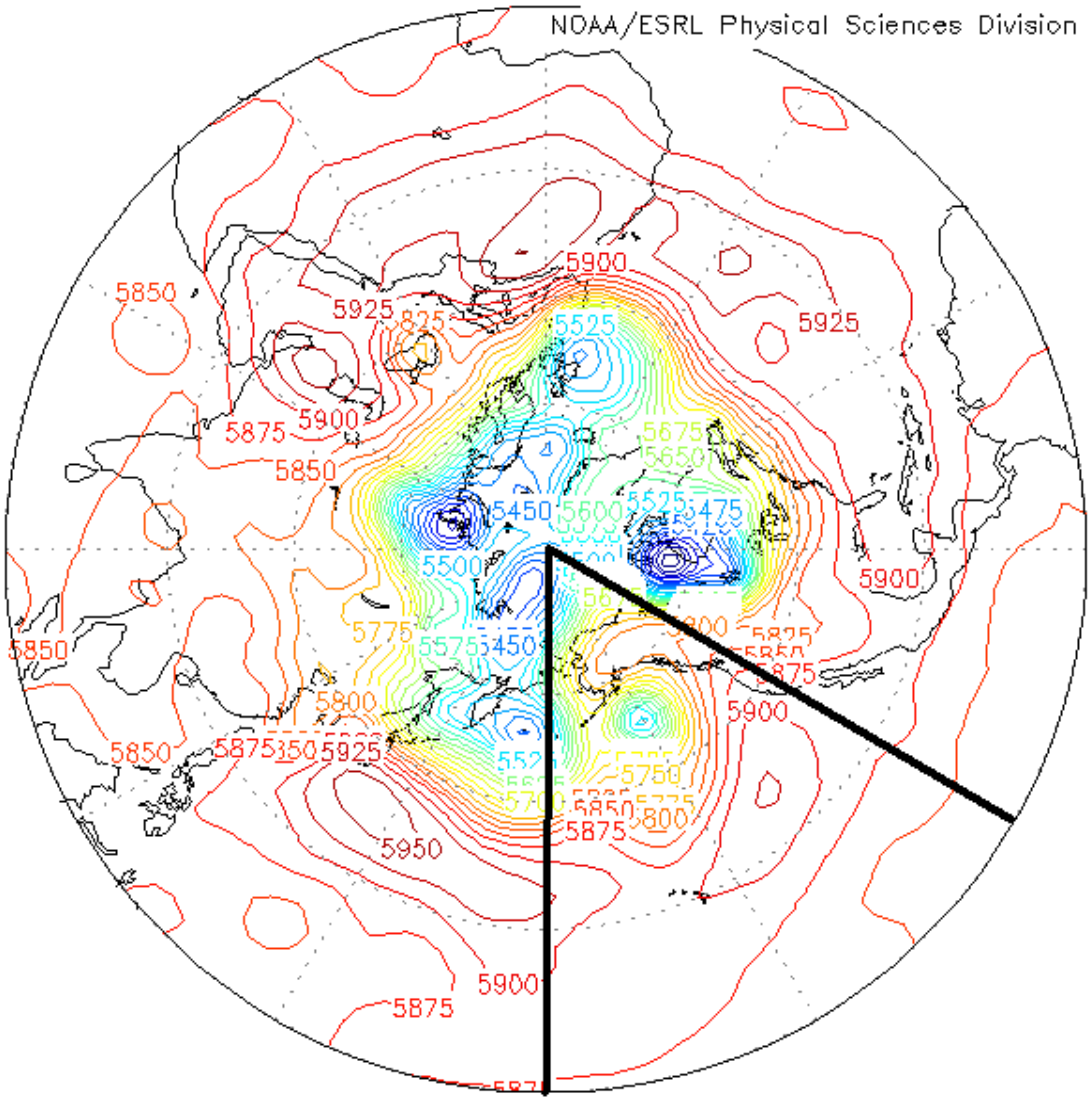

Fig. 3.3a. Same as Fig. 3.2a, except for 1200 UTC 18 August 2004 (peak activity stage). The Rex shaped blocking pattern is clearly noticeable. The NH maximum 500 mb geopotential height is 5976 m, whereas the minimum geopotential height is 5262 m. The blocking occurred inside the marked region.

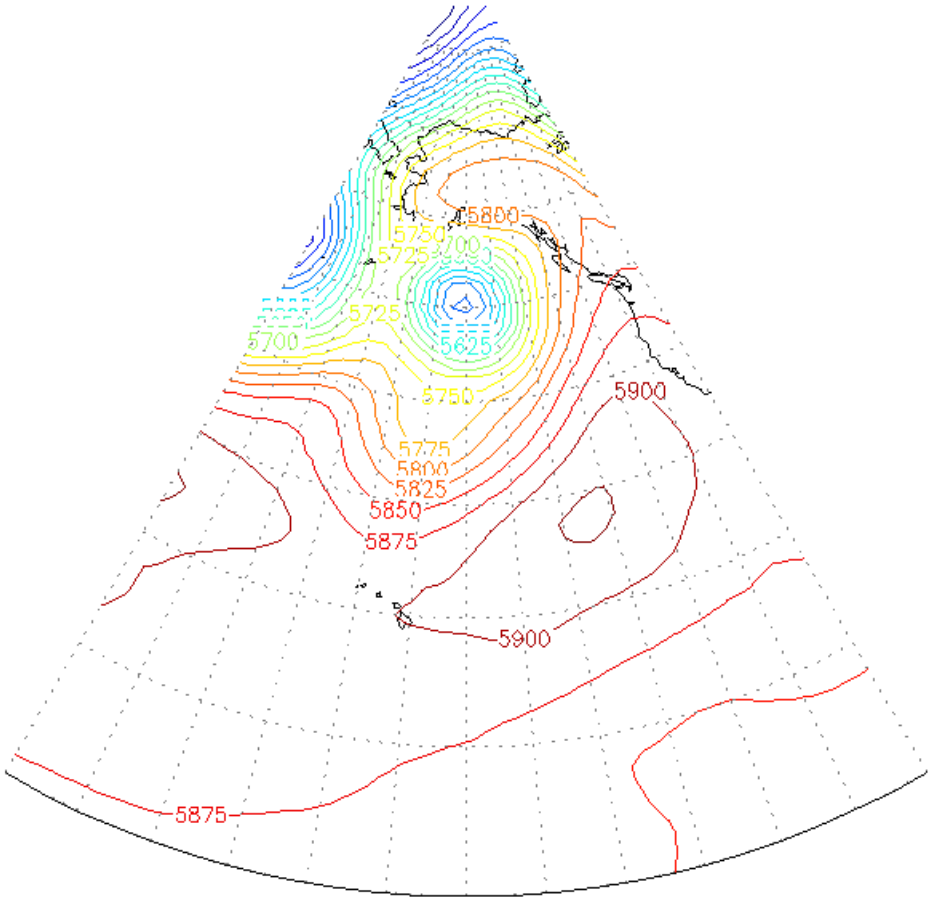

Fig. 3.3b. Same as Fig. 3.2b except for the 500 mb analyzed height for 1200 UTC 18 August 2004 for the blocking event over the North Pacific Ocean for 180^{o} through 240^{o}E during the mature stage. The analyzed 500 mb height is plotted every 25 m. The lower heights are towards the North of the high pressure ridge over the continental Alaska. The maximum geopotential height is 5959 m, whereas the minimum geopotential height is 5411 m.

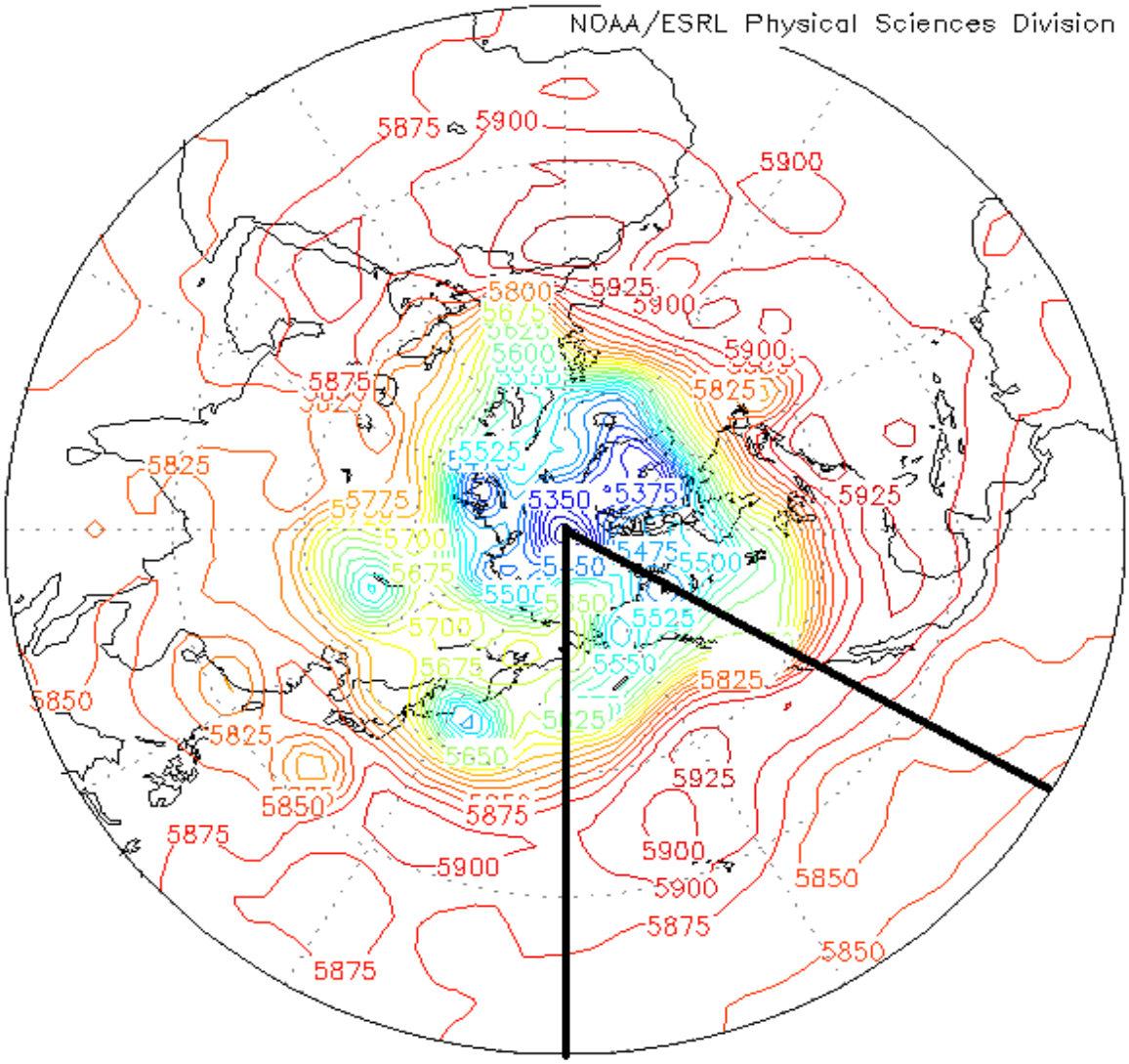

Fig. 3.4a. Same as Fig. 3.2a, except for 1200 UTC 26 August 2004 towards the end of decay stage. Note the dissolving high pressure system in Gulf of Alaska. The NH maximum geopotential height is 5975 m, whereas the minimum geopotential height is 5251 m. The blocking occurred inside the marked region.

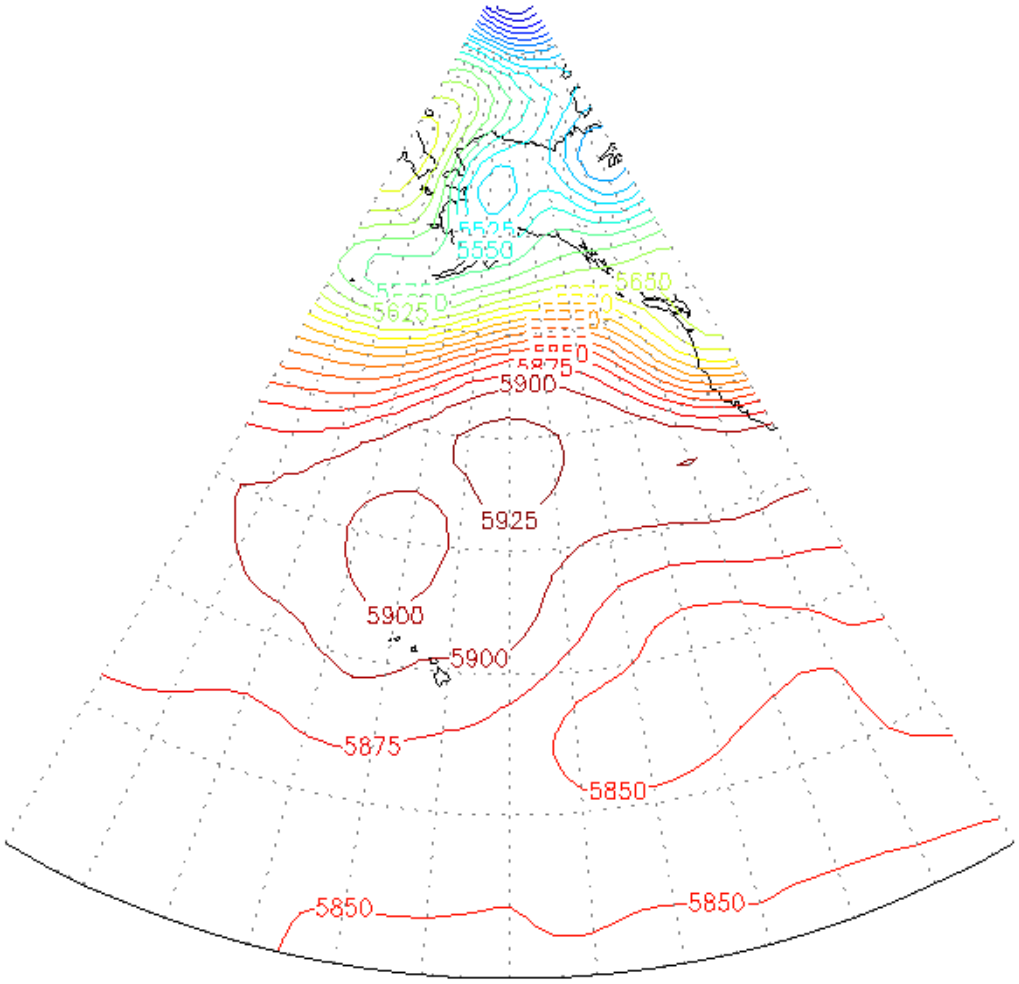

Fig. 3.4b. Same as Fig. 3.2b except for the 500 mb analyzed height for 1200 UTC 26 August 2004 for the blocking event over the North Pacific Ocean for 180^{o} through 240^{o}E during the decay stage. The analyzed 500 mb height is plotted every 25 m. The maximum geopotential height is 5940 m, whereas the minimum geopotential height is 5251 m.

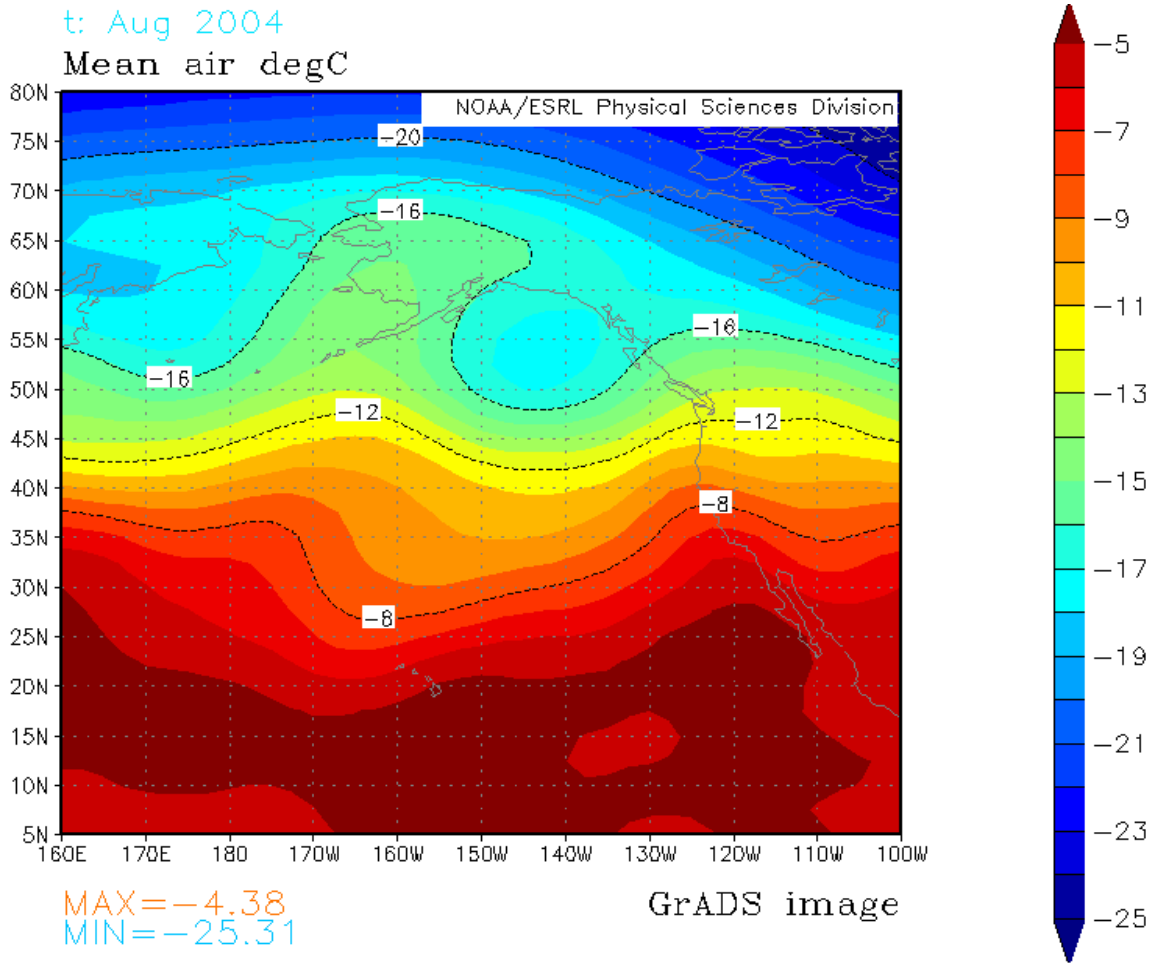

Fig. 3.5. The 500 mb analyzed temperature field (^{o}C) of the atmospheric flow region that encompasses the blocking event shown in Fig. 3.1 for August 2004. Below normal temperature is in North of the blocking ridge, whereas above normal temperatures are noticeable South of the blocking ridge (obtained from http://www.cdc.noaa.gov/).

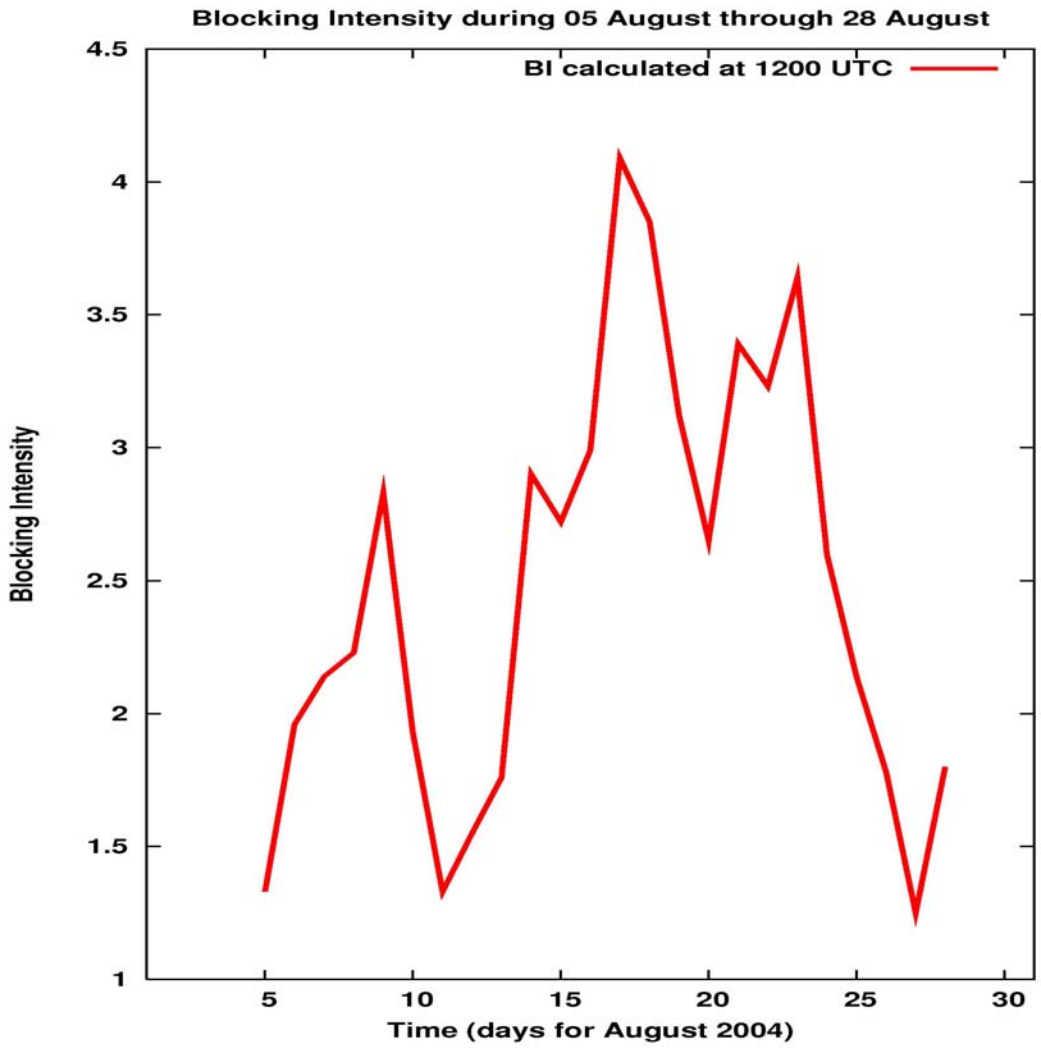

Fig. 3.6. The daily BI calculated at 1200 UTC for the entire life cycle (05–28 August 2004) of the blocking event. The oscillatory behavior attains a peak value during the maximum activity stage of the blocking (15–20 August 2004) relative to the onset (2–5 August 2004) and the decay stages (20–28 August 2004).

stage of the blocking which is 15 August through 20 August, 2004. In Fig. 3.1, we note that a relatively more negative LO index (larger hatched region) occurs between 180^{o} through 230^{o}E during approximately the same time period. Within this longitude band there is no hatched region on 11 August as the BI has a relative minimum on that day.

3.2 Scale Analysis

Figure 3.7 displays the 500 mb blocking area averaged planetary-scale height for the entire life cycle of the block. During the mature stage of the block life cycle, the height attains its relative maximum value. Note the occurrence of a positive height anomaly during the mature stage (15–20 August 2004) of the blocking as the monthly mean reference value for the entire month of August lies at 5748 m only. The median reference level for the planetary-scale geopotential height lies at 5756 m (not shown). The average heights within the box start falling until just before the block decay (day number 21). This suggests changes in the behavior of the planetary-scale flow regime.

Figure 3.8 displays the blocking area 500 mb planetary-scale geopotential height for four different isobaric levels, all at 1200 UTC. Through the entire stratosphere and the troposphere the height anomaly persists indicating that the scale dynamics of the selected blocking event is dominated by the large-scale wavelengths (the tropopause pressure averaged over the blocking life cycle was ~ 230 mb). This is in contrast to what we have noticed for the case study in the Southern Hemisphere.

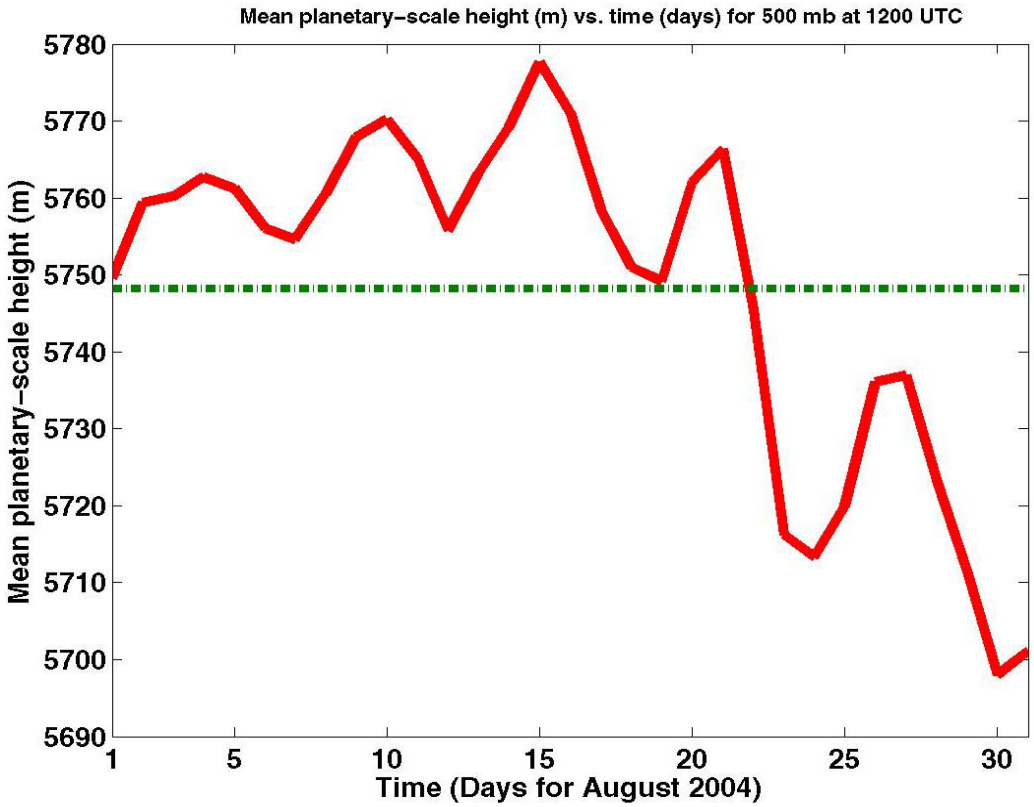

Fig. 3.7. A diagram of the mean planetary-scale 500 mb geopotential height (m) along abscissa versus time (days) along ordinate for a stationary box (5^oN to 80^oN and 260^oE to 160^oE) in the mid-latitude Northern Hemisphere flow. The dashed dotted horizontal line defines the monthly mean reference value for the planetary-scale geopotential height. The median planetary-scale geopotential height lies at 5756 m (not shown).

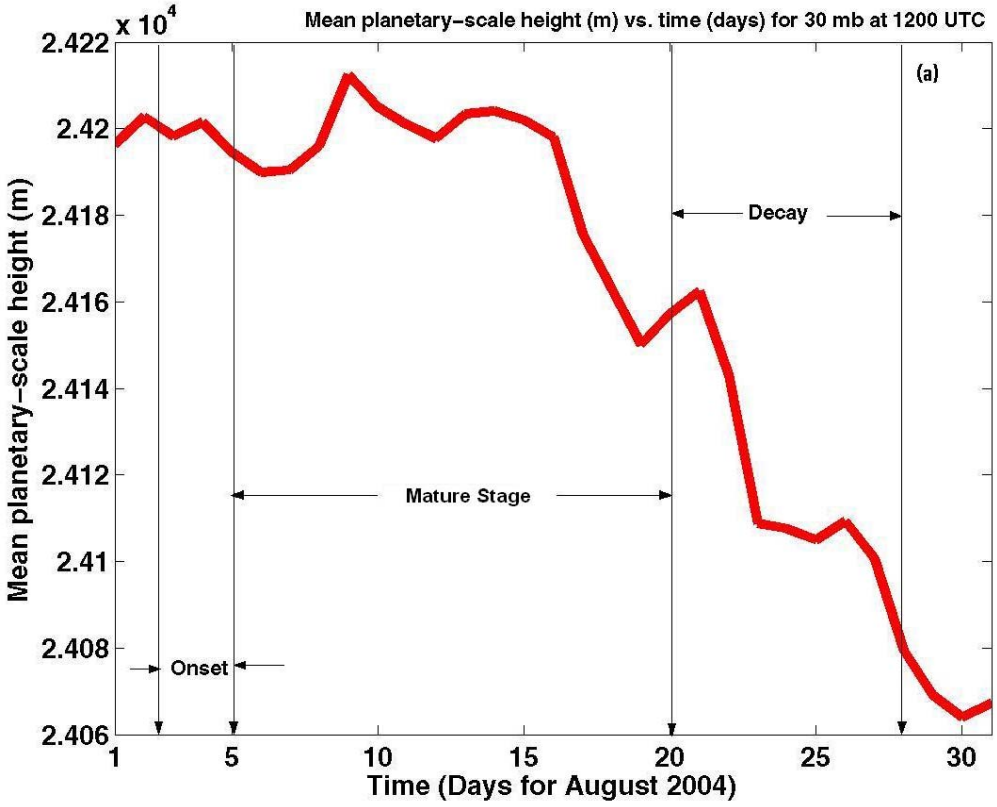
Mean planetary–scale height (m) vs. time (days) for 30 mb at 1200 UTC
x 10^4
2.422
2.42
2.418
2.416
2.414
2.412
2.41
2.408
2.406
Mean planetary–scale height (m)
(a)
Decay
Mature Stage
Onset
1
5
10
15
20
25
30
Time (Days for August 2004)

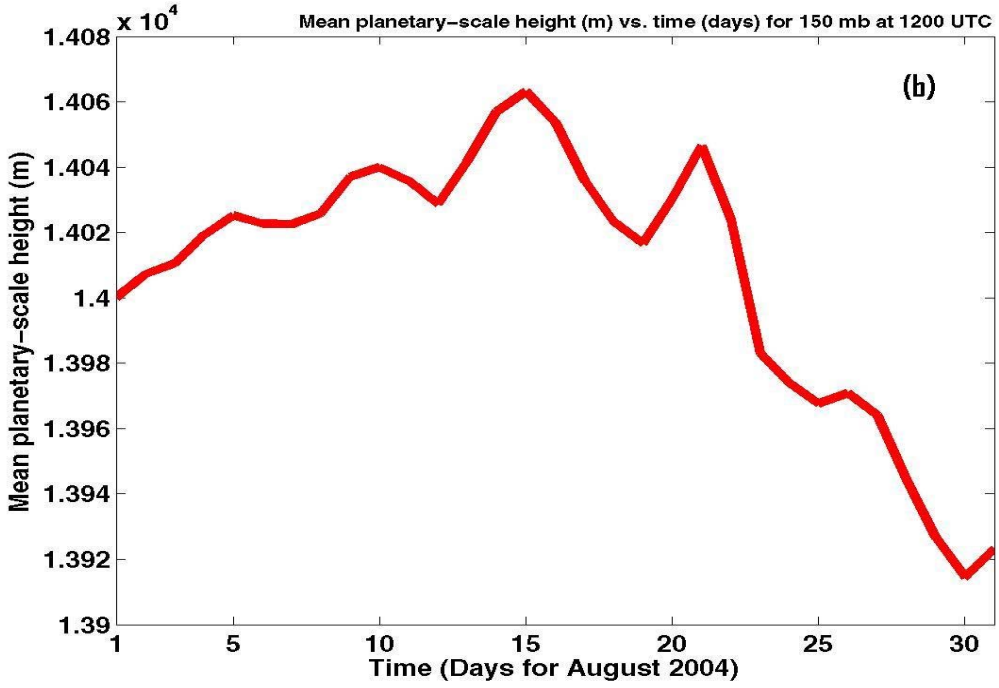
Mean planetary–scale height (m) vs. time (days) for 150 mb at 1200 UTC
x 10^4
1.408
1.406
1.404
1.402
1.4
1.398
1.396
1.394
1.392
1.39
Mean planetary–scale height (m)
(b)
1
5
10
15
20
25
30
Time (Days for August 2004)

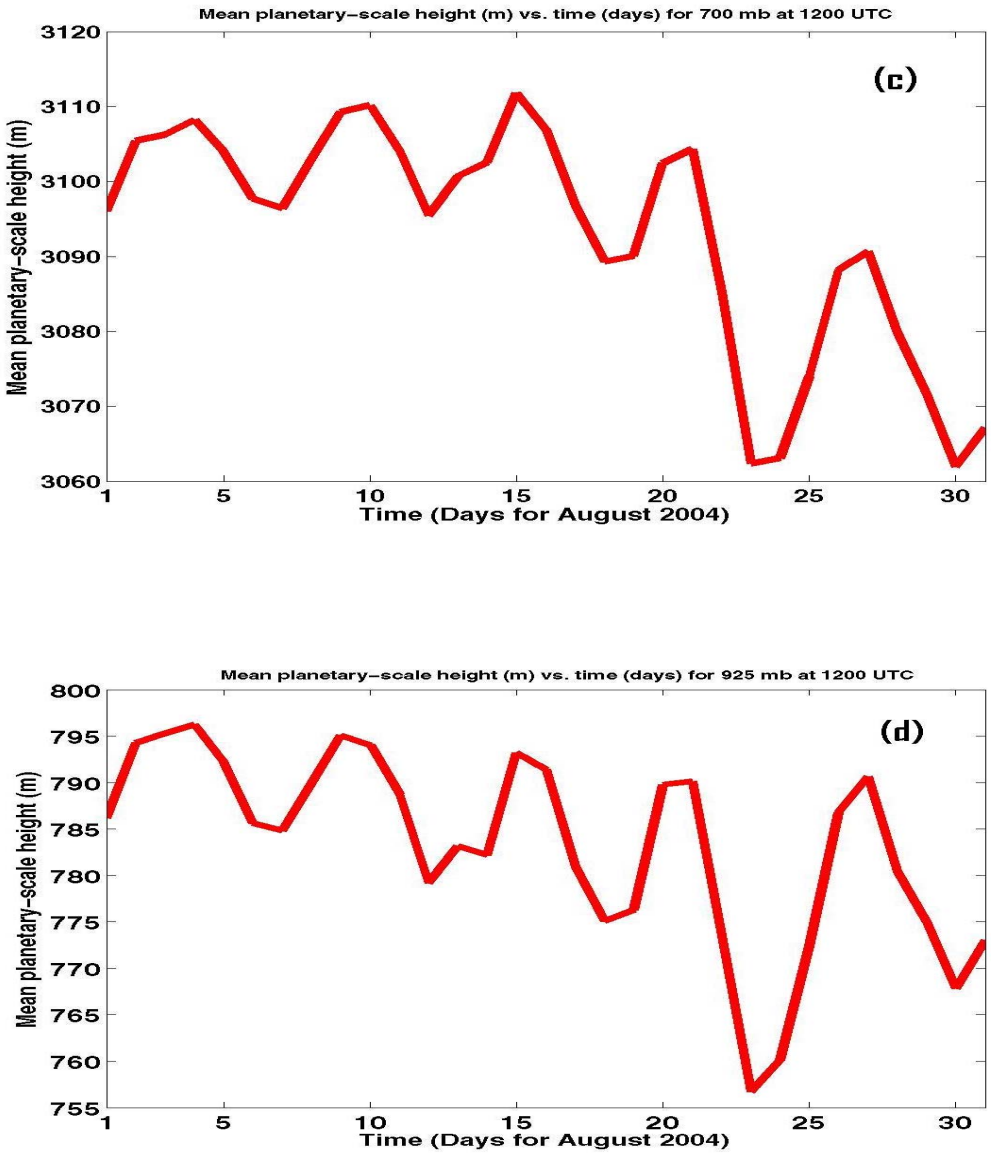

Fig. 3.8. A diagram of the mean planetary-scale geopotential height (m) along abscissa versus time (days) along ordinate for a stationary box (5^oN to 80^oN and 260^oE to 160^oE) in the mid-latitude Northern Hemisphere flow for (a) 30 mb, (b) 150 mb, (c) 700 mb, and (d) 925 mb.

The blocking area averaged synoptic-scale eddy height at 500 mb is defined as the difference between the observed and the mean planetary-scale height at this isobaric level (Eq. (1.2)). We display in Fig. 3.9 the 500 mb synoptic-scale eddy height tendency for the entire life cycle of the blocking event. During the decay stage (20–28 August), the temporal activity of the migratory synoptic-scale wavelengths is greater than during the onset and mature stages since during the decay stage, the synoptic-scale environment becomes unstable.

When stratified across the entire troposphere and stratosphere, we noticed that the blocking area averaged synoptic-scale eddies grow in amplitude in lower troposphere (925 mb) relative to upper troposphere (150 mb) and play an increasingly dominant role in destabilizing the zonal flow thus initiating the decay of the blocking state. Fig. 3.10 displays the blocking area averaged synoptic-scale eddy height for 30 mb, 150 mb, 700 mb and 925 mb. The oscillatory behavior is indicative of area averaged synoptic-scale ridge-trough dominance for the advection of the heat wave at the given isobaric level. A positive difference corresponds to the high pressure system/ridge, whereas the negative difference corresponds to the formation of a trough.

Climatologically, this blocking event is the longest blocking event in East Pacific region for the year 2004 (July 2004 through June 2005). This finding is in agreement with the blocking persistence estimates of Lupo and Smith (1995a) and of Barriopedro et al. (2006). This unusually prolonged blocking event impacted the downstream regional weather over the continental US as well. The West cost of mainland continental US experienced mild summer for August of 2004 (Glisan 2007).

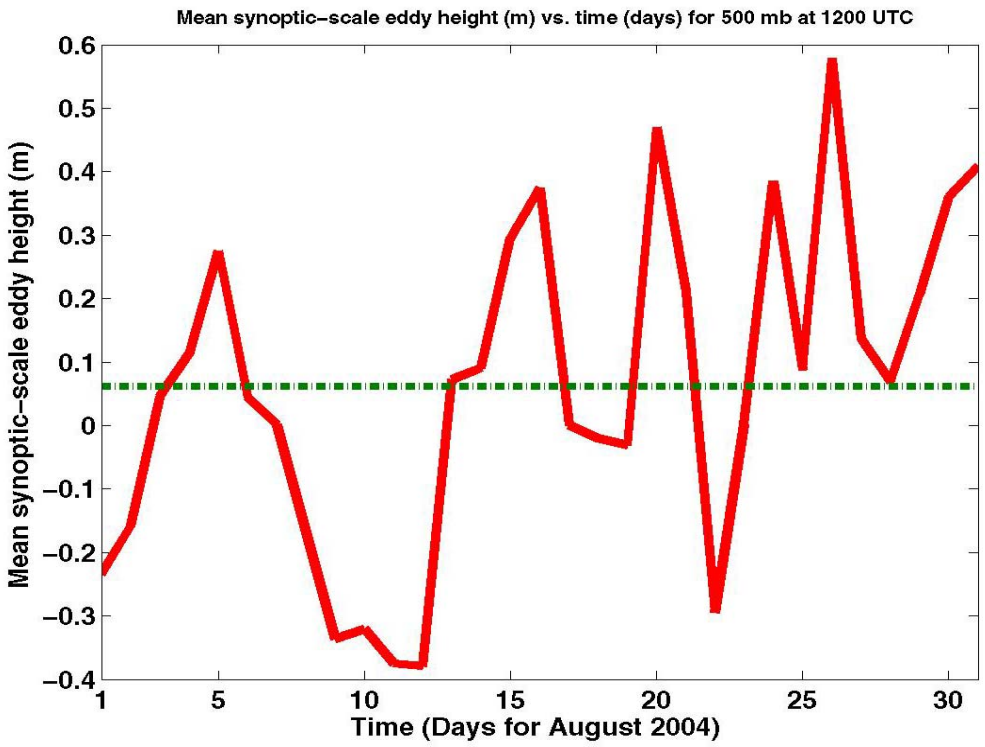

Fig. 3.9. A diagram of the mean 500 mb geopotential synoptic-scale eddy height (m) for 1200 UTC along abscissa versus time (days) along ordinate for a stationary box (5^{o}N to 80^{o}N and 260^{o}E to 160^{o}E) in the mid-latitude Northern Hemisphere flow for the entire month of August 2004. The horizontal line defines the monthly mean reference value.

This is an instance where occurrence of midtropospheric level blocking affects the regional weather though the blocking is not occurring at exactly over that region, as already pointed out in Chapter 1. For details of climatological aspects of downstream weather impacts associated with blocking, see Carrera et al. 2004.

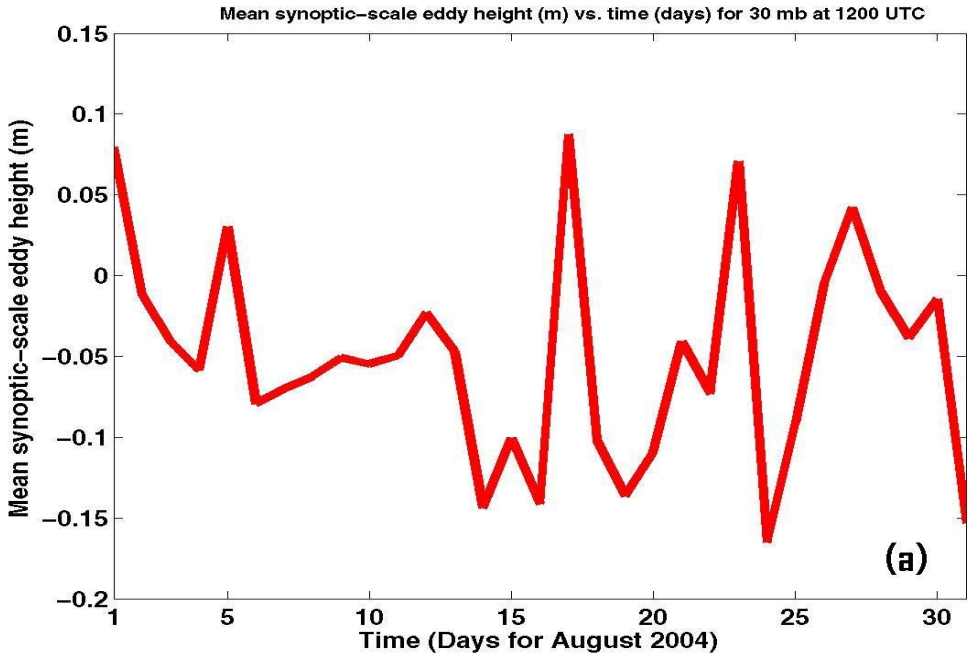
Mean synoptic–scale eddy height (m) vs. time (days) for 30 mb at 1200 UTC
Mean synoptic–scale eddy height (m)
0.15
0.1
0.05
0
−0.05
−0.1
−0.15
−0.2
1
5
10
15
20
25
30
Time (Days for August 2004)
(a)

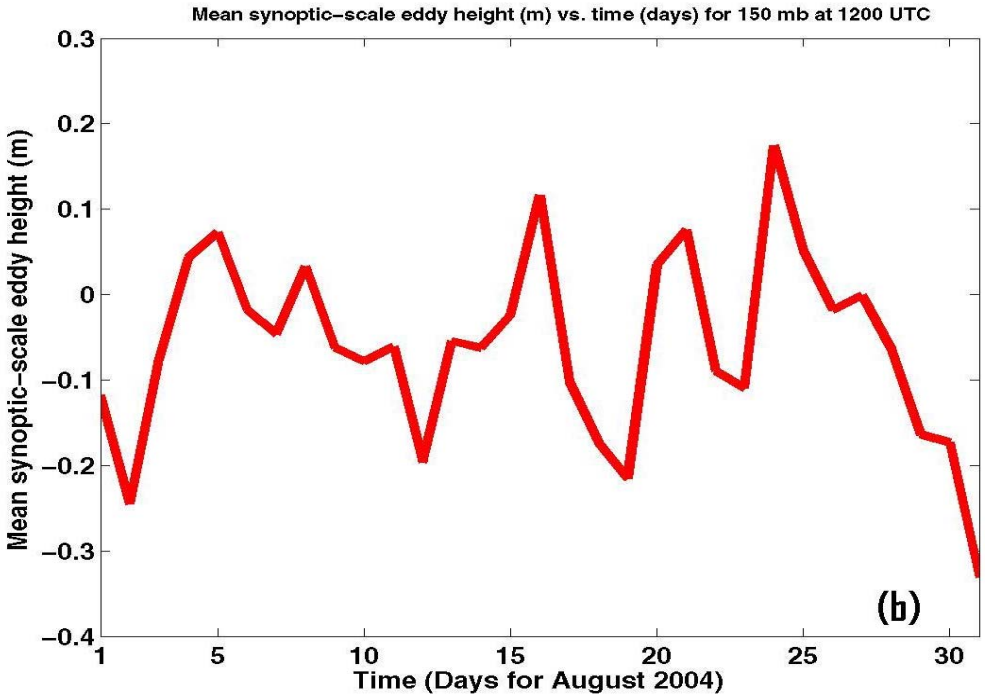
Mean synoptic–scale eddy height (m) vs. time (days) for 150 mb at 1200 UTC
Mean synoptic–scale eddy height (m)
0.3
0.2
0.1
0
−0.1
−0.2
−0.3
−0.4
1
5
10
15
20
25
30
Time (Days for August 2004)
(b)

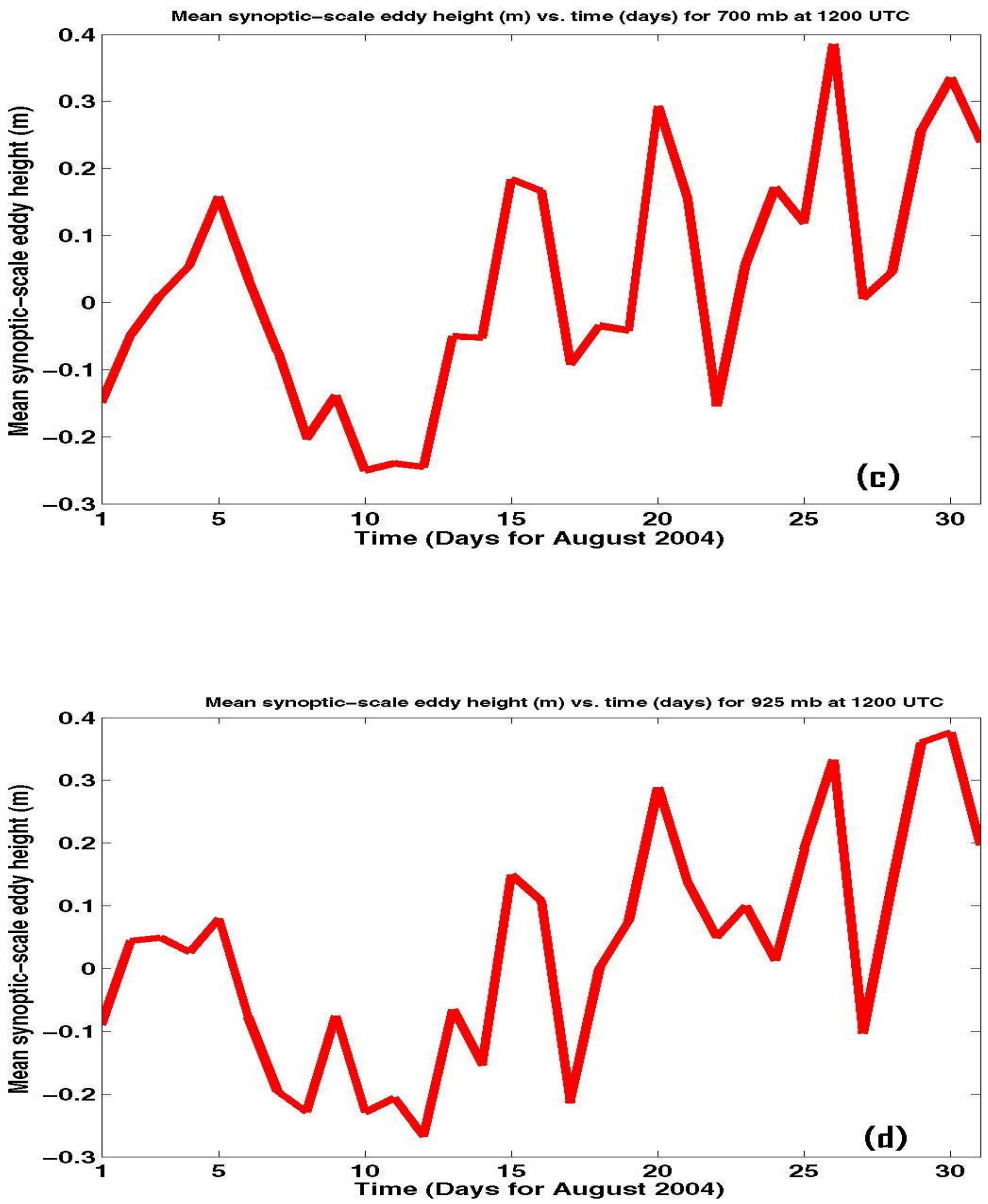

Fig. 3.10. A diagram of blocking area averaged geopotential synoptic-scale eddy height (m) for 1200 UTC along abscissa versus time (days) along ordinate for a stationary box (5^oN to 80^oN and 260^oE to 160^oE) in the mid-latitude Northern Hemisphere flow for the entire month of August 2004 for (a) 30 mb, (b) 150 mb, (c) 700 mb, and (d) 925 mb.

3.3 Stability Analysis

Fig. 3.11 displays the time variability of blocking area integrated regional enstrophy (IRE) for 500 mb planetary-scale geopotential height at 1200 UTC. Comparing this with Fig. 3.7 that gives the time variability of the planetary-scale geopotential height, we note that between 20 and 25 August, the IRE increases considerably, indicating the rise in the instability in the planetary-scale flow which corresponds well in time with the fall in amplitude of planetary-scale height during the same period. The blocking state being an anticyclone is a high pressure system and we may thus conclude that the planetary-scale relative instability formation leads to a rapid decay of the blocking high. We further note that the height stratified area averaged planetary-scale height also drops rapidly during the same duration thus confirming our above conceptual picture (Fig. 3.8).

Calculation of the IRE following Eq. (1.1) for entire life cycle of the blocking event under study demonstrates a relationship between these values and the trend displayed in Fig. 3.8 where stratified planetary-scale heights are displayed. From Fig. 3.11, we note that the area averaged enstrophy reaches a minimum shortly after block onset and is at a relative minimum during the life cycle of this blocking event. This is also consistent with the view that, in a quasi-barotropic flow, the planetary-scale flow should be strongly barotropic, see, Ghil and Childress (1987). Also that the blocking state represents a minimum state of the enstrophy [and entropy see e.g., Dymnikov and

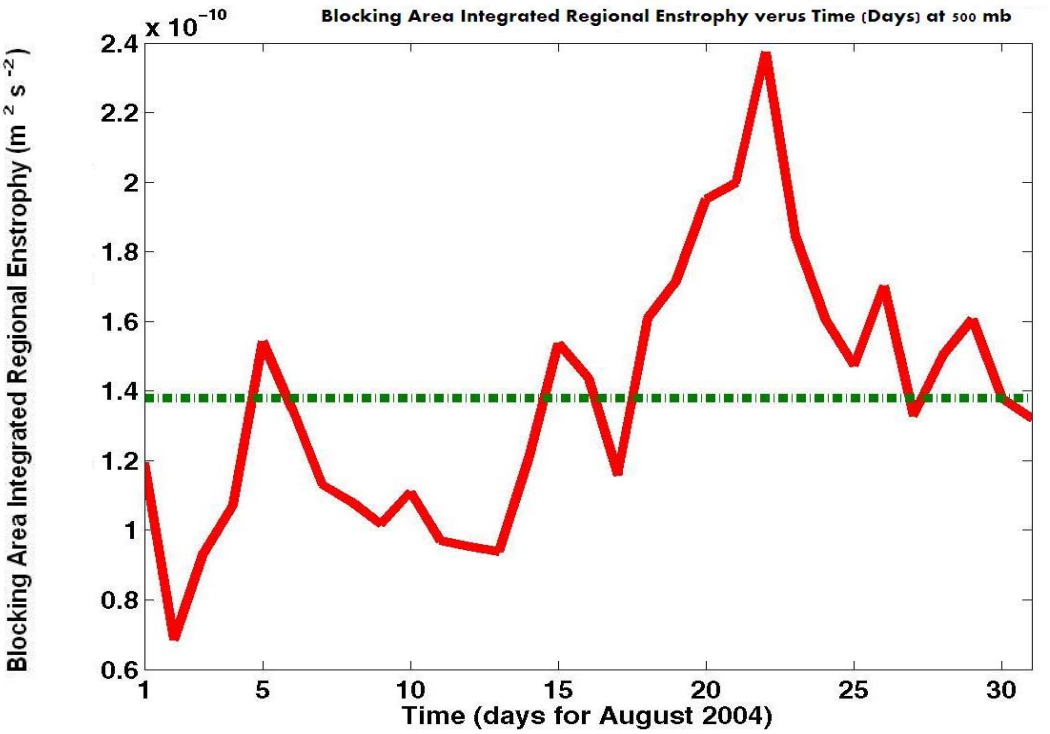

Fig. 3.11. A calculation of the area averaged enstrophy using Eq. (1.1) for the blocking event displayed in Fig. 3.7 which occurred during 05–28 August 2004.The relative stability level changes at onset (02–05 August) and at decay (20–28 August) stages. The horizontal line defines the monthly mean reference value.

Filatov (1995)]. Since enstrophy relates to the positive eigenvalues, which are relatively small here, indicates that negative values of fluid trapping (again implying more predictability, or a more stable condition) grow in concert with the intensity of the blocking event, see, Cohen and Schultz (2005). Fig. 3.12 indicates that after the onset of the blocking state, the block IRE attains relatively lower positive values. Thus,

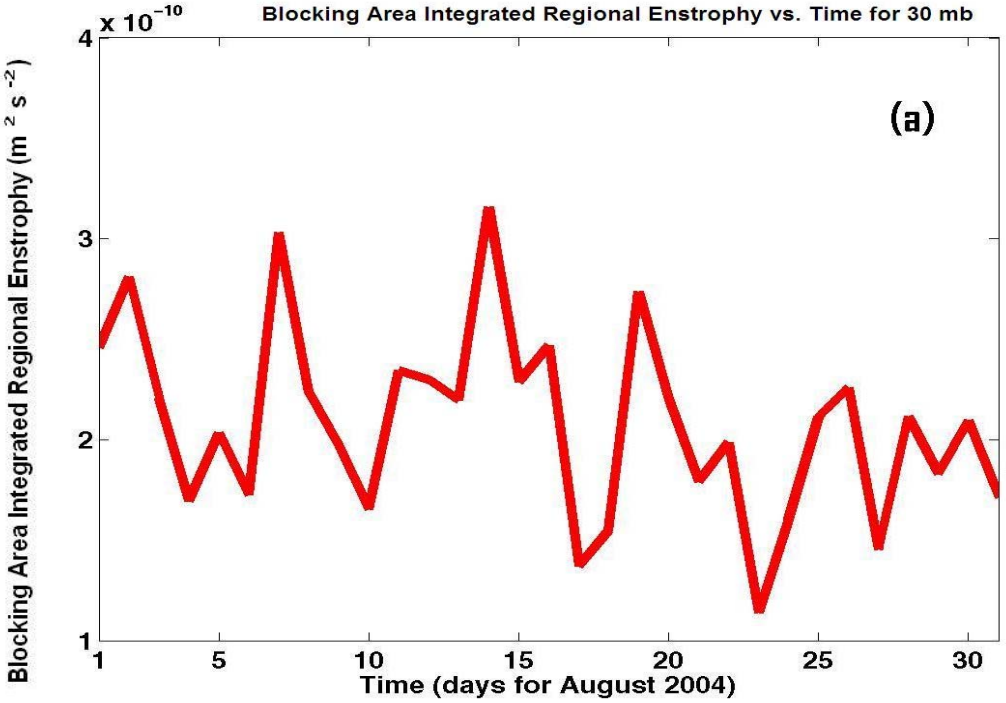
Blocking Area Integrated Regional Enstrophy vs. Time for 30 mb
x 10^-10
Blocking Area Integrated Regional Enstrophy (m^2 s^-2)
(a)
Time (days for August 2004)

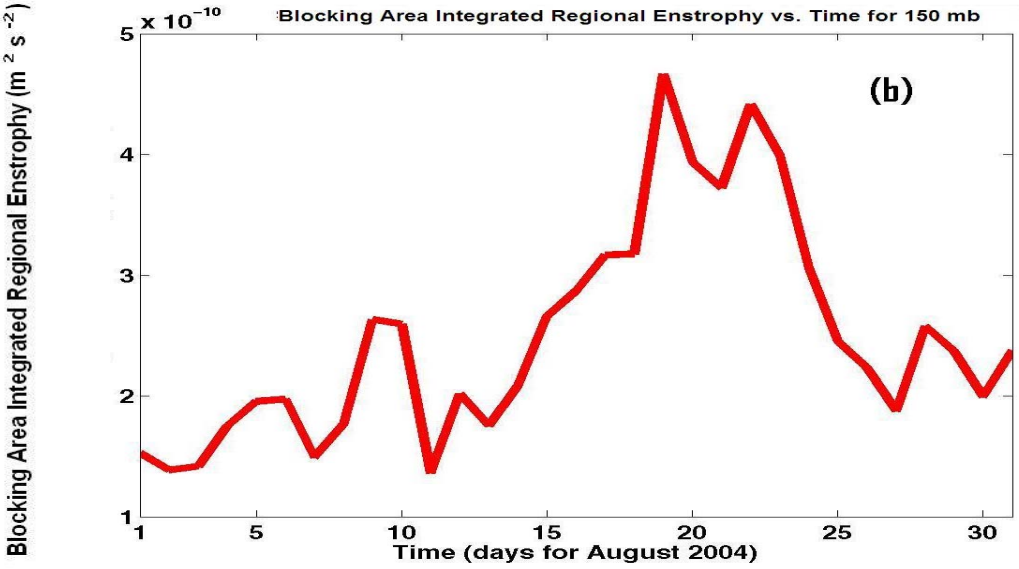
Blocking Area Integrated Regional Enstrophy vs. Time for 150 mb
x 10^-10
Blocking Area Integrated Regional Enstrophy (m^2 s^-2)
(b)
Time (days for August 2004)

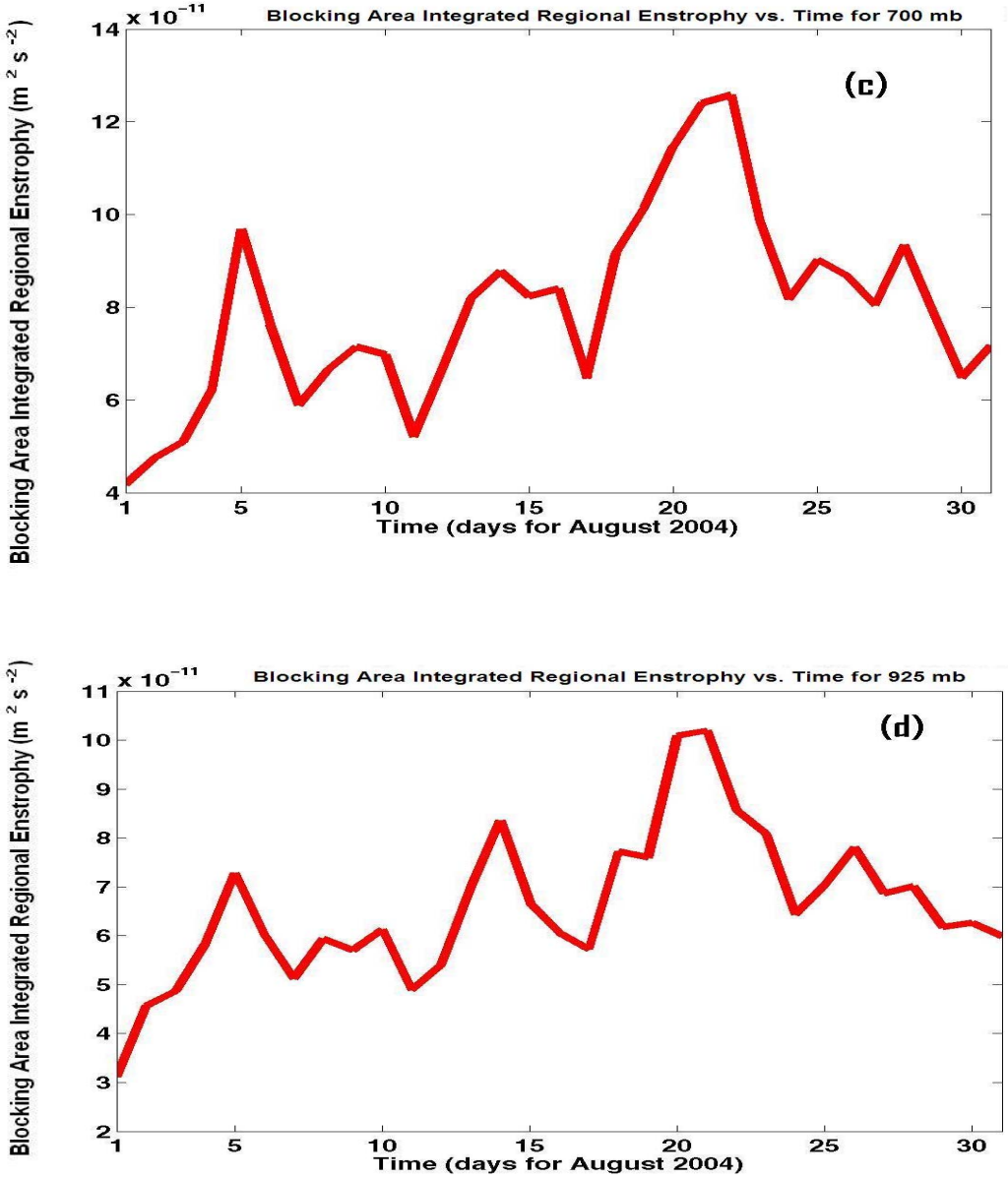

Fig. 3.12. A diagram of the mean planetary-scale geopotential height scale IRE along abscissa versus time (days) along ordinate for a stationary box (5^{o}N to 80^{o}N and 260^{o}E to 160^{o}E) in the mid-latitude Northern Hemisphere flow for (a) 30 mb, (b) 150 mb, (c) 700 mb, and (d) 925 mb.

the blocking (a mainly meridional circulation pattern) is more stable than the more frequent zonal flow.

The calculation for the IRE was also performed by taking into account the effects of synoptic-scale eddies. The result for 500 mb at 1200 UTC is displayed in Fig. 3.13. At mid tropospheric level, the synoptic-scale IRE does not exhibit a clear trend in any of the three stages of blocking. The only trend that is obvious is that just after the onset (after day 5), the IRE attains a relatively lower value, thus characterizing the relative stability of the flow at synoptic-scale.

The result of the stratified calculation of the synoptic-scale IRE is displayed in Fig. 3.14. From the Fig., we note a clearer trend that the migratory synoptic-scale eddies become relatively unstable towards the end of mature stage of the blocking leading to decay.

To access the utility and robustness of the Dymnikov et al. (1992) conjecture, we have calculated numerically two other indicators of flow regime change. These are the maximum of absolute value of stream function ($\max|\nabla\psi|$) and the maximum of absolute value of absolute vorticity ($\max|\nabla\Omega_a|$) of the flow. The two stability indicators are displayed in Fig. 3.15 for planetary-scale geopotential height. First, we calculated the gradient of the stream function (see Appendix A) and of the absolute vorticity over the blocking area and then we evaluated the maximum value of it numerically. More details of this calculation are given in the Southern Hemisphere blocking case study. The behaviors of both the indicators have simple physical meaning. Because of the presence of meridional variations in the stream function, it acquires a relative maximum

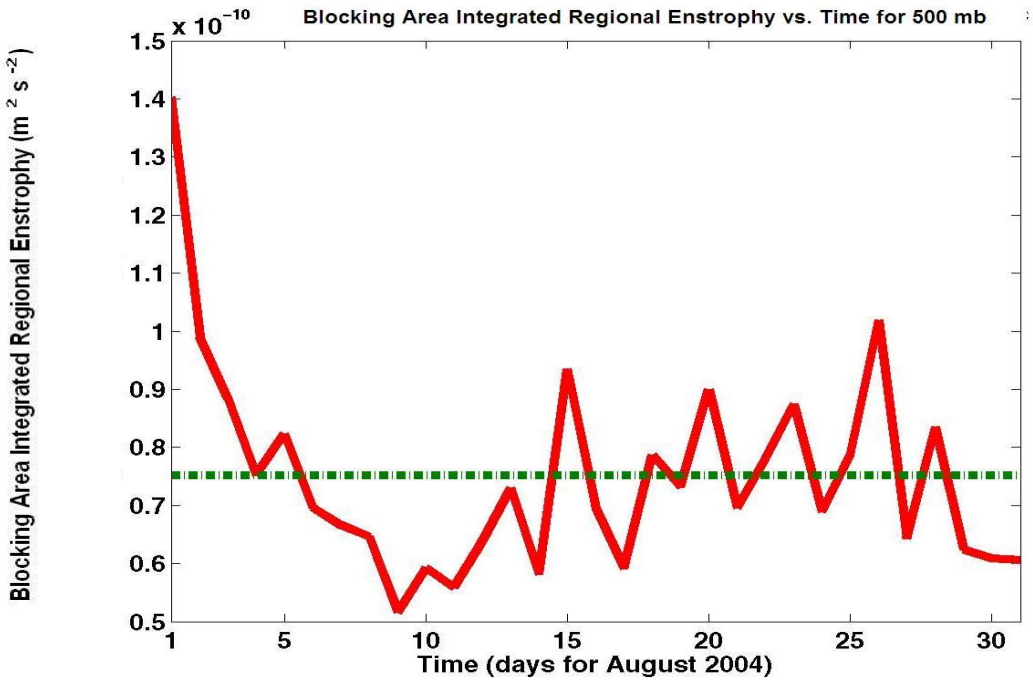

Fig. 3.13. A calculation of 500 mb blocking area averaged synoptic-scale IRE using Eq. (1.1) for the blocking event displayed in Fig. 3.6 which occurred during 05–28 August 2004. The relative stability level changes at onset (02–05 August) stage. The horizontal line defines the monthly mean reference value.

value during the blocking state and thus is akin to the time variability of BI displayed in Fig. 3.6 and the mean planetary-scale wavelength displayed in Fig. 3.7. For the second indicator, let us note that here we have made use of the observed vorticity instead of using Eq. (1.1) which defines the reduced relative vorticity only. The calculation for

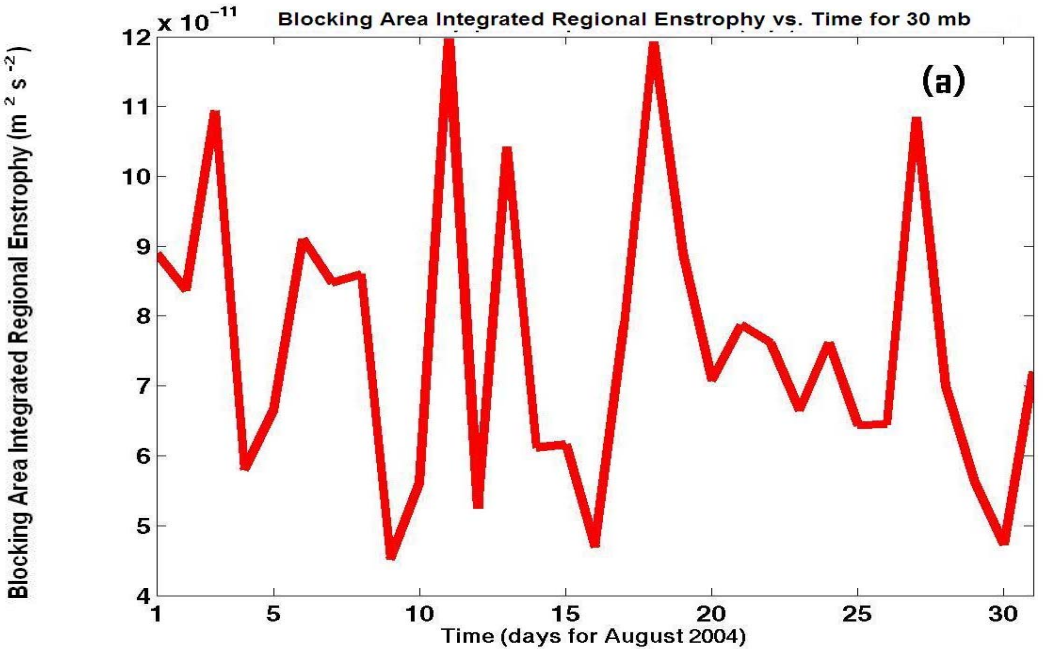
Blocking Area Integrated Regional Enstrophy vs. Time for 30 mb
x 10^-11
(a)
Blocking Area Integrated Regional Enstrophy (m^2 s^-2)
Time (days for August 2004)

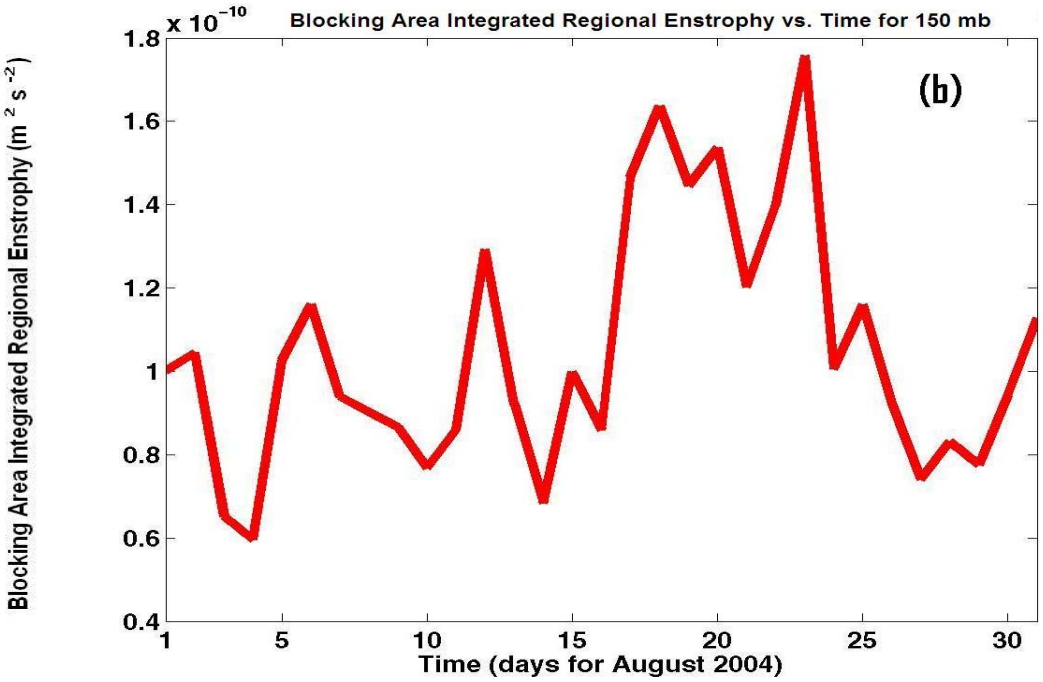
Blocking Area Integrated Regional Enstrophy vs. Time for 150 mb
x 10^-10
(b)
Blocking Area Integrated Regional Enstrophy (m^2 s^-2)
Time (days for August 2004)

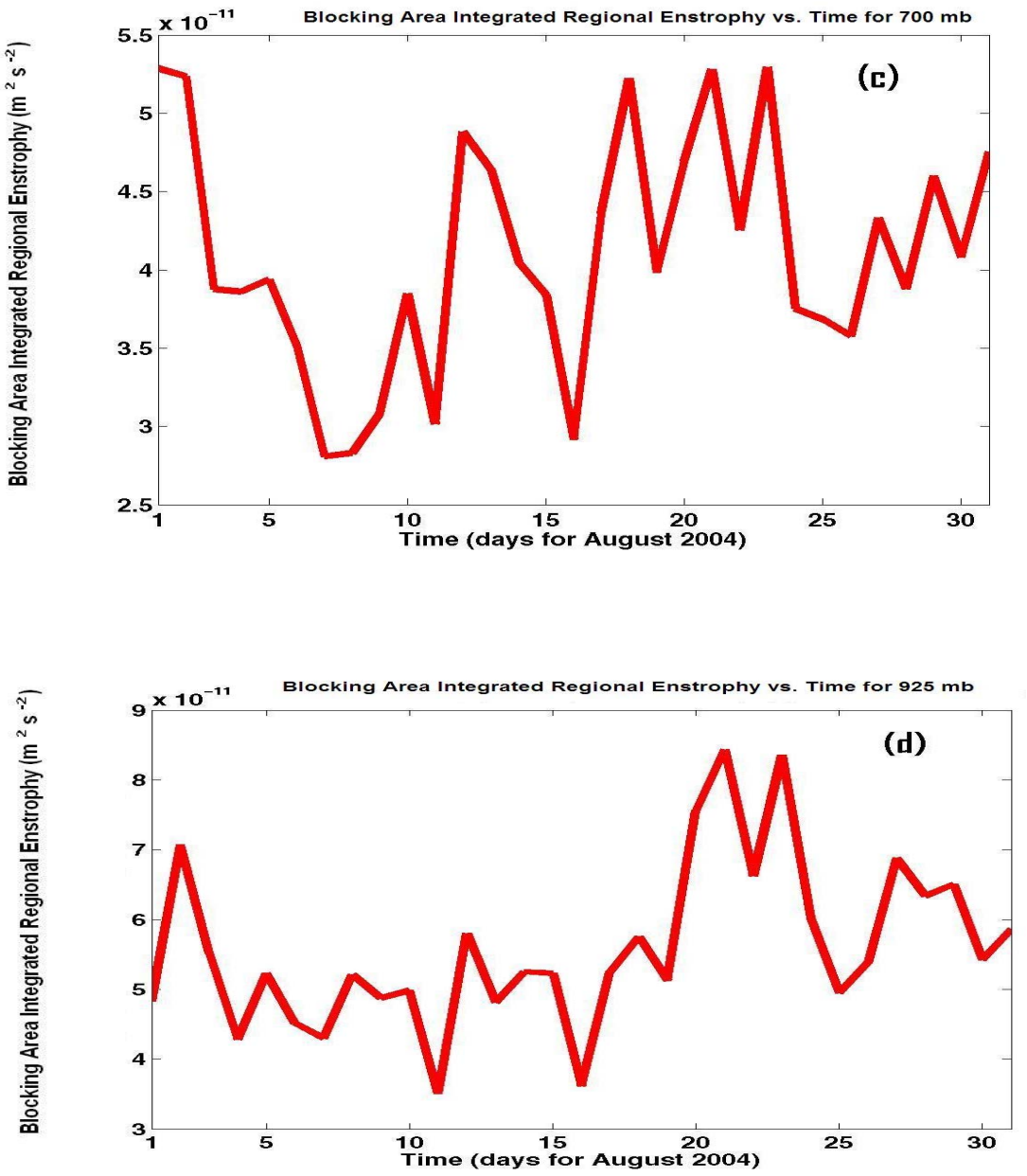

Fig. 3.14. A diagram of 1200 UTC mean synoptic-scale geopotential height scale IRE along abscissa versus time (days) along ordinate for a stationary box (5^{o}N to 80^{o}N and 260^{o}E to 160^{o}E) in the mid-latitude Northern Hemisphere flow for (a) 30 mb, (b) 150 mb, (c) 700 mb, and (d) 925 mb.

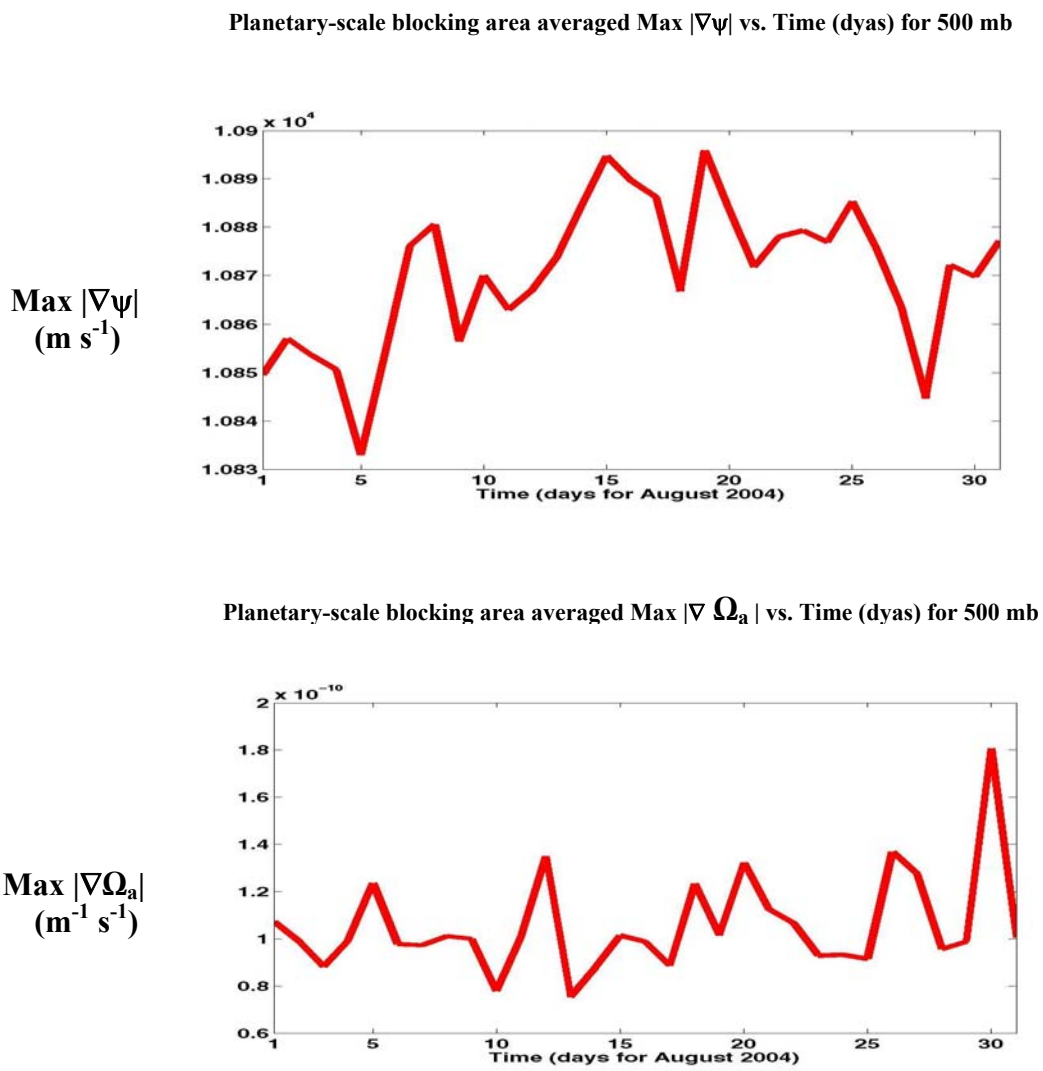

Fig. 3.15. Upper panel: A diagram of the 500 mb area averaged planetary-scale max |∇ψ| along abscissa versus time (days) along ordinate for a stationary box (5°N to 80°N and 260°E to 160°E) in the mid-latitude Northern Hemispheric flow. Mean planetary-scale geopotential height data is used here for 1200 UTC. Lower Panel: A calculation of the area averaged max |∇Ωa| for the entire life cycle of the blocking event displayed in the upper panel which occurred during 5–28 August 2004.

both the flow change indicators is carried out at 500 mb using the planetary-scale geopotential height. Following Skiba (2002), it may be concluded that if either the max|$\nabla\psi$| or max|$\nabla\Omega_a$| depicts relative changes, then the flow is becoming increasingly unstable. Thus increase/decrease in gradients of both ψ and Ω_a indicate change in the stability of the atmospheric regimes. Here ψ is the stream function of the flow and Ω_a is the absolute vorticity of the flow. An examination of Fig. 3.7 provides additional support for the observation that the changes in the planetary-scale flow leads to instability of the zonal flow. Thus, the two simple indicators mentioned above tend to mimic and follow the regime changes in the flow (from zonal to non zonal and vice versa) and may have some value as indictors of flow stability.

Fig. 3.16 is similar to Fig. 3.15 except that now we make use of the synoptic-scale eddy height to calculate the same two quantities. The appearance of the relative sharp rise during the decay stage is consistently explainable in our picture of the relative role of the two scales. The planetary-scale flow is more stable during the blocking; the synoptic-scale ridge formation destabilizes it thus causing the flow to revert back to the zonal configuration.

During the blocking events, this implies that once the blocking event established itself, the planetary-scale flow is relatively more predictable. The IRE give a relative change only and is thus alone not sufficient to identify the blocking event unambiguously. The fluctuating behavior of the IRE is a commonly occurring phenomenon in nonlinear systems (Lorenz 1963; Legras and Ghil 1985).

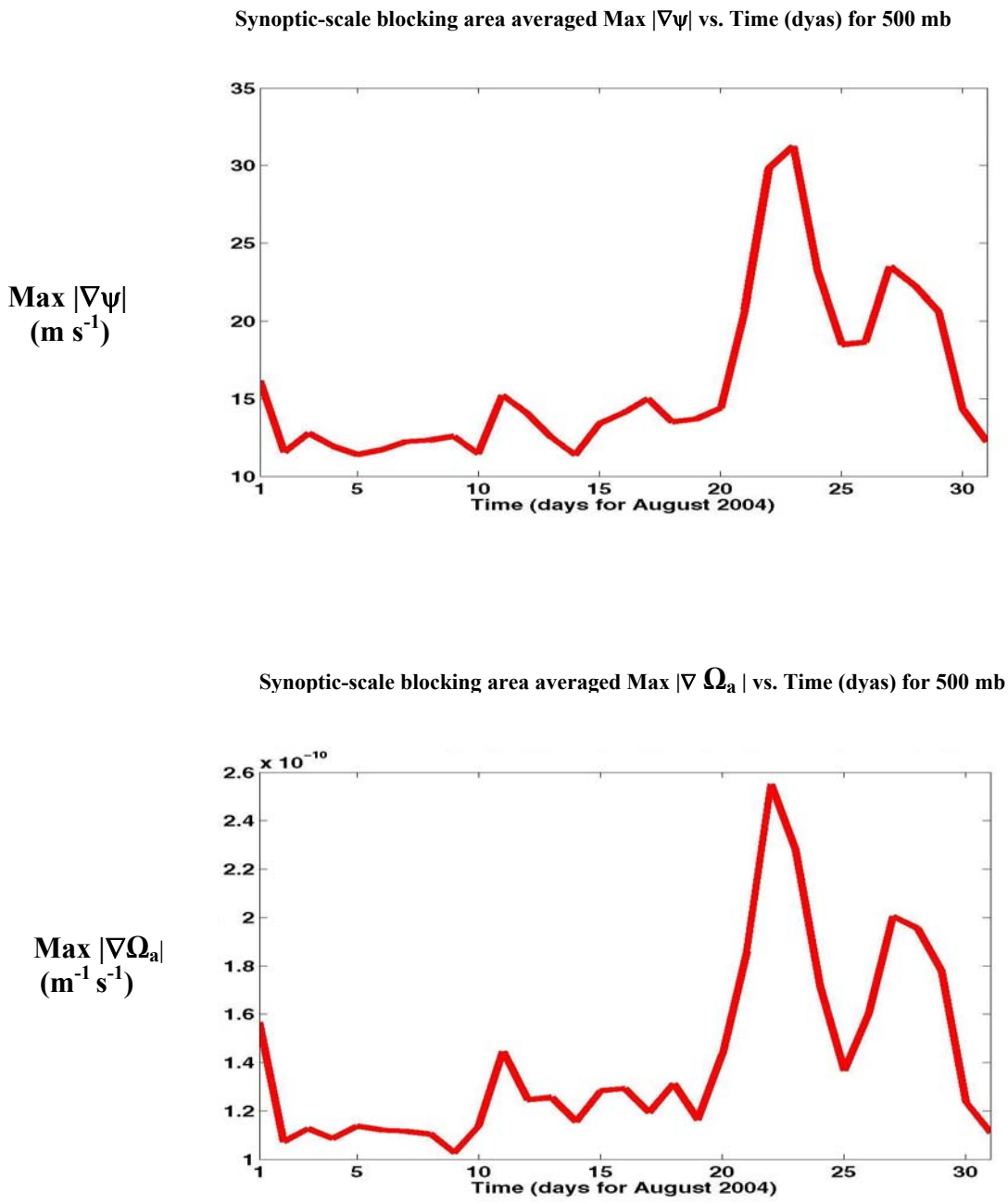

Fig. 3.16. Same as Fig. 3.15 except that now synoptic-scale eddy effect is taken into account.

Another interesting observation is that a comparison of the time variability of the positive height anomaly and the IRE for the entire life cycle of the blocking event under discussion indicates a relationship between the two as a function of pressure. The relationship is that the dominating wavelength scale stabilizes the blocking flow. A comparison of Fig. 3.7 with Fig. 3.11 reveals this relationship at 500 mb. When stratified over the troposphere, this relation holds for all mandatory levels between 30 mb and 925 mb for the entire duration of the chosen blocking event further justifying the usefulness of the IRE as a simple diagnostic tool. Deep midlatitude NH blocking anticyclones extending from upper to lower troposphere may thus be diagnosed for their stability characteristics in terms of the IRE under the assumption of barotropic and quasi-geostrophic atmospheric flow.

3.4 Discussion

Changes in the nature of the planetary-scale flow can be related with the block onset and decay supporting the general implications of the work of Tsou and Smith (1990), Haines and Holland (1998), Colucci and Baumhefner (1998), and that the planetary-scale provides an important contribution to the blocking life cycles by providing a favorable environment for the blocking event to occur, in spite of the large contributions by the synoptic-scale flow and interaction components of the forcing.

Additionally, supporting evidence for the change in planetary-scale flow regimes comes from examining the IRE (flow stability) calculations. The area

integrated regional enstrophy values (Fig. 3.11) fall to a minimum during the life cycle of the block in the blocked region in agreement with what would be expected for the selected blocking event (with planetary-scale dominance) implying that the planetary-scale flow became unstable around the time of block onset and decay. This observation was confirmed by studying all the blocking events over the 3 year period (2002–2004) for NH (for details, see Athar et al. 2007a, b).

It is possible that the planetary-scale flow at these two times moved from one (geostrophically) stable state to another, and the corresponding behavior of the other metrics shown in Fig. 3.15 and Fig. 3.16 corroborate this interpretation. Thus, the methodologies applied here, may have at least some value as a diagnostic tool for atmospheric phenomenon. It may be so because the diagnostic tools used here seems to be reliable indicators for the flow regime changes during blocking onset/decay (see Chapter 5 for comparison with the earlier work done on this blocking event) . They may even have some value as a metric for predictability; however, more study is needed in order to adequately demonstrate such value.

Earlier studies have used statistics to make a similar point (Lejenäs and Øakland 1983). Let us further remark that the blocking decay can occur when there is no longer active synoptic-scale support for the events, when the synoptic-scale impacts negatively on the blocking events, or when the planetary-scale flow regime changes character.

CHAPTER 4

CASE STUDY II: SOUTHERN HEMISPHERE

In this chapter, we present details of scale and the stability analysis of a selected blocking event in the Southern Hemisphere. All three stages of the blocking event will be analyzed.

The aim of this case study is to make an attempt to better understand the mechanisms operative in block formation in Southern Hemisphere in terms of stability indicators. Blocking area integrated regional enstrophy and maximum of absolute value of the stream function are used to quantify the stability of the zonal barotropic flow. In this context, a case study of a blocking event is performed which was studied earlier to suggest the competition between two mechanisms, namely the advection of the meridional gradient of PV and interaction between flow deformation and the PV, as a

cause of blocking onset (Dong and Colucci 2005, 2007). We use a different set of tools to analyze the entire life cycle of the blocking event that occurred in Southeastern Pacific Ocean in late July 1999 to extend and confirm the findings in the above study. We point out that the 500 mb synoptic-scale ridge formation initiated the onset by destabilizing the planetary-scale flow harboring the blocking event. The stability analysis is then extended to include all the mandatory pressure levels. The tropospheric stratified relative role of synoptic-scale and planetary-scale wavelengths for the block formation, the maintenance, and the decay is elaborated in terms of stability indicators.

In line with brief discussion in Chapter 1, we adopt the point of view that atmospheric blocking should be thought of as a stable atmospheric circulation whose state is best analyzed by its stability characteristics. In this context, we use the Dymnikov et al. (1992) conjecture which states that the sum of *positive* eigenvalues λ of the linearization operator may quantify the stability of the flow via the block area integrated regional enstrophy, i.e.,

$$\sum_i \lambda_i^+ \approx \int_D |\Omega|^2 (y) dxdy, \tag{4.1}$$

where $\Omega = -\partial u / \partial y$ and D is the blocking domain. Higher positive values correspond to more unstable flow and vice versa. Thus, the time variability of Eq. (4.1) that represents the blocking area integrated (reduced) enstrophy may be used to quantify the relative stability of the barotropic flow. We regard this as a stability indicator in our analysis.

4.1 Synoptic Analysis

The blocking event selected for the case study occurred over Southeastern Pacific Ocean during 24 July through 31 July 1999 with onset during 24–25 July and decay during 30–31 July. The blocking event lasted for 7 days. The blocking onset region was located between 60°S to 40°S and 165.5°E to 147.5°W. This is event number 5 in Table 2.3a and Table 2.5a in Chapter 2.

Climatologically, this is the fourth longest duration blocking event that occurred in the winter season of SH year 1999 (Jan.– Dec.) out of a total of 9 events which lasted for 5 days or more (see Table 2.3a). All blocking events occurred over Pacific Ocean region (130°E to 70°W). Their Blocking Intensity (BI) ranged from 1.73 to 3.47. No blocking event was detected in the month of July and August in the blocking region (165.5°E to 147.5°W) under study other than the one studied here.

Figure 4.1a displays the Southern Hemispheric flow at 500 mb on 24 July 1999. This is the onset stage of the selected blocking event. Fig. 4.1b displays the blocking pattern in the Southeastern Pacific only. The appearance of inverted omega shaped flow is clearly noticeable in Fig. 4.1 (a and b) at the onset stage.

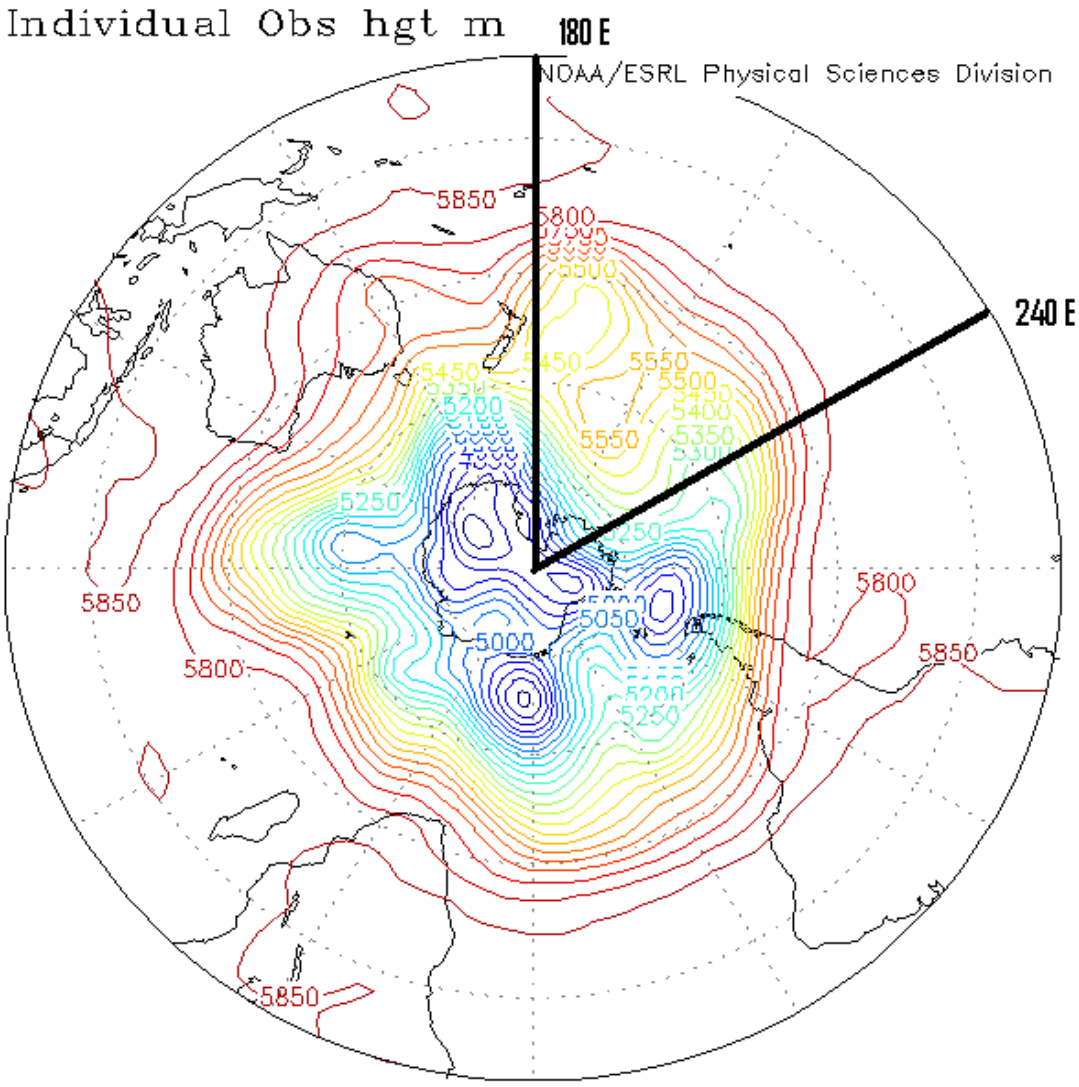

Fig. 4.1a. 500 mb Southern Hemisphere flow for 1200 UTC 24 July 1999. The onset of blocking can be seen inside 180^{o} and 240^{o}E as an inverted omega shape. The contour interval is 50 m. The maximum geopotential height is 5893 m, whereas the minimum geopotential height is 4721 m (obtained from http://www.cdc.noaa.gov).

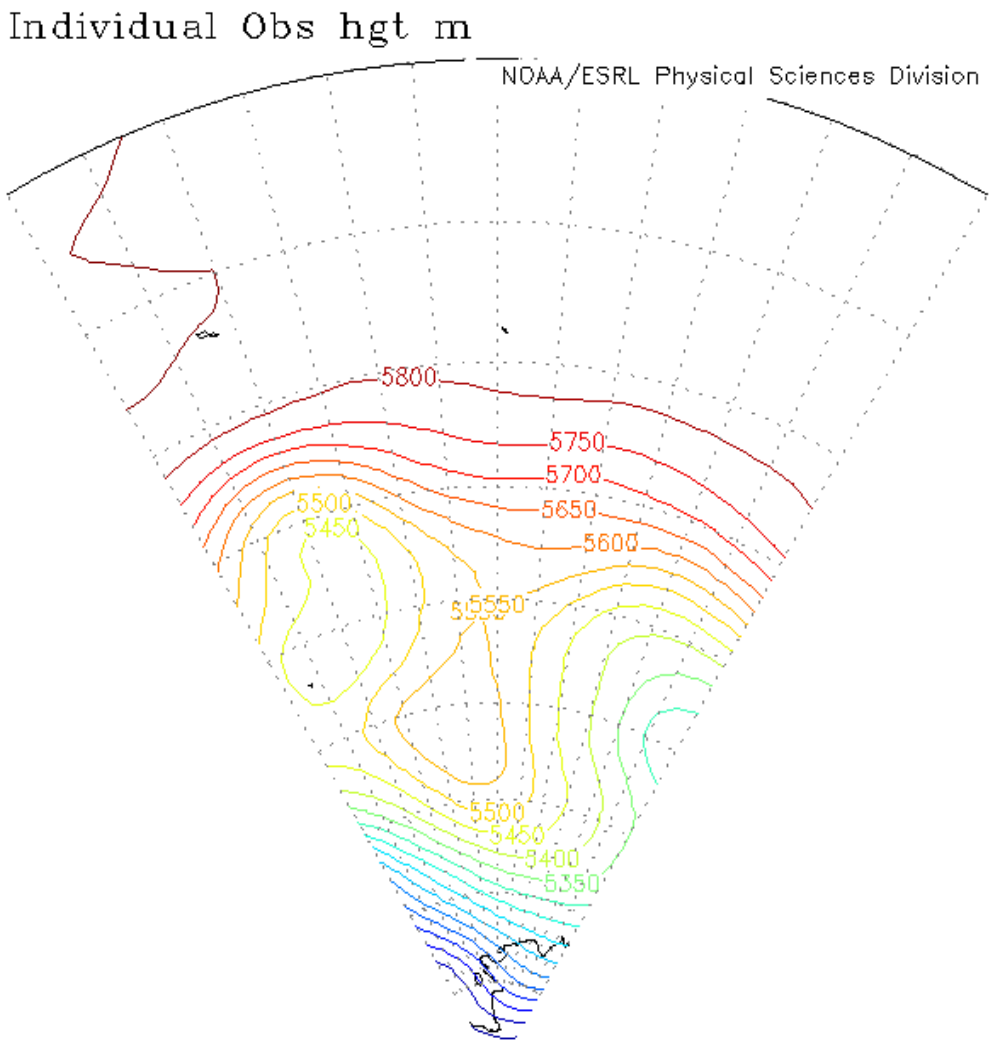

Fig. 4.1b. 500 mb Southern Hemisphere flow between 180^{o} and 240^{o}E for 1200 UTC 24 July 1999. At the onset of the blocking, the flow has as an inverted omega shape. The contour interval is 50 m. The maximum geopotential height is 5858 m, whereas the minimum geopotential height is 4809 m (obtained from http://www.cdc.noaa.gov).

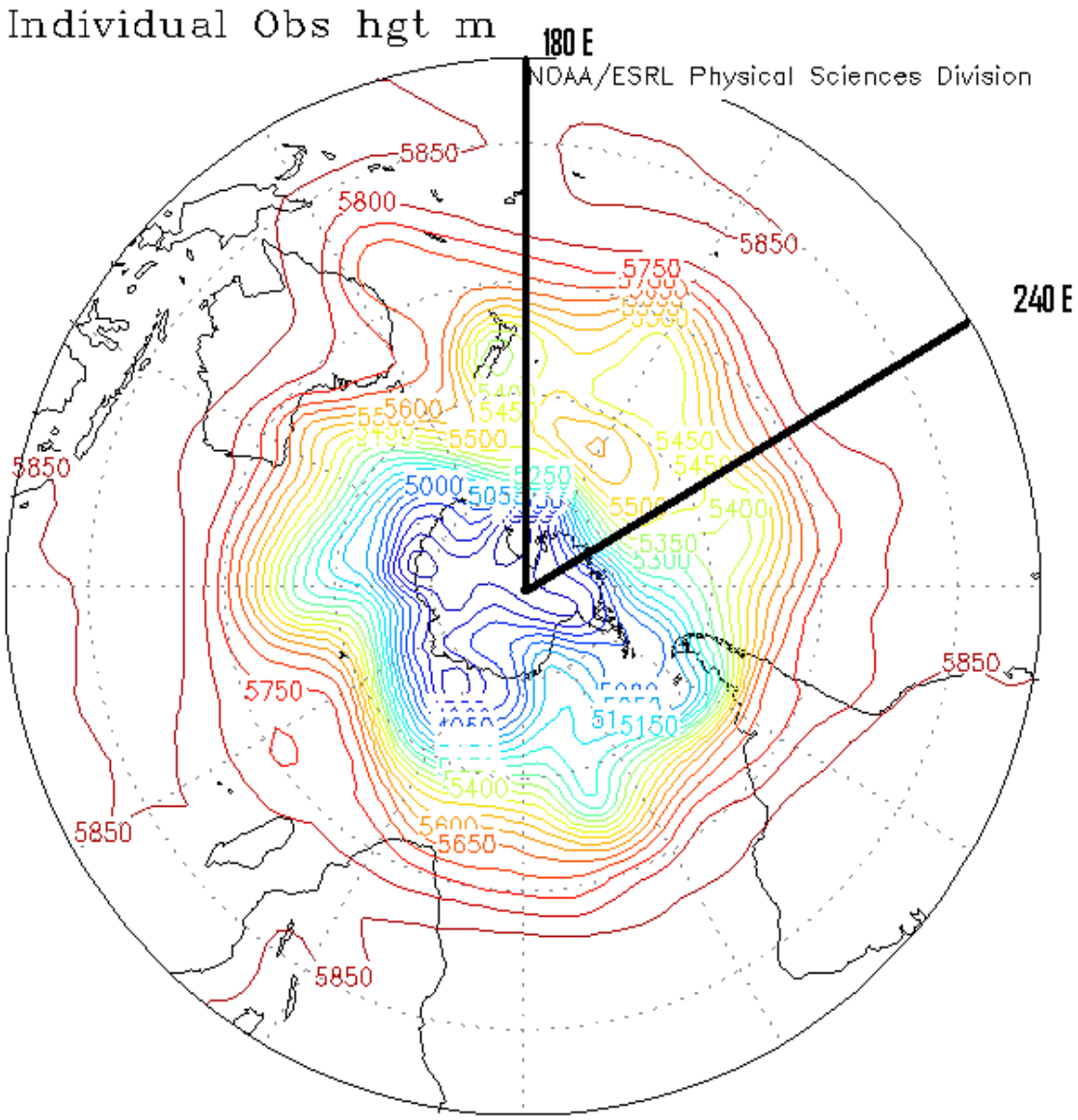

Fig. 4.2a. Same as Fig. 4.1a except for 500 mb Southern Hemisphere flow for 1200 UTC 26 July 1999. The mature stage of the blocking is marked by the formation of a dipole. The contour interval is 50 m. The maximum geopotential height is 5899 m, whereas the minimum geopotential height is 4710 m.

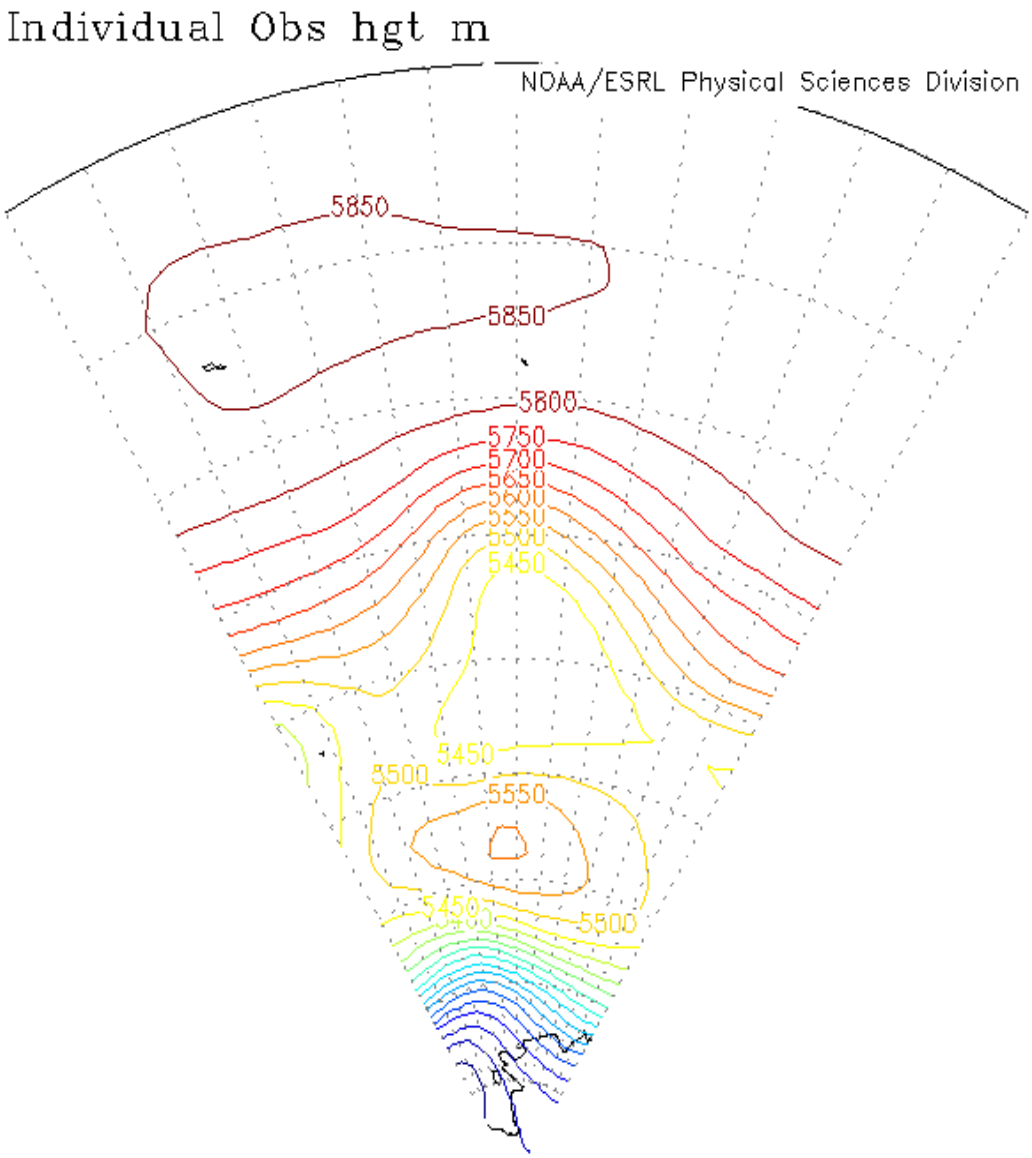

Fig. 4.2b. Same as Fig. 4.1b except for 500 mb Southern Hemisphere flow between 180^{o} and 240^{o}E for 1200 UTC 26 July 1999. In the mature stage of the blocking, the flow develops a dipole structure. The contour interval is 50 m. The maximum geopotential height is 5862 m, whereas the minimum geopotential height is 4725 m.

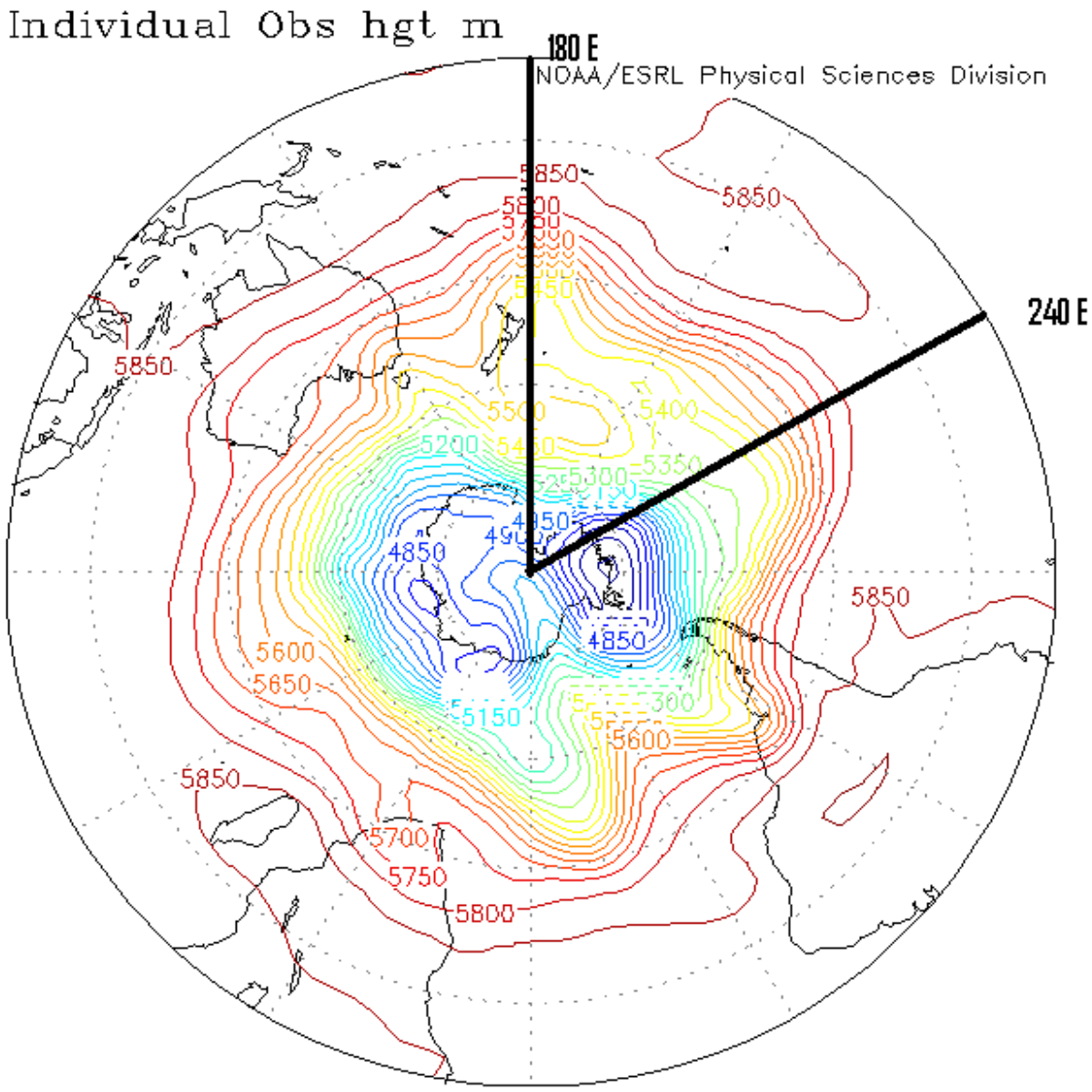

Fig. 4.3a. Same as Fig. 4.1a except for 500 mb Southern Hemisphere flow for 1200 UTC 30 July 1999. The decay stage of the blocking resulted in the dissolving of the dipole structure. The contour interval is 50 m. The maximum geopotential height is 5904 m, whereas the minimum geopotential height is 4641 m.

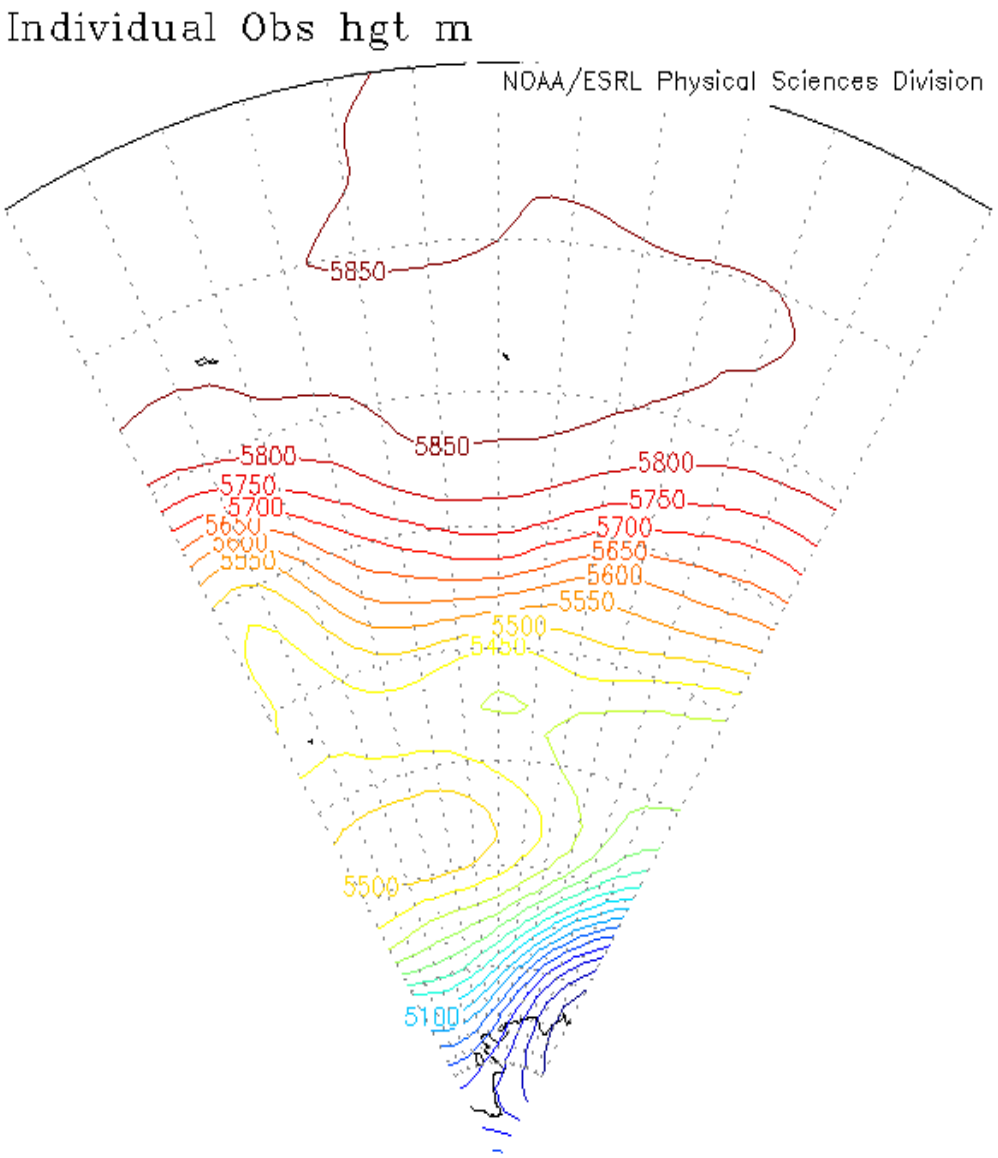

Fig. 4.3b. Same as Fig. 4.1b except for 500 mb Southern Hemisphere flow between 180^{o} and 240^{o}E for 1200 UTC 30 July 1999. At the decay stage of the blocking, the dipole structure disappears. The contour interval is 50 m. The maximum geopotential height is 5873 m, whereas the minimum geopotential height is 4720 m.

Figure 4.2a displays the Southern Hemispheric flow at 500 mb on 26 July 1999. This is the mature stage of the chosen blocking event. Fig. 4.2b displays the blocking pattern in the Southeastern Pacific only. The appearance of commonly occurring dipole shaped flow is clearly noticeable in Fig. 4.2 during the mature stage.

Figure 4.3a displays the Southern Hemispheric flow at 500 mb on 30 July 1999. This is the decay stage of the chosen blocking event. Fig. 4.3b displays the blocking pattern in the Southeastern Pacific only. The disappearance of the dipole shaped flow marked the decay stage.

Figure 4.4 displays the Blocking Intensity (BI) calculated using the Wiedenmann et al. (2002) criterion for the entire duration of the blocking event. Note the presence of sharp rise in the BI value during peak activity stage of the blocking event in Fig. 4.4. The BI gives the combined effect of planetary-scale and synoptic-scale wavelengths towards the entire life cycle of the blocking. The BI averaged over the entire life cycle of the blocking event was found to be 2.70. Since, the BI falls within the range: $2.0 < BI < 4.3$, so it corresponds to a moderate intensity blocking event (for further details, see Wiedenmann et al. 2002).

In what follows, we study the relative role of the planetary- and synoptic-scale wavelengths in initiating a transition from mainly zonal to meridional flow and vice versa by first filtering the planetary-scale wavelength contribution from observed Z, then separating the synoptic-scale contribution (using Eq. (1.2)) and then comparing the two with the BI profile given by Fig. 4.4. In this context, we perform a case study of

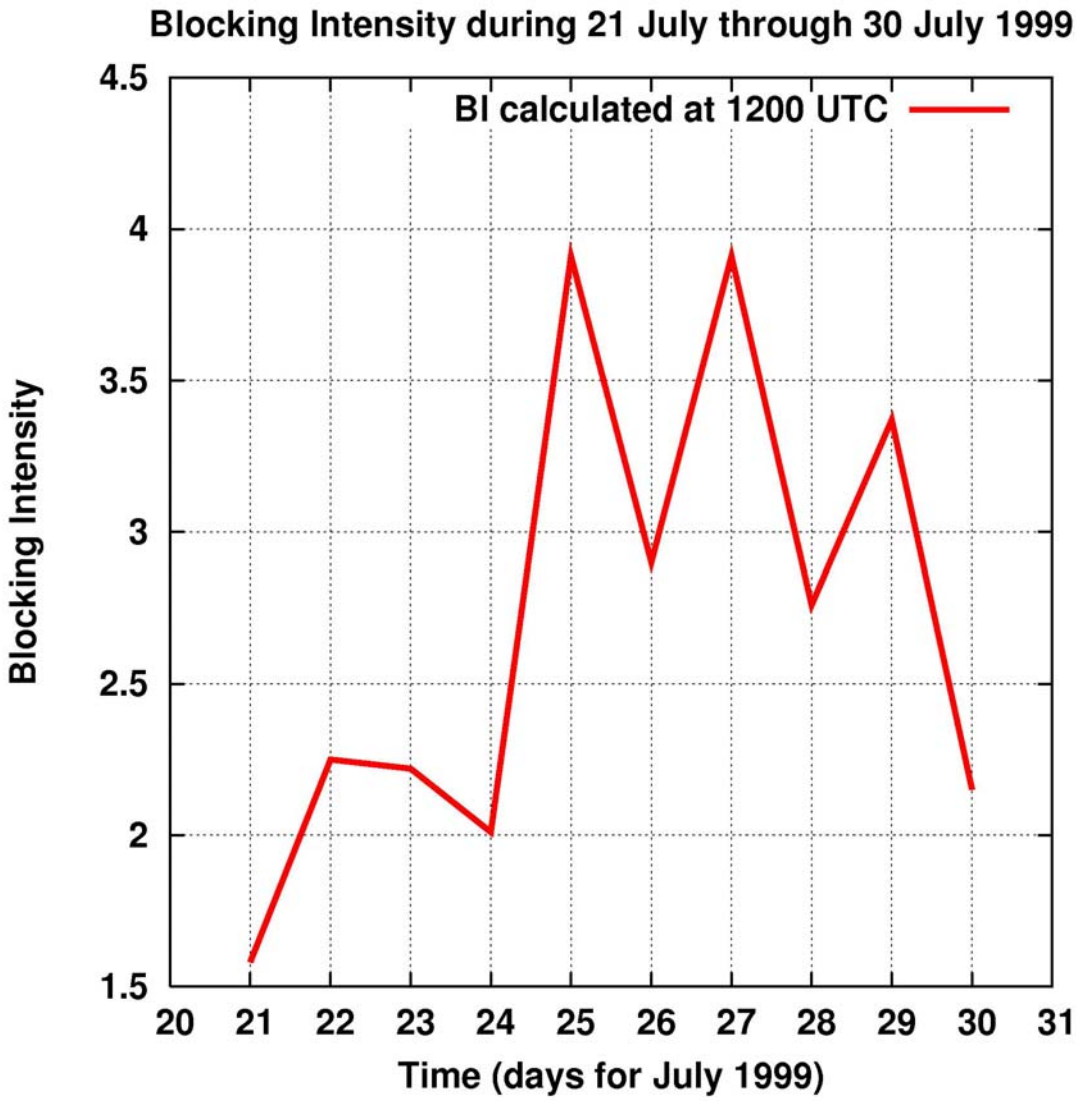

Fig. 4.4. The daily BI calculated at 1200 UTC for the entire life cycle (24–30 July 1999) of the blocking event. The oscillatory behavior peaks during the maximum activity stage of the blocking (25–27 July 1999). The BI calculation is shown up to 3 days prior to the blocking onset.

an isolated Southern Hemisphere blocking event that occurred in Pacific Ocean in late July 1999 as mentioned earlier. To our knowledge, this type of detailed relative stability analysis of a SH blocking event has not been performed earlier.

We choose the blocking event that has also been studied by Dong and Colucci (2005, 2007). There, the emphasis was to present a scenario in which two opposing mechanisms lead to the onset of blocking. Our intention is to find the *corresponding* stability signatures not only for the onset but also for the mature stage and the decay stage as well. The formation of an instability/locally diffluent flow initiates the onset of the blocking and later during the mature stage of the blocking leads to the formation of the anti cyclonic vortex and eventually leads to decay. We thus study the stability signatures in terms of stability indicators.

4.2 Scale Analysis

Figure 4.5 displays the blocking area averaged planetary-scale height (m) as a function of days for the month of July and August 1999 for 500 mb at 1200 UTC. A longer term evaluation of the 500 mb height is indicative of the flow pattern before, during and after the blocking. From the figure, we note that the planetary-scale geopotential height has a pronounced *relative minimum* that coincides with the blocking onset on 25 July. This trend continues during the early mature stage of the blocking and

then reverses itself during the later half of the blocking life cycle to accommodate the contribution from synoptic-scale wavelengths. The mean reference value of the planetary-scale geopotential height for the month of July and August lies at 5529 m, and is shown by the dash-dotted horizontal line. The median reference value of the planetary-scale geopotential height for the month of July and August lies at 5533 m (not shown). The mean monthly standard deviation was also calculated for the planetary-scale geopotential height and was found to be 71.2 m.

We have studied the role of the stratified mean planetary-scale geopotential heights over the entire troposphere and into the lower stratosphere. It is done by evaluating the blocking area averaged mean planetary-scale height for all the 17 mandatory levels (from 1000 mb to 10 mb). We have found that relatively lower heights persisted over the whole blocking region for the entire life cycle of the block indicating that this scale has not played a dominant role in blocking the zonal flow, at all isobaric levels. This observation can be clearly noticed by comparing Fig. 4.5 and Fig. 4.6. The trend of falling heights becomes more evident in the mid to lower troposphere (Fig. 4.6 (e)-(g)).

Figure 4.7 displays the blocking area averaged synoptic-scale eddy height (m) as a function of the days for the month of July and August 1999 at 500 mb. We have used our MATLAB code to isolate the synoptic-scale eddy height from the planetary-scale height and the observed geopotential height (see appendix A.1). Note, the area averaged synoptic-scale eddy height at 500 mb is defined as the difference between the observed

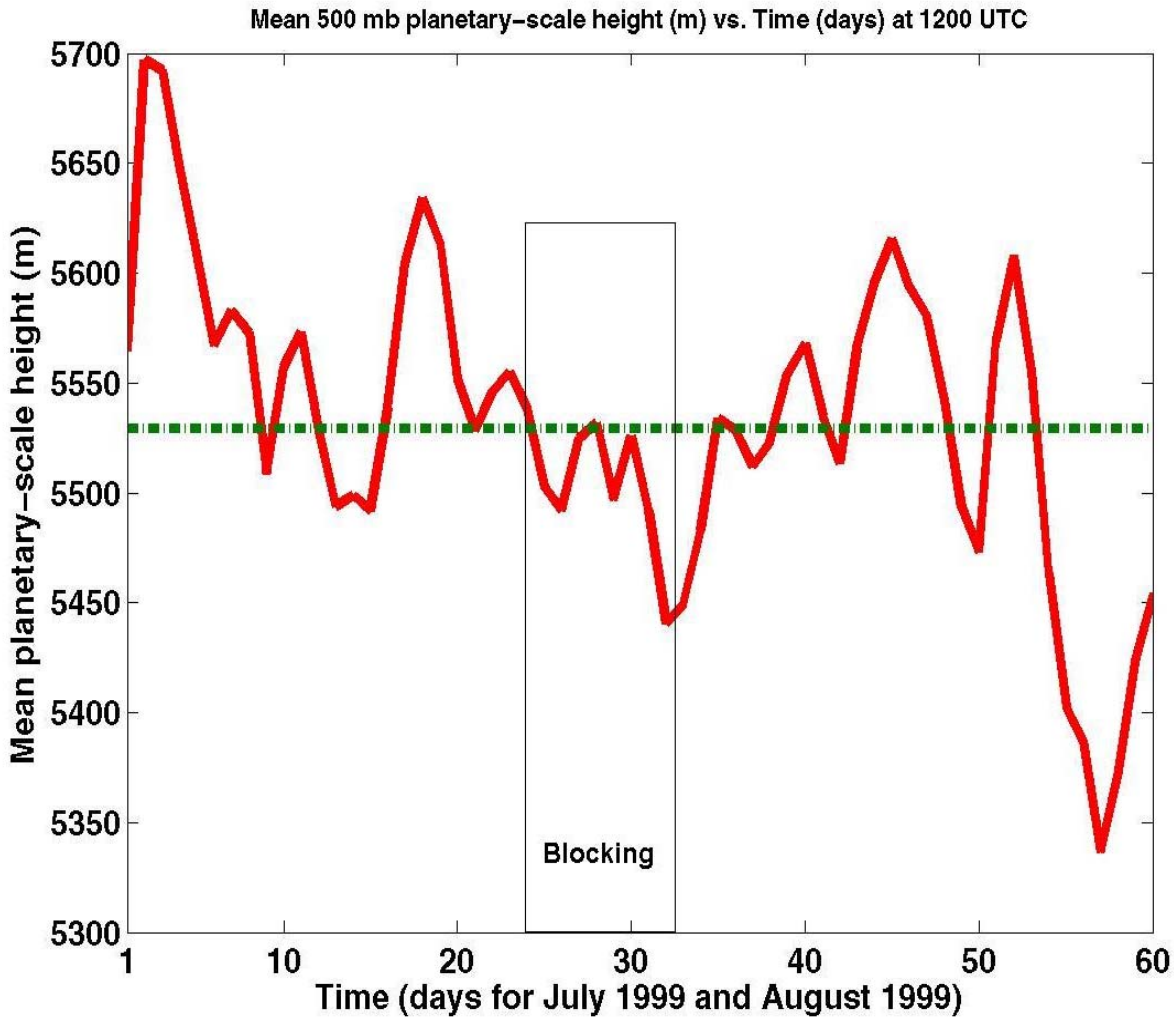

Fig. 4.5. A diagram of the mean planetary-scale 500 mb geopotential height (m) along abscissa versus time (days) along ordinate for a stationary box at 1200 UTC for July and August 1999 ($60^{o}S$ to $40^{o}S$ and $212.5^{o}E$ to $192.5^{o}E$) in the mid latitude Southern Hemisphere flow over Southeastern Pacific Ocean. The horizontal line defines the monthly mean reference value.

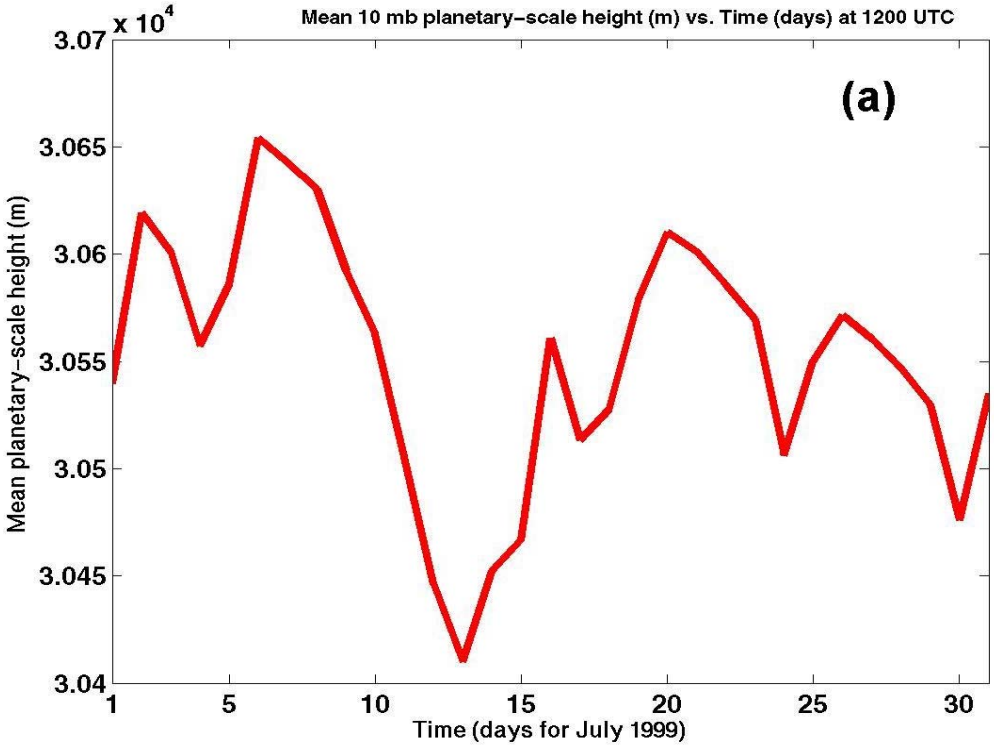
Mean 10 mb planetary–scale height (m) vs. Time (days) at 1200 UTC
x 10^4
(a)
Mean planetary–scale height (m)
3.07
3.065
3.06
3.055
3.05
3.045
3.04
1
5
10
15
20
25
30
Time (days for July 1999)

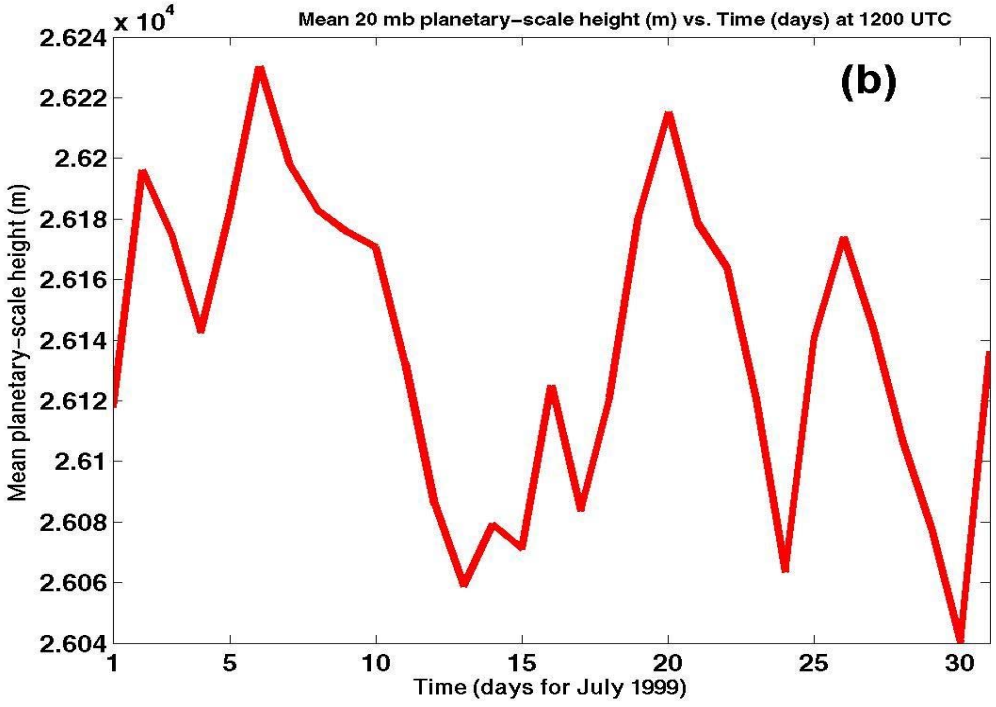
Mean 20 mb planetary–scale height (m) vs. Time (days) at 1200 UTC
x 10^4
(b)
Mean planetary–scale height (m)
2.624
2.622
2.62
2.618
2.616
2.614
2.612
2.61
2.608
2.606
2.604
1
5
10
15
20
25
30
Time (days for July 1999)

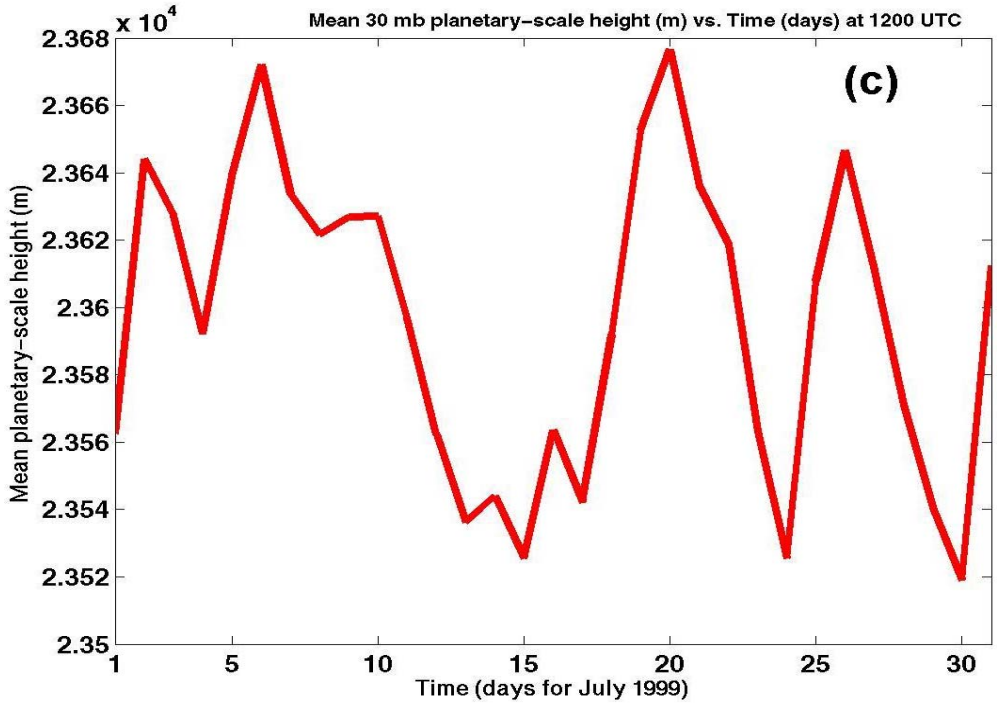
Mean 30 mb planetary–scale height (m) vs. Time (days) at 1200 UTC
x 10^4
(c)
Mean planetary–scale height (m)
2.368
2.366
2.364
2.362
2.36
2.358
2.356
2.354
2.352
2.35
1
5
10
15
20
25
30
Time (days for July 1999)

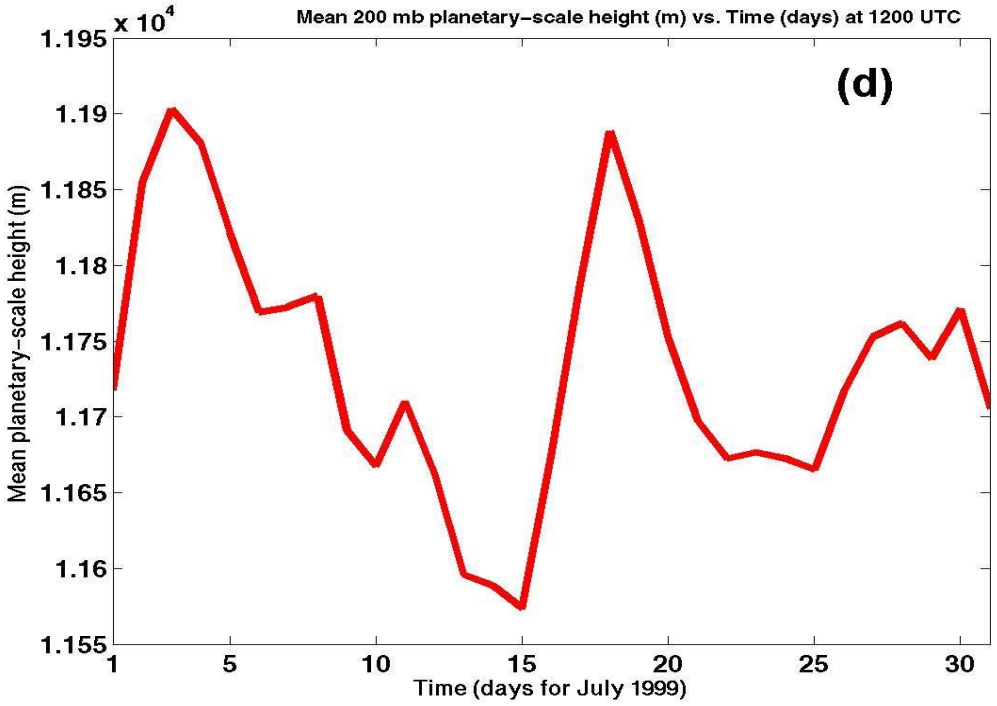
Mean 200 mb planetary–scale height (m) vs. Time (days) at 1200 UTC
x 10^4
(d)
Mean planetary–scale height (m)
1.195
1.19
1.185
1.18
1.175
1.17
1.165
1.16
1.155
1
5
10
15
20
25
30
Time (days for July 1999)

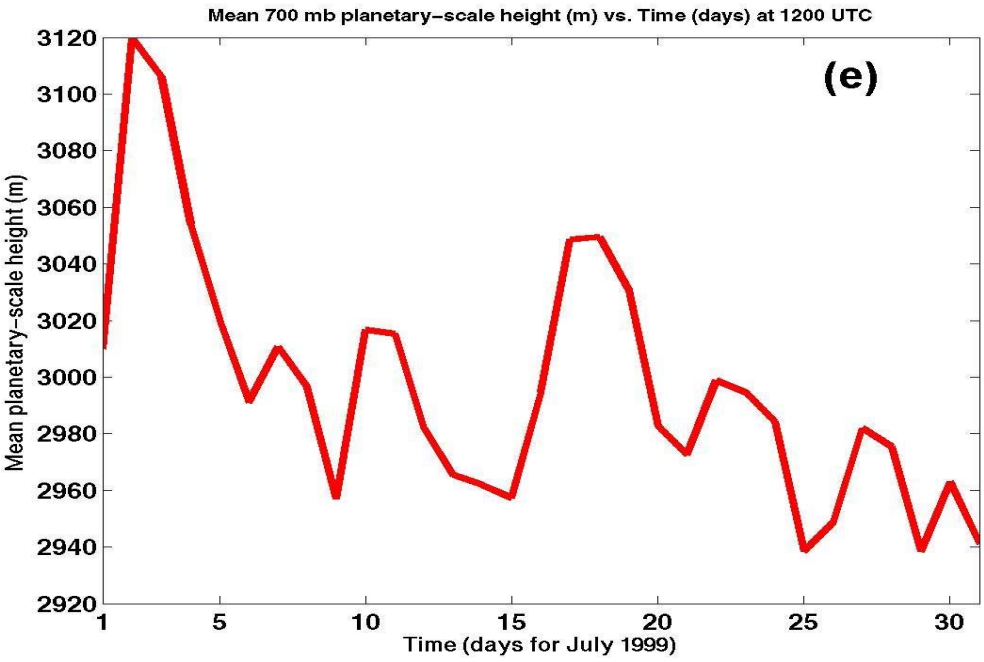
Mean 700 mb planetary–scale height (m) vs. Time (days) at 1200 UTC
(e)
Mean planetary–scale height (m)
3120
3100
3080
3060
3040
3020
3000
2980
2960
2940
2920
1
5
10
15
20
25
30
Time (days for July 1999)

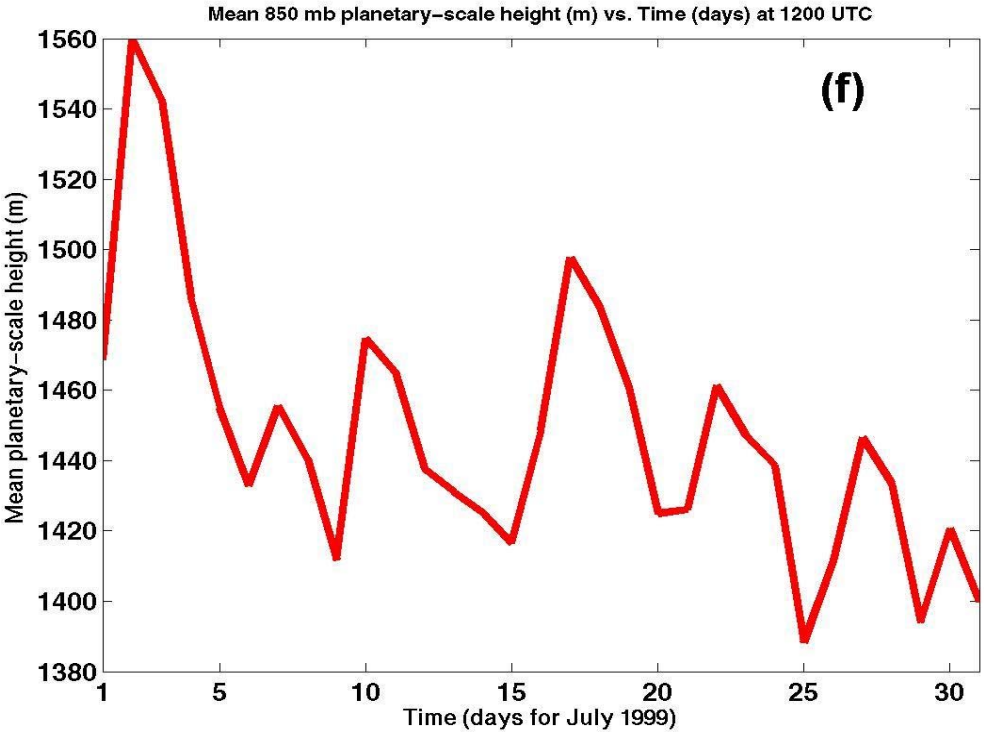
Mean 850 mb planetary–scale height (m) vs. Time (days) at 1200 UTC
(f)
Mean planetary–scale height (m)
1560
1540
1520
1500
1480
1460
1440
1420
1400
1380
1
5
10
15
20
25
30
Time (days for July 1999)

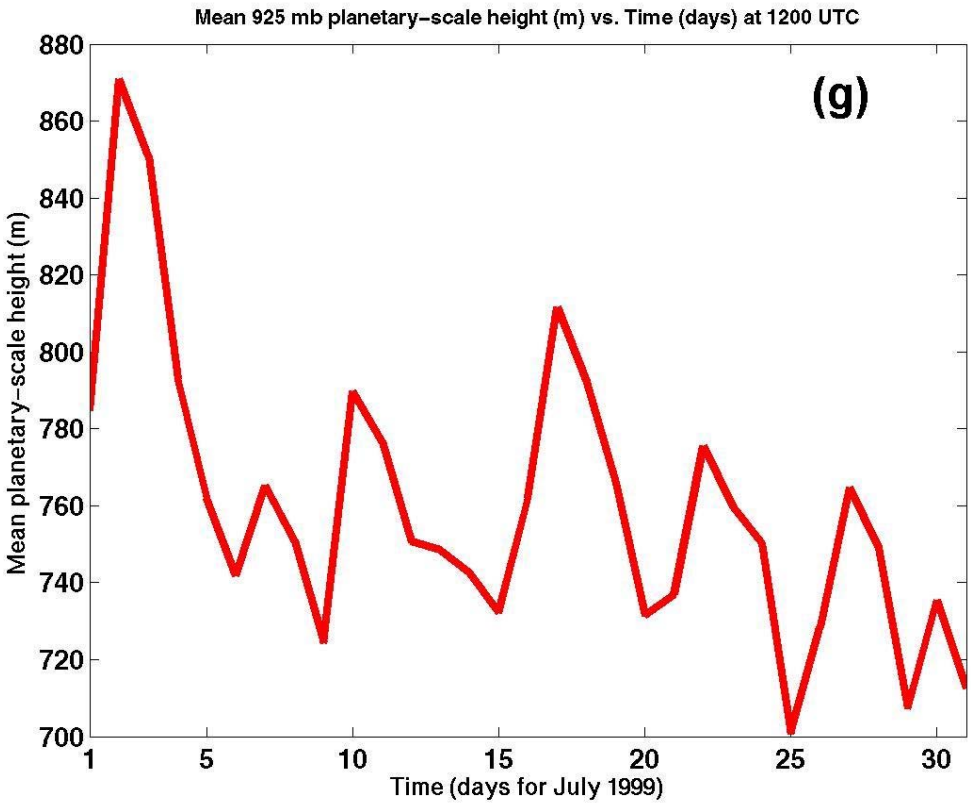

Fig. 4.6. The blocking area averaged planetary-scale geopotential height at 1200 UTC for the entire month of July 1999. (a) 10 mb, (b) 20 mb, (c) 30 mb, (d) 200 mb, (e) 700 mb, (f) 850 mb, and (g) 925 mb. Note the falling height trend throughout the plotted isobaric levels during the entire life cycle (24–30 July 1999) of the selected blocking event. The pressure at the tropopause was found to be ~ 250 mb when averaged over the life cycle of the blocking event. Thus, in the figure, diagrams (a)–(d) display the time variability of the mean planetary-scale geopotential height in the stratosphere, whereas the diagrams (e)–(g) display the same in the troposphere.

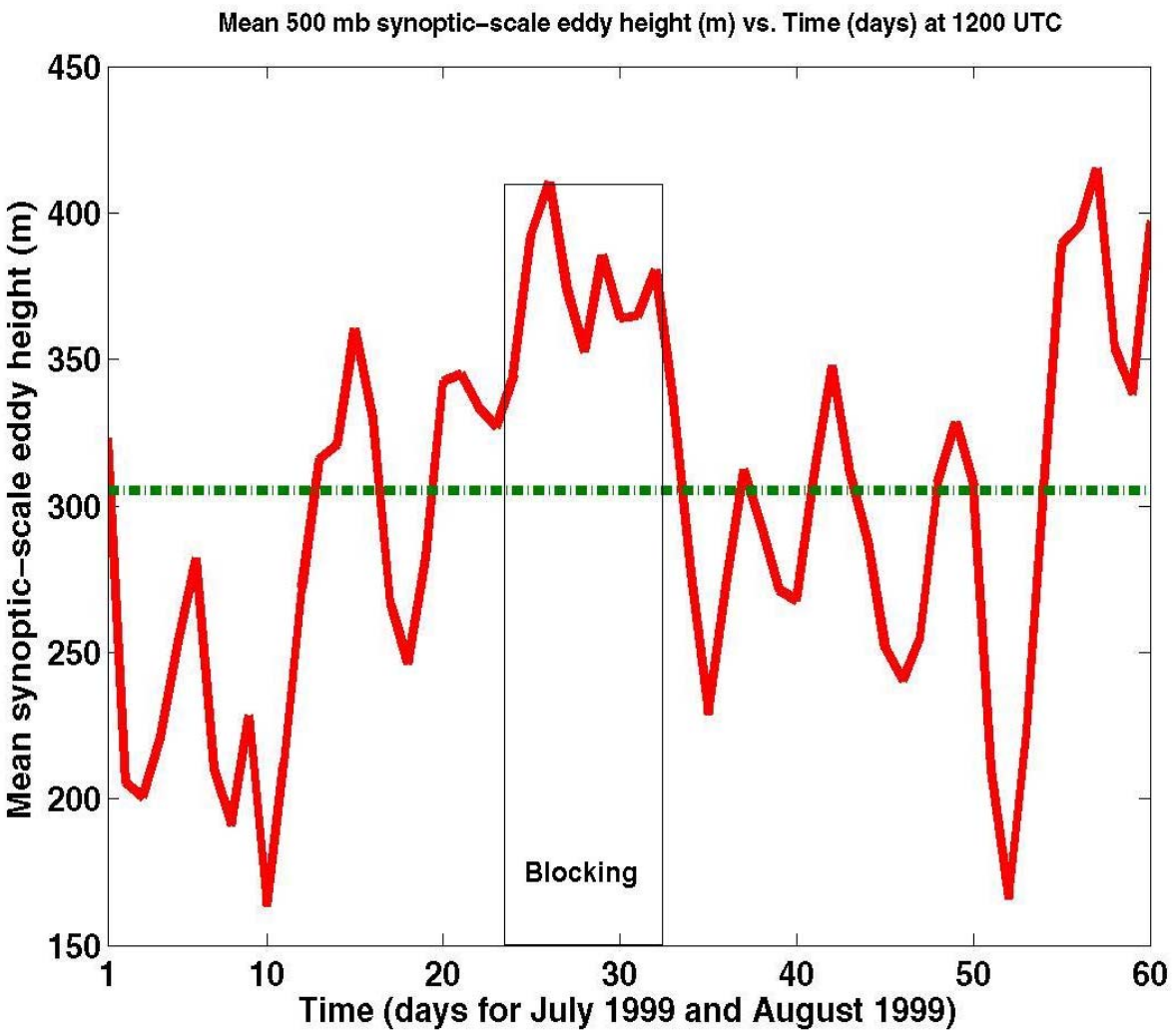

Fig. 4.7. A diagram of the mean 500 mb synoptic-scale geopotential eddy height (m) for 1200 UTC along abscissa versus time (days) along ordinate for a stationary box (60^oS to 40^oS and 212.5^oE to 192.5^oE) in the mid latitude Southern Hemisphere flow for the entire month of July and August 1999 over Southeastern Pacific Ocean. The horizontal line defines the monthly mean reference value.

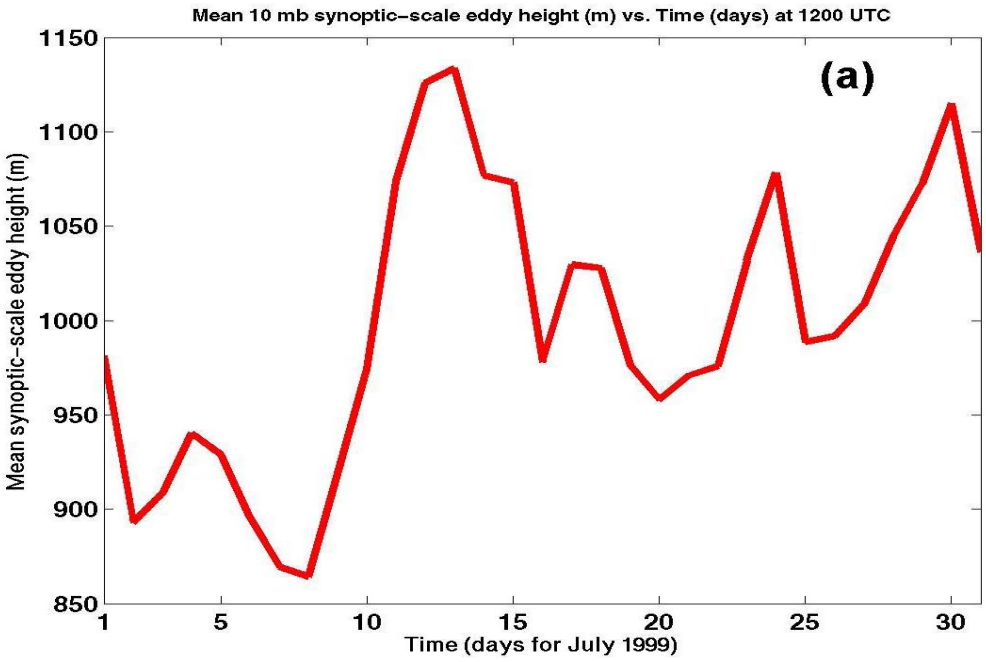
Mean 10 mb synoptic–scale eddy height (m) vs. Time (days) at 1200 UTC
(a)
Mean synoptic–scale eddy height (m)
1150
1100
1050
1000
950
900
850
1
5
10
15
20
25
30
Time (days for July 1999)

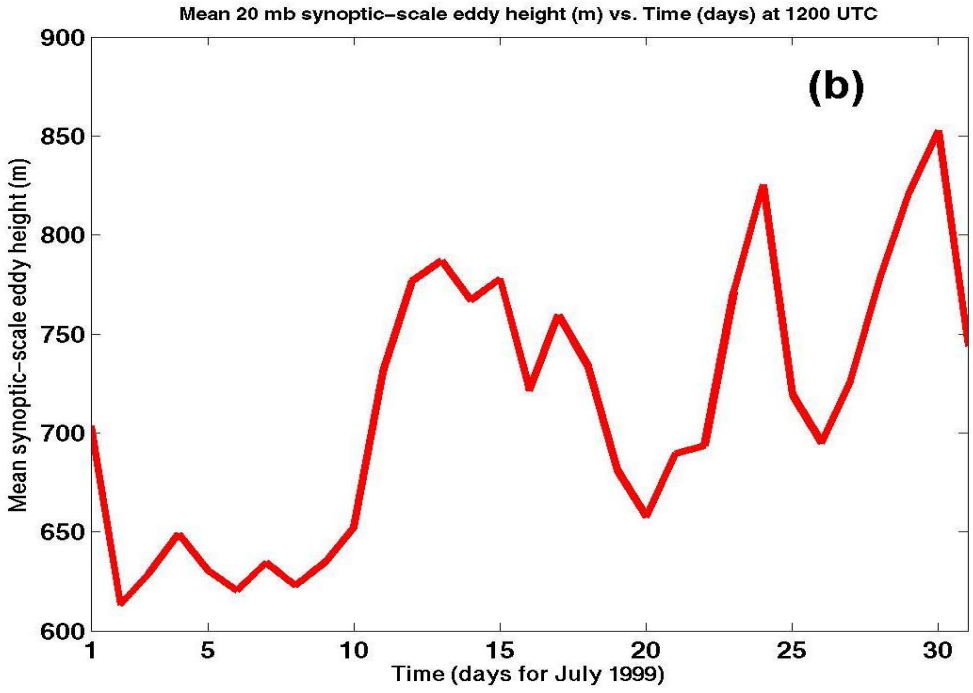
Mean 20 mb synoptic–scale eddy height (m) vs. Time (days) at 1200 UTC
(b)
Mean synoptic–scale eddy height (m)
900
850
800
750
700
650
600
1
5
10
15
20
25
30
Time (days for July 1999)

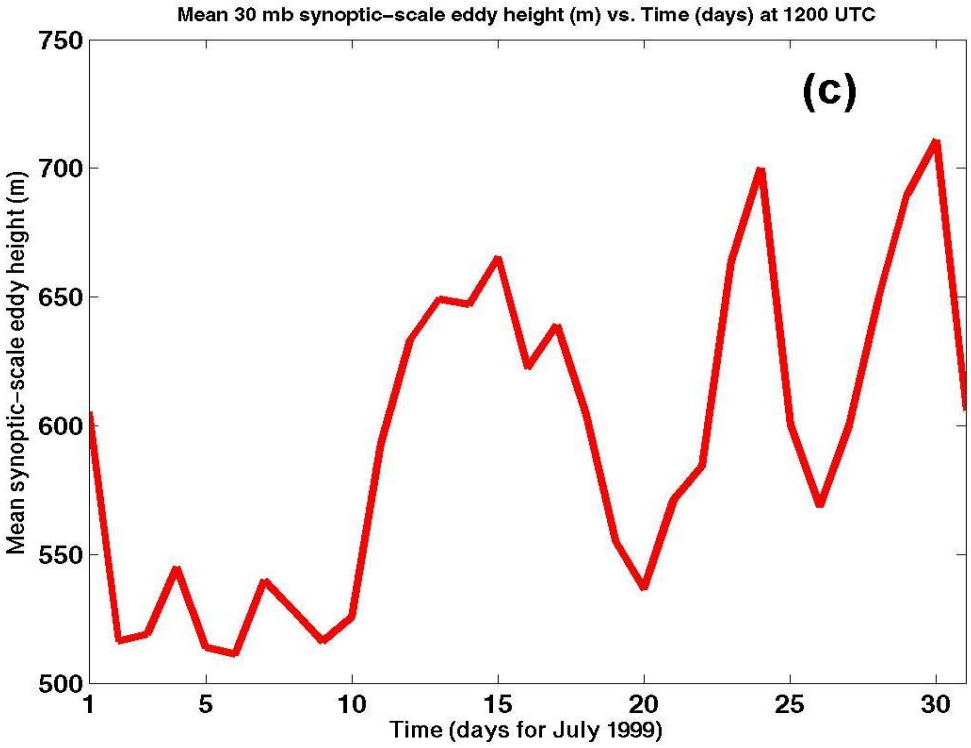
Mean 30 mb synoptic–scale eddy height (m) vs. Time (days) at 1200 UTC
(c)
Mean synoptic–scale eddy height (m)
750
700
650
600
550
500
1
5
10
15
20
25
30
Time (days for July 1999)

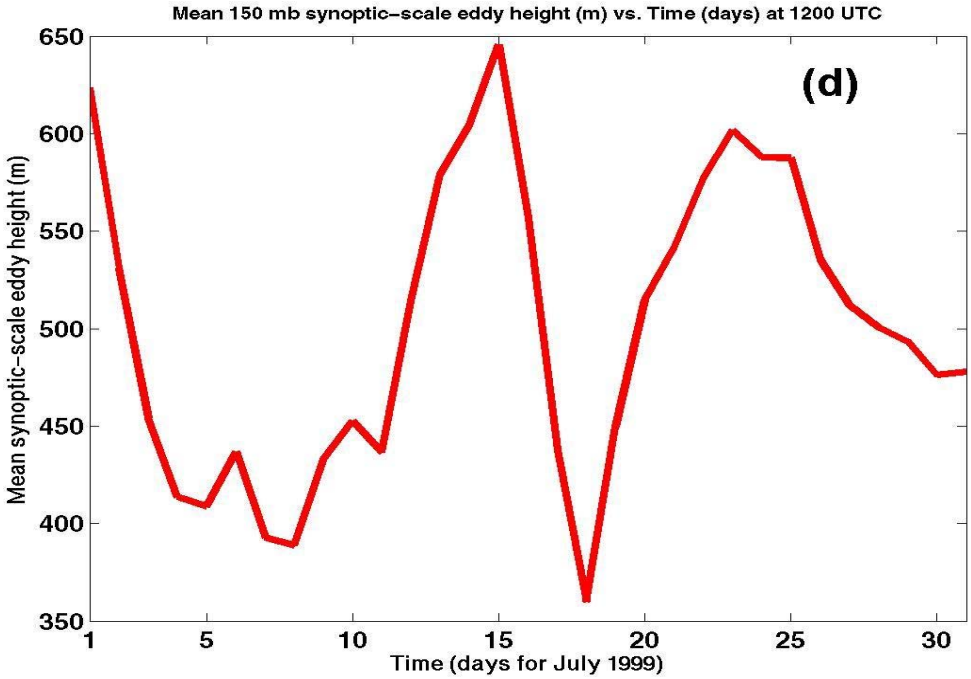
Mean 150 mb synoptic–scale eddy height (m) vs. Time (days) at 1200 UTC
(d)
Mean synoptic–scale eddy height (m)
650
600
550
500
450
400
350
1
5
10
15
20
25
30
Time (days for July 1999)

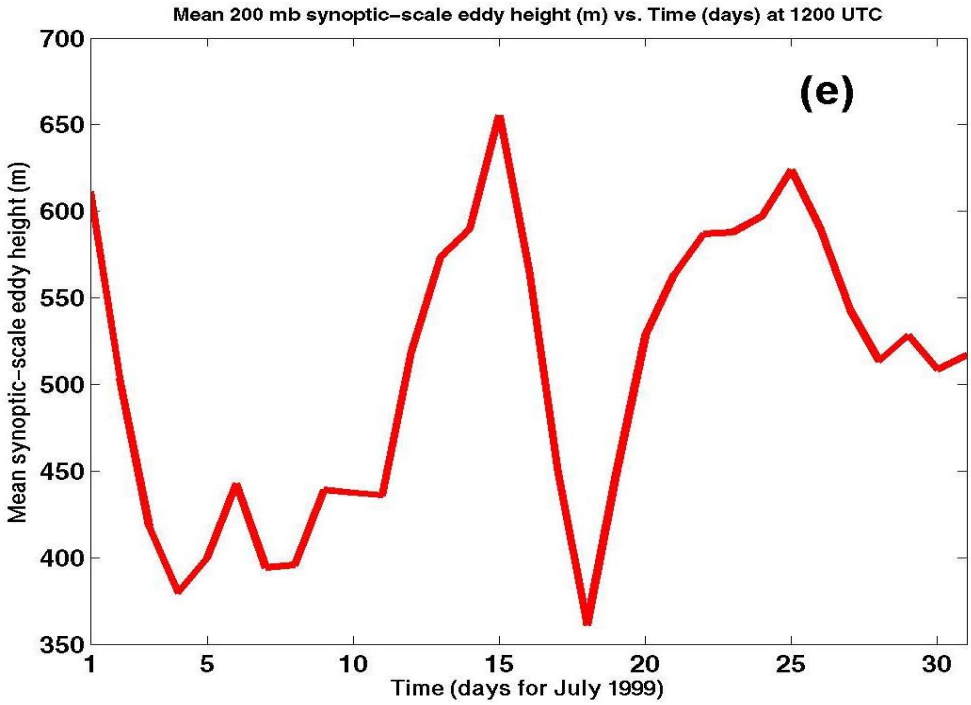
Mean 200 mb synoptic–scale eddy height (m) vs. Time (days) at 1200 UTC
(e)
Mean synoptic–scale eddy height (m)
700
650
600
550
500
450
400
350
1
5
10
15
20
25
30
Time (days for July 1999)

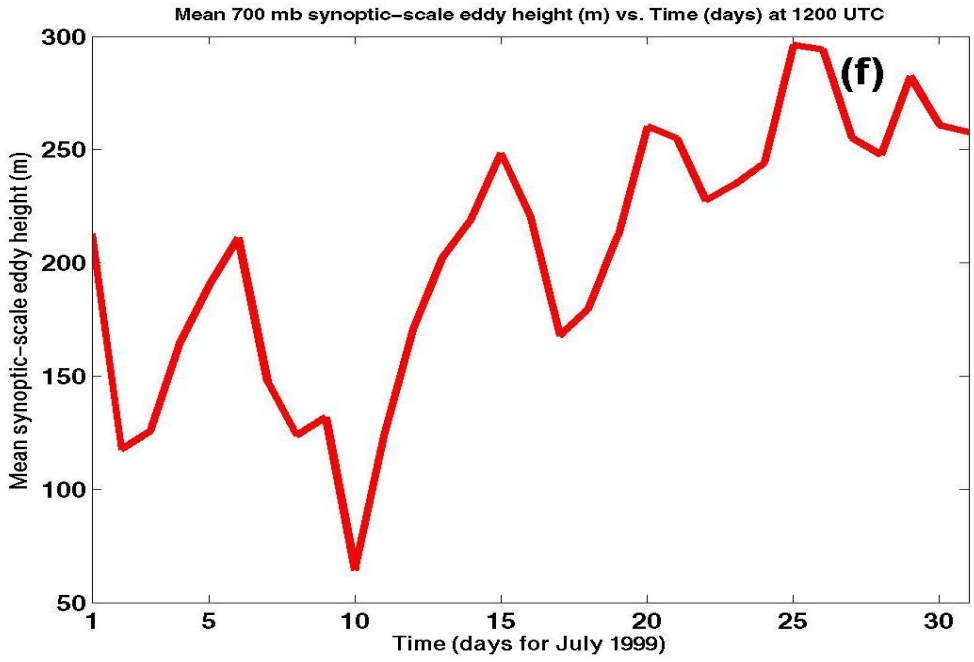
Mean 700 mb synoptic–scale eddy height (m) vs. Time (days) at 1200 UTC
(f)
Mean synoptic–scale eddy height (m)
300
250
200
150
100
50
1
5
10
15
20
25
30
Time (days for July 1999)

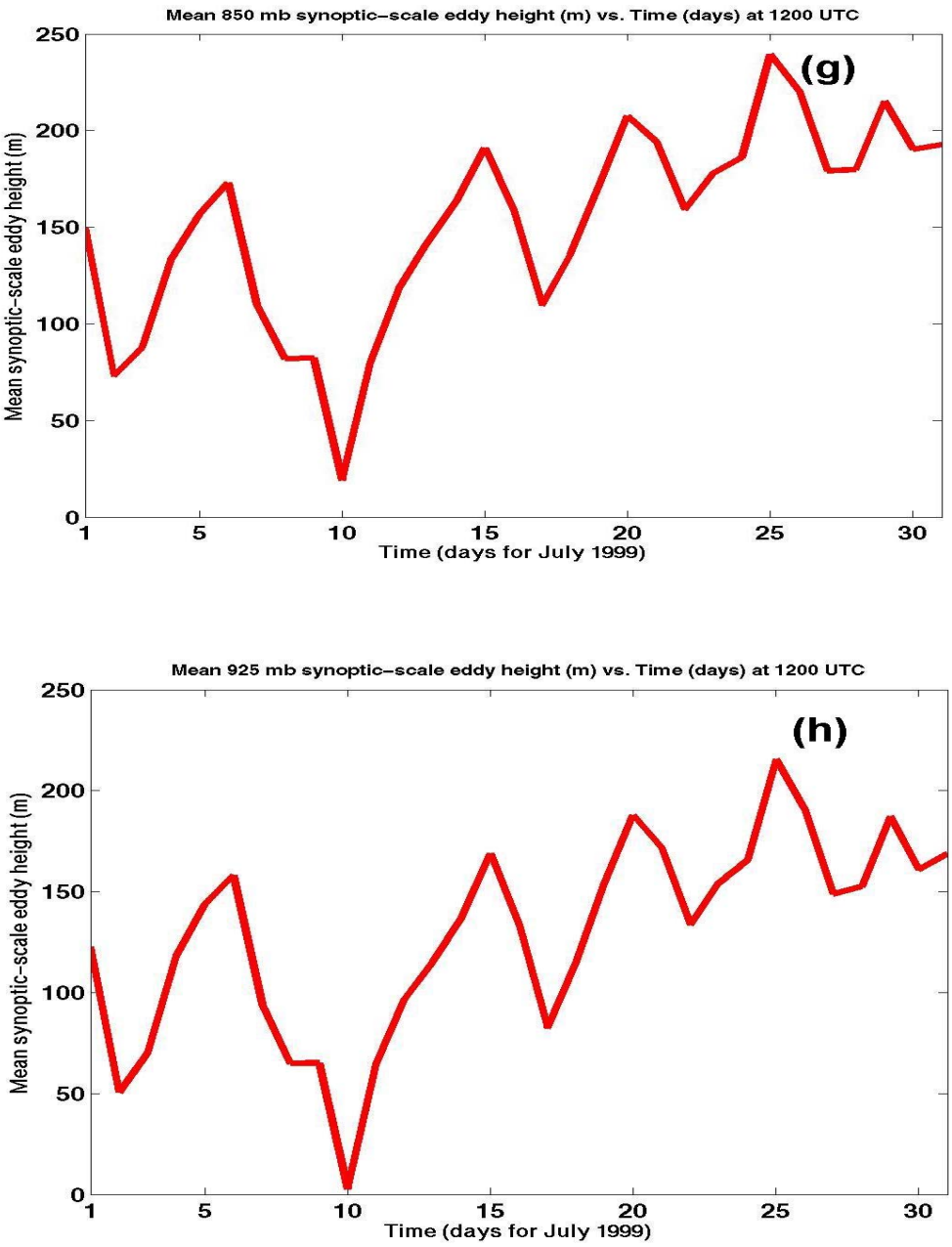

Fig. 4.8. Blocking area averaged synoptic-scale geopotential height at 1200 UTC for the entire month of July 1999. (a) 10 mb, (b) 20 mb, (c) 30 mb, (d) 150 mb, (e) 200 mb, (f) 700 mb, (g) 850 mb, and (h) 925 mb.

and the mean planetary-scale height at this isobaric level. A positive difference corresponds to the high pressure system/ridge, whereas the negative difference corresponds to the formation of a trough. Note that all the synoptic-scale heights are positive along the vertical axis in Fig. 4.7. Also note that the synoptic-scale height acquires a *relative maximum* during the blocking onset. We thus conclude that the synoptic-scale wavelengths contribute dominantly towards the formation of the blocking ridge. This finding is consistent with the findings by Dong and Colucci (2005, 2007) using a different set of diagnostic tools. They have used the quasi-geostrophic zonal wind tendency equation as their diagnostic tool to analyze the selected SH blocking event. Moreover, this is in contrast to our findings in the Northern Hemisphere case study.

Comparing with Fig. 4.4 which gives the cumulative effect of both the scales, we conclude that the synoptic-scale eddies play a dominant role during the onset, maintenance as well as decay stages of the blocking event. The BI thus provides a good diagnosis of the blocking event by mimicking the overall height pattern during the blocking and in our case as a good cross check.

When stratified over the stratosphere, from 10 mb to 300 mb, the synoptic-scale eddies do not seem to play a dominant role in the entire life cycle of the blocking event. The relative height averaged over the entire month of July 1999 falls, indicating a possible contribution towards stratospheric cooling (O' Neill and Taylor 1979; Austin 1980; Baldwin and Dunkerton 2001). Between 400 mb and 1000 mb, the relative ridge

height in the region of blocking increases especially during the onset of blocking, indicating a contribution towards possible tropospheric heating, see Fig. 4.8. A detailed heat budget study is called for at this stage to further investigate this observation. At the same time, we have relative lower planetary-scale heights in the same area (compare Fig. 4.6 and Fig. 4.8). Thus, the scale dynamics of the blocking event under study is dominated by the synoptic-scale eddies. We further note that from Fig. 4.5 and Fig. 4.7 that the selected blocking event is indeed isolated, so that its stability characteristics are not impacted by the onset/decay of other blockings in the vicinity.

4.3 Stability Analysis

We note that the blocking pattern remained quite stationary over its entire life cycle thus reasonably justifying the assumption that we are using to quantify the stability of the flow that blocking is assumed to be a relatively stationary state of the flow (see Section 1.3). During the mature and decay stages of the blocking, the Westward retrogression is $\leq 4^{o}$ as can be noticed from Fig. 4.1b and Fig. 4.2b.

We have noticed quite a different behavior of planetary- and synoptic-scale wavelengths during the life cycle of SH blocking events as compared to the selected NH blocking events. In NH blocking events, the planetary- and synoptic- scales tend to act in a synergistic manner to form the blockings. On the other hand, in SH blocking event,

single wavelength dominance seems to be operative in the life cycle of blocking event. In the selected blocking case, it is the synoptic-scale wavelength that dominates. This is consistent with Burkhardt and Lupo (2005) analysis in that their selected SH blocking event formation is a result of the superposition of the synoptic-scale on the planetary-scale. The planetary-scale height fall at the blocking onset may be associated with the diffluence of this wavelength however since it is the synoptic-scale wavelength that dominated so overall the BI starts rising at the onset as shown in Fig. 4.4.

Fig. 4.9 displays the time variability of the IRE for planetary-scale height at 500 mb for 1200 UTC. This figure gives the tendency of the IRE for the entire life cycle of the blocking event. Note that between 25 and 30 July, the IRE increases considerably, indicating the rise in the instability in the planetary-scale flow. This related well in time with the corresponding fall in amplitude of the synoptic-scale IRE (Fig. 4.10).

The blocking state being a high pressure system and we may thus conclude that the synoptic-scale ridge formation leads to rapid decay of the blocking high. We further note that the area averaged planetary-scale height also drops rapidly during the same time period thus confirming our above conceptual picture (Fig. 4.5).

Calculation of the IRE following Eq. (1.1) for the entire life cycle of the blocking event under study demonstrates a relationship between these values and those displayed in Fig. 4.10. From Fig. 4.10, we note that the IRE reaches a minimum shortly after the block onset and is at a relative minimum during the mature stage of this blocking event.

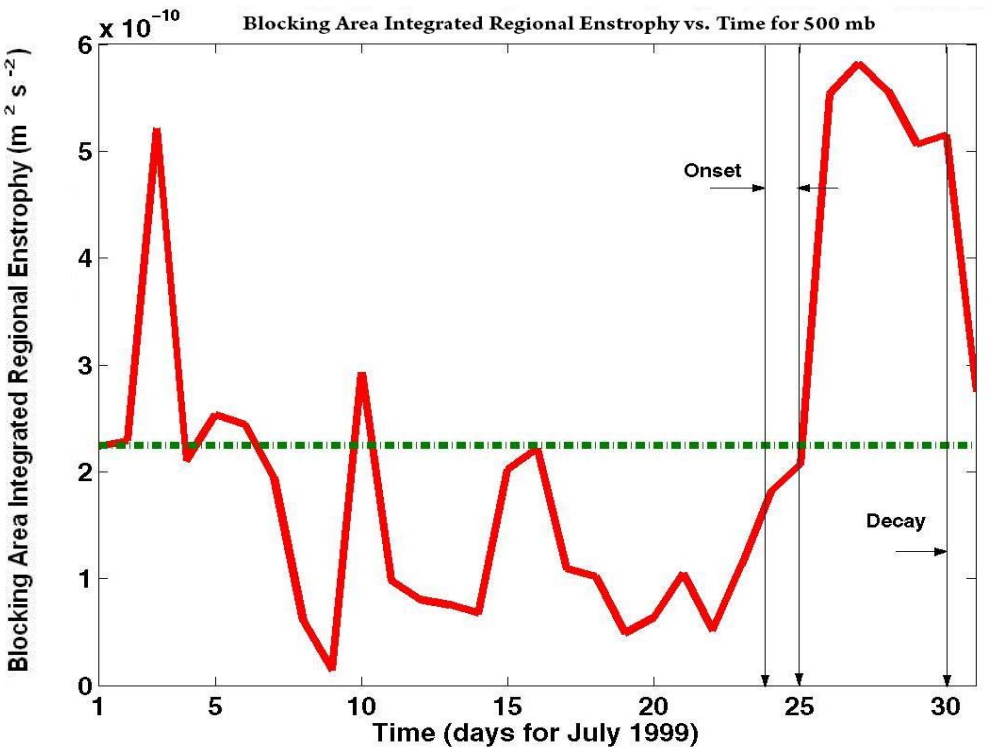

Fig. 4.9. A calculation of the planetary-scale area averaged enstrophy using Eq. (1.1) for the blocking event displayed in Fig. 4.4 which occurred during 24–31 July 1999 in the Pacific Ocean. The relative stability level changes at onset (24–25 July) and at decay (30–31 July) stages. The horizontal line defines the monthly mean reference value.

This is also consistent with the view that, in a quasi-barotropic flow, the scale dependent flow should be strongly barotropic, and that the blocking state represents a minimum state of enstrophy [and entropy see e.g., Dymnikov and Filatov (1995)]. Since these relate to the IRE which is relatively small here, indicates that negative

values of fluid trapping (again implying more predictability, or a more stable condition) grow with corresponding rise in the intensity of the blocking event.

We also note from Fig. 4.10 that after the onset of the blocking state, the IRE at synoptic-scale attains relatively lower positive values relative to its monthly mean value. Thus, the blocking (a mainly meridional circulation pattern) is more stable than the more frequent zonal flow. A comparison of Fig. 4.9 and Fig. 4.10 also indicates that planetary-scale wavelength becomes unstable whereas the synoptic-scale eddies becomes more stable during the mature stage of the blocking life cycle.

To further access the utility and robustness of the Dymnikov et al. (1992) conjecture, we have calculated numerically two other indicators of flow regime change and they are displayed in Fig. 4.11 and Fig. 4.12 for planetary- (upper panel) and synoptic-scale heights (lower panel) at 500 mb, respectively. These are the maximum of the absolute value of the gradient of the stream function, $\max|\nabla\psi|$, and the maximum of absolute value of the absolute vorticity of the flow, $\max|\nabla\Omega_a|$. Here

$$\psi = gZ/f, \tag{4.2}$$

where Z is the geopotential height and $f = 2\omega Sin(\phi)$ is the Coriolis parameter with latitude denoted by ϕ. The ω is the Earth rotation speed (ω is taken as 7.292×10^{-5} rad/s) and acceleration due to gravity is g (g is taken as 9.81 m/s^2). Also,

$$\Omega_a = \nabla^2\psi + f\ . \tag{4.3}$$

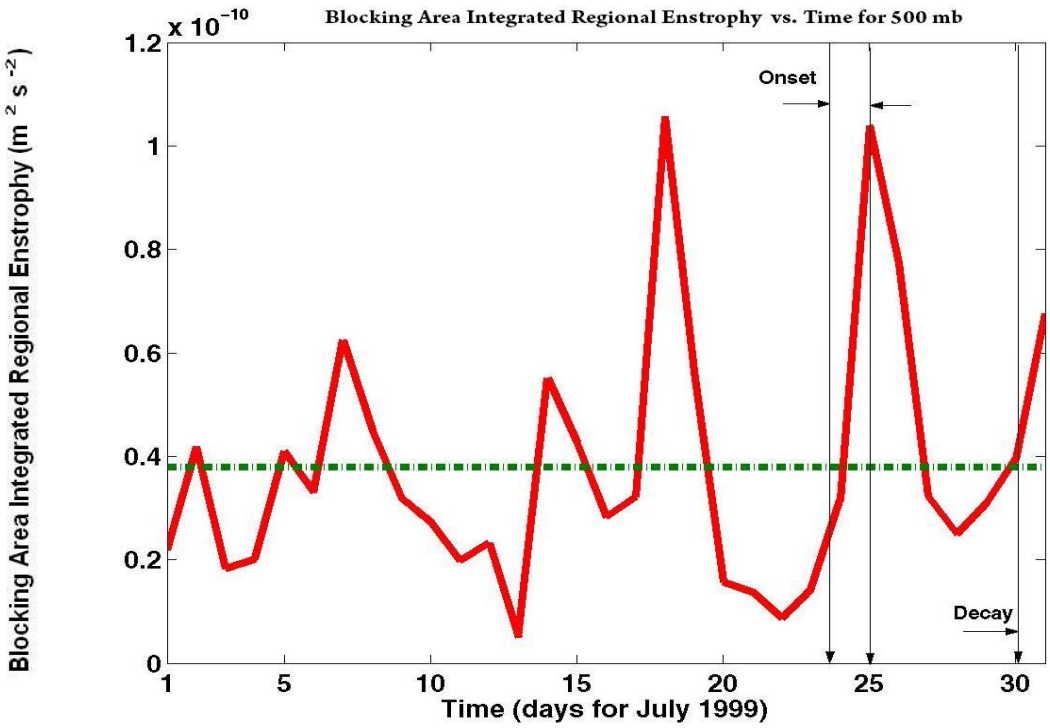

Fig. 4.10. A calculation of the synoptic-scale area averaged enstrophy using Eq. (1.1) for the blocking event displayed in Fig. 4.4 which occurred during 24–31 July 1999 in Pacific Ocean. Note the sharp relative decrease in enstrophy between the onset (24–25 July) and the decay (30–31 July) stages. The horizontal line defines the monthly mean reference value.

The behaviors of both the indicators have simple physical sense. Because of the presence of meridional variations in the stream function, it acquires a relative maximum during blocking state and thus is akin to the time variability of BI displayed in Fig. 4.4.

Comparing the upper panel of Fig. 4.11 with the lower panel, we note that planetary-scale wavelengths become more unstable than the synoptic-scale wavelengths. This explanation is consistent with the findings indicated by the stability indicator given by Eq. (4.1) and displayed in Fig. 4.9 and Fig. 4.10. The same tendency can be noticed in Fig. 4.12 which displays the time variability of stability indicator given by Eq. (4.3) for both components of the barotropic atmospheric flow.

Like in the NH case study, following Skiba (2002), it may be concluded that if either the maximum of absolute value of $\nabla\psi$ or maximum of absolute value of $\nabla\Omega_a$ depicts relative change, then the flow is becoming increasingly unstable. The two quantities may be considered as defining the instability of the flow. Here ψ is the stream function of the flow and Ω_a is the absolute vorticity of the flow. An examination of Fig. 4.9 provides additional support for the observation that the changes in the planetary-scale flow leads to instability of the zonal flow.

Thus, the two simple indicators given by Eq. (4.2) and Eq. (4.3) tend to mimic the regime changes in the flow (from zonal to non zonal and vice versa) and may have some value as indictors of flow stability. The planetary-scale flow is relatively unstable during the blocking; the synoptic-scale ridge formation destabilizes it thus causing the flow to revert back to the zonal configuration. The stratified behavior of both the above indicators of stability over the 17 mandatory levels confirms our findings displayed in Fig. 4.11 and Fig. 4.12. During blocking events, this implies that once the blocking event established itself, the synoptic-scale flow is relatively more predictable.

Planetary-scale blocking area averaged Max |∇ψ| vs. Time (dyas) for 500 mb

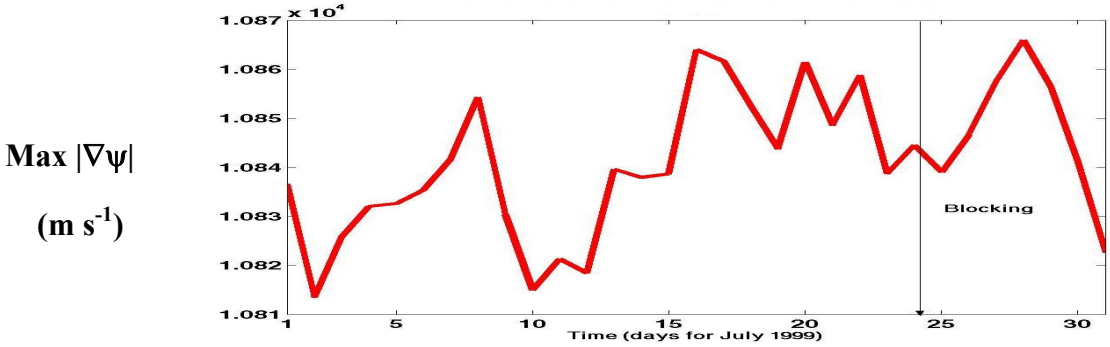

Synoptic-scale blocking area averaged Max |∇ψ| vs. Time (dyas) for 500 mb

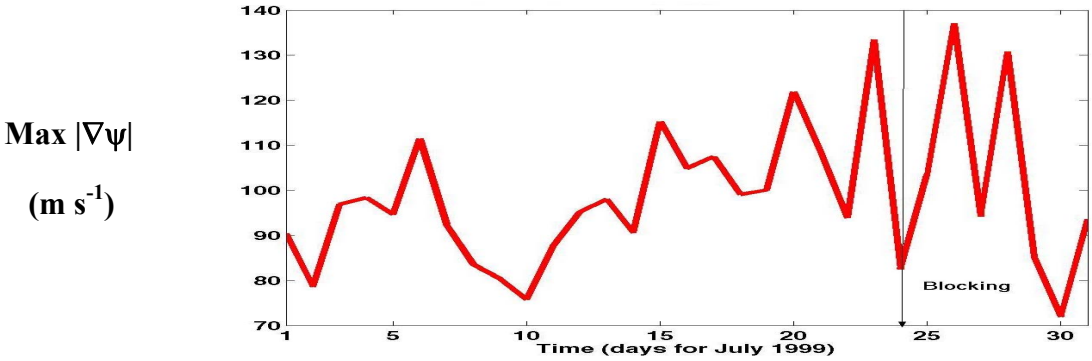

Fig. 4.11. Upper panel: A diagram of the blocking area averaged max |∇ψ| along abscissa versus time (days) along ordinate for a stationary box (60°S to 40°S and 212.5°E to 192.5°E) in the mid latitude Southern Hemispheric flow. Mean planetary-scale height data is used here for 1200 UTC. Lower Panel: Same as upper panel except for synoptic-scale wavelength.

Planetary-scale blocking area averaged Max $|\nabla \Omega_a|$ vs. Time (dyas) for 500 mb

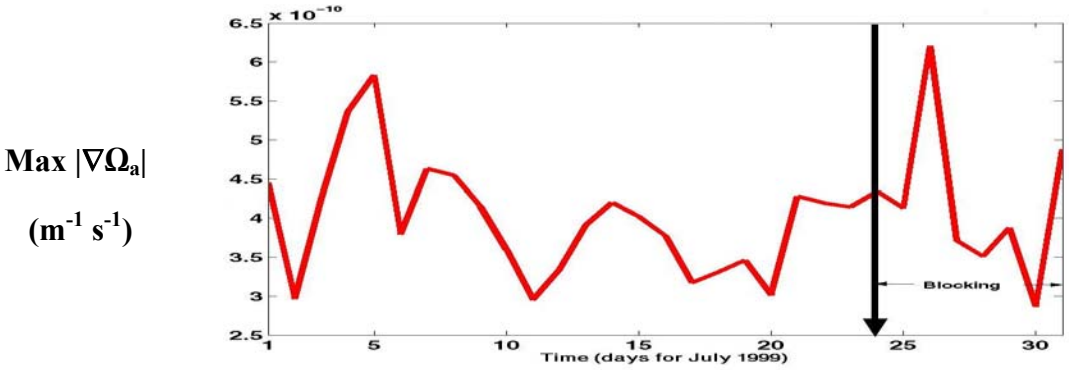

Synoptic-scale blocking area averaged Max $|\nabla \Omega_a|$ vs. Time (dyas) for 500 mb

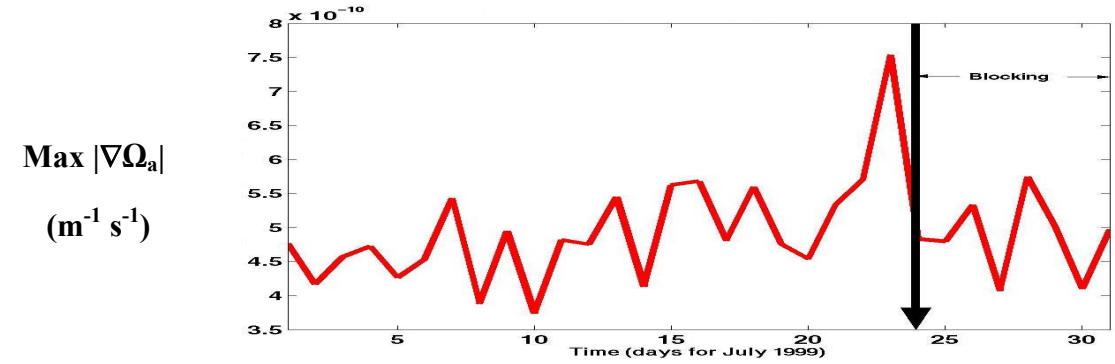

Fig. 4.12. Upper panel: A diagram of the blocking area averaged max $|\nabla\Omega_a|$ along abscissa versus time (days) along ordinate for a stationary box (60^oS to 40^oS and 212.5^oE to 192.5^oE) in the mid latitude Southern Hemispheric flow. 1200 UTC mean planetary-scale height data is used. Lower Panel: Same as upper panel except for synoptic-scale.

Another interesting observation is that a comparison of positive height anomaly and the IRE for the entire life cycle of the blocking event under discussion indicates a relation between the two as a function of pressure, as explained in Chapter 3. A comparison of Fig. 4.10 with Fig. 4.7 reveals this relation at 500 mb.

When stratified over the troposphere, this relation seems to hold for all mandatory levels for the entire duration of the selected blocking event further justifying the usefulness of the IRE as a simple diagnostic tool. Namely, the relative height rise corresponds to more stable flow configuration and hence in lower values of the IRE. Deep midlatitude SH blocking anticyclones extending from upper to lower troposphere may thus be diagnosed for their stability characteristics in terms of the IRE under the assumption of barotropic and quasi-geostrophic atmospheric flow.

4.4 Discussion

Based on the observations made in this case study, changes in the nature of the scale dependent flow can be related with the block onset and decay supporting the general implications of the earlier works, and that the planetary-scale provides an important contribution to blocking life cycles by providing a favorable environment for the blocking event to occur, in spite of the large contributions by the synoptic-scale flow and interaction components of the forcing.

Additionally, supporting evidence for the change in planetary- and synoptic-scale flow regimes at the block onset and decay stages comes from examining the i) IRE (flow stability) calculations, ii) max $|\nabla\psi|$, and iii) max $|\nabla\Omega_a|$. The area integrated enstrophy values (Fig. 4.10) fall to a minimum during the life cycle of the block in the blocked region in agreement with what would be expected for the selected blocking event implying that the synoptic-scale flow became unstable around the time of block onset and decay. Note that this feature is absent in the NH case study.

It is possible that the scale dependent flow at these two times moved from one (geostrophically) stable state to another, and the corresponding behavior of the other metrics shown in Fig. 4.11 and Fig. 4.12 corroborate this interpretation. Thus, the analyses presented here, which are relatively easy to generate, have at least some value as a diagnostic tool for atmospheric phenomena. These include the BI, the scale (planetary/synoptic) analysis and the stability indicator analysis. They may even have some value as a metric for predictability; however, more study is needed in order to adequately demonstrate such value.

CHAPTER 5

SUMMARY AND CONCLUSIONS

In this chapter we first summarize our findings for the six year global scale dynamics climatology and then present our analysis results for the Northern Hemisphere case study and then for the Southern Hemisphere case study.

5.1 Global Six Year Scale Dynamics Climatology

The scale analysis is performed by decomposing the observed 500 mb geopotential height into the blocking area averaged planetary-scale and the synoptic-scale eddy wavelengths and then the time variability of both the contributions is analyzed during the onset, the maintenance and the decay stages for the entire set of the blocking events. See section 1.5 of Chapter 1 for details of methodology.

Using the NCEP/NCAR gridded climatological data for 1999-2004, and averaging over the $40^{o}\times60^{o}$ latitude longitude box harboring the blocking event and based on our criterion of scale dominance as a height value above the monthly mean value for that height during the month in which the blocking occurs, we summarize our findings as follows.

- An event by event synoptic and stability analysis of all the blocking events occurring during 1999 through 2004 is performed to assess the role of scale dynamics. Such a detailed study is currently not available elsewhere.
- A total of 274 events were analyzed to determine the scale dominance of the planetary- and/or synoptic- scales during the blocking of the zonal flow. 83% of the total analyzed events have single wavelength dominance. Out of these, 48% have planetary-scale dominance, whereas 35% have synoptic-scale dominance in scale dynamics. The remaining 17% of the blocking events are categorized as alternating scale dominance blocking events.
- All previous studies of scale dynamics are based on individual case studies. Though these studies do provide useful insight for the selected blocking event, however they do not provide a global climatological perspective of scale dynamics.
- The sensitivity of our results for blocking domain size variation was studied. When the blocking domain size was varied from $40^{o}\times60^{o}$ to

$70^{o}\times90^{o}$, the deviation of the quantities that are averaged over it was found to be of the order of 2%. This indicates that our conclusions are insensitive to the blocking domain size variation within the above latitude and longitude range.

- The duration and geographic location of each analyzed blocking event is presented in tabular form in Chapter 2 and in appendix B. The scale dynamics results for all the blocking events for the same period are also presented in tabular form in the same format in Chapter 2 and appendix B for convenience.
- The variability of scale dependent flow in blocking events for the six year duration is displayed graphically (see Fig. 2.2). It is pointed out that during the later half of 1999-2004, the number of blocking events with planetary-scale dominance is higher by 28% relative to those with synoptic-scale dominance in NH.

In next two sections, we summarize and contrast our findings for the two case studies in the NH and SH respectively. For both case studies, we have extended our scale and stability analysis over the stratosphere for operational relevance.

5.2 Northern Hemisphere Case Study

The synoptic analysis as well as the scale and the stability analysis of an unusually prolonged and a moderately extreme blocking event occurring in the Gulf of

Alaska during the month of August 2004 is presented. See section 1.5 of Chapter 1 for details of analysis methodology. This blocking event resulted in a prolonged high pressure system that persisted in Gulf of Alaska for the entire month of August resulting in a heat wave (4.6^{o} F higher than normal 1971–2000 mean temperatures in Alaska region). Our analyzed results are as follows.

- The Dymnikov et al. (1992) conjecture is used to study the stability of the barotropic mid latitude NH flow, which relates the sum of positive eigenvalues of the linearization operator in barotropic flow with the blocking area regional enstrophy of the flow (IRE). See section 1.3 in Chapter 1 for details. Two diagnostic tools (namely, the mean geopotential planetary- and/or synoptic-scale eddy height and the IRE) providing valuable information about the change in the flow pattern during the blocking event are used to study the stability properties of the flow.
- It is noticed that the planetary-scale environment becomes unstable during the onset and then stabilizes during the peak activity of the blocking, whereas the synoptic-scale wavelengths play a dominant role in destabilizing the planetary-scale flow during peak activity/maintenance of the blocking life cycle thus initiating the blocking decay. The stability behavior of the barotropic flow containing the blocking when quantified in terms of the IRE indicates that the flow during blocking is more stable than the more frequent zonal flow.

- When stratified over the entire troposphere, the difference in the relative role of the two contributions is noticed. The synoptic-scale eddy wavelength played a dominant role in the lower troposphere during the entire life cycle of the blocking event. Interplay of both the contributions is found to be the case during the three stages of the blocking when their relative role is assessed in terms of the IRE and the gradient of stream function of the flow.
- From the comparative stability analysis of the selected blocking event, we point out that the planetary-scale provided a conducive environment for block onset and maintenance, whereas the relatively rapid formation of synoptic-scale eddies play a dominant role in the decay stage of the block life cycle. It is thus concluded that both the planetary-scale and the synoptic-scale wavelengths are necessary by their own as well as their interaction (in particular, at the decay stage for the blocking). We arrived at this conclusion by comparing the area averaged planetary-scale and synoptic-scale contributions to the IRE (mimicking the characteristic stability) of the flow that attended the blocking.
- The presence of an unusually long duration blocking pattern over Gulf of Alaska forced warm air pole ward resulting in warm air advection over the continental Alaska. It is noted that the planetary-scale height variation in the atmospheric flow follow the changes in the flow during the blocking event which are characteristically different from the

unblocked flow pattern upstream as well as the downstream. The 500 mb planetary-scale geopotential height variation for the considered blocking event over its entire life cycle ranged approximately between 80 m to 100 m.

- The synoptic-scale wavelength dominance is noticed in the present case only during the decay stage of the blocking under the assumption of barotropic atmospheric flow in quasi-geostrophic balance. This observation is supported by first isolating the time variability of the synoptic-scale eddies during the entire life cycle of the blocking event and then comparing it with the sum of planetary-scale and synoptic-scale wavelength contributions via the BI calculation.

Combining these with the results presented in Athar et al. (2007a, b), where the IRE for NH blocking events during the 3 year period (2002–2004) was calculated, we may arrive at a tentative conclusion that the IRE seems to mimic the (in) stability of the planetary-scale and the synoptic-scale atmospheric flow during blocking event and may thus qualify as a climatologically reliable diagnostic tool for the atmospheric blocking. We thus also confirm the tentative conclusions of earlier studies that the planetary- and synoptic- scales act in a synergistic manner to form the blockings in the mid latitude NH zonal flow.

5.2.1 Comparison with Earlier Works

This blocking case was studied earlier by Glisan (2007) as mentioned briefly in Chapter 1. Here we present a brief summary of his findings and relevance to our work.

- Glisan (2007) has performed a synoptic study of this event using BI and pressure at the dynamic tropopause at 2 PVU surface, where PVU is potential vorticity unit with 1 PVU equals 10^{-6} $m^2s^{-1}Kkg^{-1}$. Through visual inspection of a series of NCEP/NCAR reanalysis data generated plots of observed geopotential height, it was concluded that the blocking anticyclone is a positive height anomaly encompassing 25^oN-80^oN and 140^oE-100^oW. Our detailed analysis presented in Chapter 2 as well as the specific case study presented in Chapter 4 also confirms this. We arrived at this conclusion using a different set of diagnostic tools, namely; by first filtering the observed geopotential height and then averaging over the blocking domain. This positive comparison lends confidence in our diagnostic analysis procedure outlined in Chapter 1. We thus have performed an explicit calculation to obtain the same result and thus have provided an independent verification of visual observations. Our analysis is more exhaustive and precise since we have not only studied the role of both the synoptic- and planetary-scale contributions towards scale dynamics but also their relative stability role as well.

- Glisan (2007) noticed a gradual amplification of positive height anomaly during the first half of the blocking event life cycle (5-20 August 2004) and then later a de-amplification during later half of the blocking event life cycle (20-26 August 2004) based on same observational procedure. Our Fig. 3.7 confirms this finding.
- At 850 mb, a positive height anomaly was concluded. Our Fig. 3.8 confirms this as well. However, Glisan (2007) did not extend this analysis to include the stratospheric signals of the blocking event. Our analysis includes these signals. Our conclusion is that the selected blocking event leads to positive height anomaly in the stratosphere. This observation may have operational relevance. Glisan (2007) did extended the analysis into tropopause to study the role of wind fields only, however Glisan (2007) did not extend the height anomaly observations into the stratosphere.
- It was concluded that the synoptic-scale eddies do not play a main role in this event by subtracting the zonal mean from the mean tropopause pressure plots. It was point out that planetary-scale is more stable. We support these conclusions through a different set of tools. Furthermore, we have also analyzed the relative stability role of the two scales under the working assumption of Dymnikov et al. (1992) conjecture. Fig. 3.11 and Fig. 3.13 display our findings for the relative stability role of the planetary- and synoptic- scales respectively.

- Glisan (2007) noticed an extreme meridional gradient of the height field at midtropospheric level through visual inspection. Our results displayed in Fig. 3.15 and Fig. 3.16 confirm this finding. This in turn provide support for using simple variable such as max $|\nabla\psi|$ as a stability indicator of the flow.

5.3 Southern Hemisphere Case Study

We have used the same methodology to study this blocking event as for the selected blocking event in NH. Our findings for this case study are summarized as follows.

- On contrary to the stability characteristics of the NH blocking event, where planetary-scale and synoptic-scale wavelength seem to act in a synergistic manner to form the blocking event in the midlatitude NH zonal flow, in the selected SH blocking event, it is the synoptic-scale wavelength that dominantly determined the overall stability and scale dynamics of the blocking event.
- The stratified behavior of the height scales and the stability indicator behavior over the stratosphere and troposphere indicates a relatively dominant contribution of synoptic-scale eddies towards stratospheric cooling and tropospheric warming over the blocking region. This height stratified reversal of synoptic-scale eddies is absent for the planetary-scale wavelength during the life cycle of the selected SH blocking event.

- We have presented a comparison of the contributions from the two wavelengths (planetary- and synoptic-scale) as our scale analysis via Fig. 4.5 and Fig. 4.7 and then have made use of indicators of stability such as the IRE to quantify the underlying stability characteristics of the flow during the blocking via Fig. 4.9 and Fig. 4.10.
- We conclude that synoptic-scale eddies played a dominant role in the onset, maintenance and decay stages of the considered blocking event. We arrived at this conclusion by considering the IRE of the flow in the blocked region as a measure of the stability of the flow and then comparing it with its monthly mean reference value.
- We have studied the relative and tropospherically stratified role of the planetary- and synoptic-scale wavelengths towards the various stages of the blocking event. Blocking is treated as a meridionally perturbed stationary state in the zonal flow.

Summarizing, local weakening of the westerlies or local strengthening of the easterlies may be interpreted as a meridional perturbation of the zonal flow and then the flow stability characteristics may be quantified in terms of the IRE. We have used Dymnikov et al. (1992) conjecture to relate this with the blocking area enstrophy of the flow. The relative spatial and temporal isolation of the selected blocking event provide a good test example of Dymnikov et al. (1992) conjecture.

5.3.1 Comparison with Earlier Works

As mentioned in Chapter 1, Dong and Colucci (2005, 2007) pointed out that the interplay of local flow deformation and potential vorticity (PV) and/or the advection of the meridional gradient of PV seems to be the cause of the *local weakening of the geostrophic westerlies* prior to the onset of the midtropospheric SH blocking event which we also have analyzed. They used the quasi-geostrophic zonal wind tendency equation as their diagnostic tool to analyze the selected blocking event in SH. They supported their conjecture through case study of 30 SH blocking events that seems to broadly fall within this category. The comparison includes the following points.

- Dong and Colucci (2005) have applied the scale partitioning to the quasi-geostrophic zonal wind equation and have used the two dimensional Fourier transform analysis to 500 mb height at the block onset on 25 July 1999 (Dong and Colucci 2007) to obtain the synoptic-scale dominance results. However, these studies are limited to the onset stage of blocking only. We have extended their analysis to include all three stages of blocking life cycle using a different set of tools and have performed stability analysis of the event as well.
- A closely associated point is that the meridional variations of (potential) vorticity was found to play an important role in the onset of the selected blocking event (Dong and Colucci 2005, 2007). Our results displayed in Fig. 4.11 and Fig. 4.12 confirm this point of view via the stability

indicators, namely; via the maximum of the absolute value of the gradient of the stream function, max|$\nabla\psi$|, and the maximum of absolute value of the absolute vorticity of the flow, max|$\nabla\Omega_a$|, from a different perspective. The main emphasis in that case study was to pinpoint the relation and extent of the two opposing blocking mechanisms for onset of SH blockings, here we have extended that analysis by incorporating and emphasizing the (in)stability considerations.

- Our results corroborate and extend the conjecture developed by Dong and Colucci (2005, 2007) that weakening of westerlies seem to be the precursor condition of the blocking onset and that synoptic-scale eddies played a dominant role in all the three stages of the blocking event.

The above observations in the two case studies are true irrespective of whether the blocking event occurs entirely over land, over sea or partially over land and partially over sea (Athar et al. 2007a, b). This may indicate more dominating role played by the different scales and their interactions in atmospheric flow (as noted in earlier studies too) once the blocking sets in instead of orographic forcings.

The use of stability indicators such as max|$\nabla\psi$| shall have some implications for medium range weather forecast, since an early indication of relative variation in max|$\nabla\psi$| is suggestive of flow instability.

A yet another potential implication of diagnostic study carried out in this work is that the flow stability analysis tools developed here can be used to extract useful information about the dynamics of the atmospheres of other Earth like planets, as well.

At least for the selected case studied here, the IRE seems to characterize the stability of the planetary/synoptic-scale flow in barotropic circulation. The stability theory is thus investigated in order to evaluate its use as a simple diagnostic tool. A simultaneous knowledge of the two diagnostic tools however seems to provide a more reliable scenario for the existence/occurrence, sustenance as well as decay of a blocking event. The IRE based on Dymnikov et al. (1992) conjecture gives only the relative stability of the flow. Geopotential height variations alone however do not provide any underlying insight into the dynamics and the stability of the atmospheric flow during the blocking period. A simultaneous estimate of both should suffice to establish the presence and the stability behavior of the flow. The above observations made in this study find some justification in light of the previous studies mentioned in Chapter 1, where it was concluded that both the planetary-scale as well as the synoptic-scale wavelengths seems to play some role in essentially all stages of blocking life cycle. Though depending upon the specific case study, the relative strength of the role seems to vary.

Given, the analyzed blocking event cases for scale dominance and the stability character of the scales for a six year period (1999-2004), globally, the blocking of the zonal flow seems to be dominated by a single wavelength (either planetary or synoptic) and that the dominating scale determines the stability of the flow, especially during the peak activity/ mature phase of the flow. Furthermore, under the assumption of the barotropic flow in the mid latitude blocking events, the blocking area integrated regional enstrophy can be used as a climatologically reliable diagnostic tool.

APPENDIX A- MATLAB Codes

This appendix describes the MATLAB codes used to calculate the blocking area integrated regional enstrophy, the filtered heights and the space derivatives. The codes take input variables from the netCDF files which are opened in the main code in MATLAB given in appendix A.1.

A.1 MATLAB Code for Calculating the Integrated Regional Ensrophy

The netCDF files ‘hgt.1999.nc’, ‘uwnd.1999.nc’ and ‘vwnd.1999.nc’ used in this code were downloaded from the website **http://www.cdc.noaa.gov/**. For the filter subroutine named shapiro, see appendix A.2, whereas for the calculation of space derivatives via suroutine named jet_dz, see appendix A.3.

```
clear; close all; more off;
warning off MATLAB:divideByZero;
nc=netcdf('hgt.1999.nc','nowrite');
ncu=netcdf('uwnd.1999.nc','nowrite');
ncv=netcdf('vwnd.1999.nc','nowrite');
time=datevec(nc{'time'}(:)/24+365);
```

```
lon=0:2.5:357.5;
lat=0:-2.5:-90;
a=find(time(:,2)>=7 & time (:,2)<=8 & time(:,4)==12);
for i=1:length(a)
  disp(i)
  z=squeeze(nc{'hgt'}(a(i),find(nc{'level'}(:)==500),...
  37:73,:).*nc{'hgt'}.scale_factor+nc{'hgt'}.add_offset);
  zfil=shapiro(z);
  zfilt=z-zfil;
  zstore(i,:,:)=zfilt(:,:);
  ustore(i,:,:)=squeeze(ncu{'uwnd'}(a(i),...
  find(ncu{'level'}(:)==500),:,:).*ncu{'uwnd'}.scale_factor+...
  ncu{'uwnd'}.add_offset);
  vstore(i,:,:)=squeeze(ncv{'vwnd'}(a(i),...
  find(ncv{'level'}(:)==500),:,:).*ncv{'vwnd'}.scale_factor+...
  ncv{'vwnd'}.add_offset);
end
save ireshsynpt zstore ustore vstore;


clear; close all; more off;
load ireshsynpt;
lon=0:2.5:357.5;
```

```
lat=0:-2.5:-90;
lona=144;
lonb=1;
lata=37;
latb=73;
f=-(2.*7.29e-5*sin((0:-2.5:-90).*2.*pi./360))';
fmat=repmat(f,1,144);
g=9.81;
ER=6.371e6; % earth radius in meters
dy=2.*pi.*ER./144;
dx(1:(latb-lata+1),1)=dy;
dx=dx.*cos(linspace(0,-pi/2,latb-lata+1))';
dx=repmat(dx,1,lona-lonb+1);
dy=repmat(dy,latb-lata+1,lona-lonb+1);
dA=dx.*dy;

for i=1:size(zstore,1)
  % read and filter z
  disp(i)
  z=squeeze(zstore(i,:,:));
  u=squeeze(ustore(i,:,:));
  v=squeeze(vstore(i,:,:));
```

```
  [dzdx,dzdy]=jet_dz(flipud(z));
  dzdy=-flipud(dzdy);
  dzdx=flipud(dzdx);
  ug=-g./fmat.*dzdy;
  vg=g./fmat.*dzdx;
  [junk,dudy]=jet_dz(flipud(ug));
  [dvdx,junk]=jet_dz(flipud(vg));
  dudy=-flipud(dudy);
  dvdx=flipud(dvdx);
  %vor = dvdx - dudy + fmat;
  vor =-dudy;
  lona=find(lon==212.5); lonb=find(lon==192.5);
  lata=find(lat==-40); latb=find(lat==-60);
  vors(i)=sum(sum(vor(lata:latb,lonb:lona).^2.*dA(lata:latb,lonb:lona)));
  ire(i)=vors(i)./sum(sum(dA(lata:latb,lonb:lona)));
end
plot (ire);
xlabel('Time (days for July 1999 and August 1999)');
ylabel('Synoptic-Scale IRE');
title ('Integrated Regional Enstrophy vs. Time (days) at 500 mb for 1200 UTC');
set(findobj(gca,'Type','line','Color',[0 0 1]),...
    'Color','red','LineWidth',4);
```

A.2 MATLAB Code for Shapiro Filter

The following subroutine is called by the main code in MATLAB to filter the planetary-scale heights from the height variables of the netCDF files (see appendix A.1).

```
function s=shapiro(dat)
for iter=1:1250
  for el=1:2
    ip0jp0=dat(3:35,:);
    ip1jp0=[dat(3:35,2:end) dat(3:35,1)];
    ip2jp0=[dat(3:35,3:end) dat(3:35,1:2)];
    im1jp0=[dat(3:35,end) dat(3:35,1:end-1)];
    im2jp0=[dat(3:35,end-1:end) dat(3:35,1:end-2)];

    ip0jp1=dat(2:34,:);
    ip1jp1=[dat(2:34,2:end) dat(2:34,1)];
    ip2jp1=[dat(2:34,3:end) dat(2:34,1:2)];
    im1jp1=[dat(2:34,end) dat(2:34,1:end-1)];
    im2jp1=[dat(2:34,end-1:end) dat(2:34,1:end-2)];

    ip0jp2=dat(1:33,:);
```

```
ip1jp2=[dat(1:33,2:end) dat(1:33,1)];
ip2jp2=[dat(1:33,3:end) dat(1:33,1:2)];
im1jp2=[dat(1:33,end) dat(1:33,1:end-1)];
im2jp2=[dat(1:33,end-1:end) dat(1:33,1:end-2)];

ip0jm1=dat(4:36,:);
ip1jm1=[dat(4:36,2:end) dat(4:36,1)];
ip2jm1=[dat(4:36,3:end) dat(4:36,1:2)];
im1jm1=[dat(4:36,end) dat(4:36,1:end-1)];
im2jm1=[dat(4:36,end-1:end) dat(4:36,1:end-2)];

ip0jm2=dat(5:37,:);
ip1jm2=[dat(5:37,2:end) dat(5:37,1)];
ip2jm2=[dat(5:37,3:end) dat(5:37,1:2)];
im1jm2=[dat(5:37,end) dat(5:37,1:end-1)];
im2jm2=[dat(5:37,end-1:end) dat(5:37,1:end-2)];

switch el
case 1
  dat(3:35,:)=1/256.*(100.*ip0jp0 + 40.*(ip1jp0 + ip0jp1 + im1jp0 + ip0jm1) ...
    + 16.*(ip1jp1 + ip1jm1 + im1jp1 + im1jm1) ...
    -10.*(ip2jp0 + im2jp0 + ip0jp2 + ip0jm2) ...
```

```
        -4.*(ip1jp2 + im2jm1 + im1jm2 + im1jp2 + im2jp1 + ip2jm1 + ip1jm2 + ip2jp1) ...
        + (ip2jp2 + im2jm2 + ip2jm2 + im2jp2));
    case 2
      dat(3:35,:)=1/256.*(484.*ip0jp0 - 88.*(ip1jp0 + ip0jp1 + im1jp0 + ip0jm1) ...
        + 16.*(ip1jp1 + ip1jm1 + im1jp1 + im1jm1) ...
        + 22.*(ip2jp0 + im2jp0 + ip0jp2 + ip0jm2) ...
        -4.*(ip1jp2 + im2jm1 + im1jm2 + im1jp2 + im2jp1 + ip2jm1 + ip1jm2 + ip2jp1) ...
        + (ip2jp2 + im2jm2 + ip2jm2 + im2jp2));
    end
  end
end
s=dat;
```

A.3 MATLAB Code for Calculating the Space Derivatives

The following MATLAB code calculates the space derivatives on variables from the netCDF files that are read from the main code in MATLAB (see appendix A.1).

```
function [dzdx,dzdy] = jet_dz(z)
%   function [dzdx,dzdy] = jet_dz(z) is expecting 37x144 matrix of data
%   Returns dzdx and dzdy matrices which are the first derivatives of z in x and y
%   For SH data, put in entire hemisphere flipud, then flipud results and multiply dzdy
%   by -1

lat=90:-2.5:0;
dlat=2*6.371E6*pi/360; % distance for 1 degree latitude (m) = C/360 = 2*r*pi/360
% set dy constant (dlat is y-axis North-South spacing between parallels)
dlat=abs(lat(2)-lat(3))*dlat; % distance for given data spacing
% set dx matrix ("dlon" is x-axis, East-West spacing between meridians)
% This matrix is same size as hgt field allowing NaN at -2.5 and 90 N
dlon_mat=dlat.*cos(lat.*2*pi/360); % set a meridian of values
dlon_mat=repmat(dlon_mat',1,144); % spin it around the globe
dlon_mat(1,:)=NaN; % to prevent infinite differences

dzdy(37,144)=NaN; dzdy(:,:)=NaN; % initialize for size
dzdx(37,144)=NaN; dzdx(:,:)=NaN; % initialize for size
```

```
dzdy(1,:)=(3.*z(1,:)-4.*z(2,:)+z(3,:))./(dlat.*2);

dzdy(end,:)=(-z(end-2,:)+4.*z(end-1,:)-3.*z(end,:))./(dlat.*2);

% now dzdy is straight forward central difference:

dzdy(2:end-1,:)=(z(1:end-2,:)-z(3:end,:))./(dlat.*2); % (z(y1)-z(y3))/(2*dlat) for z(y2)


% dzdx requires some shuffling:

% this code moves the first column to the end and calls that upper

%   then it moves the last column to the front and calls that lower

%   these two will be subtracted and divided by dlon*2

%   It's setting up   2 3 4 5 6 7 8 9 1

%                  - 9 1 2 3 4 5 6 7 8

%                   --------------------

%                  (a central finite difference ) ... 3-1 goes on 2, 4-2 goes on 3

upper(:,:) = [z(:,2:end) z(:,1)];

lower(:,:) = [z(:,end) z(:,1:end-1)];

dzdx(:,:)=(upper - lower) ./ (dlon_mat.*2);

% (z(x3)-z(x1))/(2*dlon) for z(x2)
```

APPENDIX B- Tables of Blocking Events

This appendix provides the blocking event details for the years 2000, 2001 and 2003.

Table B.1a. Blocking event details for NH 2000. For each blocking event, the start date is displayed in column 2, the end date in column 3, the event duration in column 4, the BI averaged over the entire life cycle of the blocking event in column 5, and the geographic location in column 6. For further details, see Chapter 2.

EVENT NO.	START DATE	END DATE	DURATION (DAYS)	BI	GEOGRAPHIC LOCATION
1	09 Jan.	23 Jan.	14	2.73	Atlantic
2	29 Jan.	07 Feb.	10	2.61	Atlantic
3	11 Feb.	23 Feb.	12	4.22	Pacific
4	23 Feb.	05 Mar.	10	2.30	Atlantic
5	12 Mar.	20 Mar.	8	1.73	Atlantic
6	18 Mar.	31 Mar.	13	2.68	Pacific
7	11 Apr.	20 Apr.	9	1.47	Atlantic
8	11 Apr.	17 Apr.	6	1.00	Pacific
9	24 Apr.	06 May	12	2.39	Continental
10	03 May	13 May	10	1.93	Atlantic
11	17 May	28 May	11	2.50	Atlantic
12	22 May	30 May	8	2.00	Continental
13	06 Jun.	13 Jun.	7	1.63	Atlantic
14	10 Jun.	18 Jun.	8	2.27	Continental
15	15 Jun.	29 Jun.	14	1.47	Pacific
16	22 Jun.	28 Jun.	6	1.43	Atlantic
17	30 Jun.	07 Jul.	8	0.96	Pacific
18	11 Jul.	25 Jul.	14	1.14	Continental
19	14 Jul.	20 Jul.	6	0.75	Pacific
20	17 Aug.	24 Aug.	7	1.20	Atlantic
21	18 Sep.	03 Oct.	15	2.80	Atlantic
22	06 Oct.	14 Oct.	8	2.30	Atlantic
23	16 Oct.	21 Oct.	5	3.19	Atlantic
24	06 Nov.	11 Nov.	5	2.70	Continental
25	19 Nov.	24 Nov.	5	1.60	Atlantic
26	09 Dec.	16 Dec.	7	3.09	Pacific
27	20 Dec.	25 Dec.	5	2.81	Pacific
28	22 Dec.	29 Dec.	7	2.42	Atlantic

Table B.1b. Same as Table B.1a except for NH 2001.

EVENT NO.	START DATE	END DATE	DURATION (DAYS)	BI	GEOGRAPHIC LOCATION
1	02 Jan.	11 Jan.	9	3.09	Atlantic
2	10 Feb.	15 Feb.	5	3.60	Pacific
3	23 Feb.	03 Mar.	8	2.51	Pacific
4	26 Feb.	06 Mar.	8	2.55	Continental
5	04 Mar.	10 Mar.	6	4.17	Pacific
6	15 Mar.	23 Mar.	8	4.18	Pacific
7	21 Mar.	30 Mar.	9	2.16	Atlantic
8	29 Mar.	07 Apr.	9	2.02	Pacific
9	02 Apr.	08 Apr.	6	2.37	Atlantic
10	25 Apr.	05 May	10	2.60	Atlantic
11	10 May	19 May	9	2.37	Atlantic
12	15 May	21 May	6	2.62	Pacific
13	18 May	26 May	8	3.61	Pacific
14	23 May	01 Jun.	9	3.46	Atlantic
15	03 Jun.	13 Jun.	10	2.43	Atlantic
16	17 Jun.	22 Jun.	5	1.93	Continental
17	09 Jul.	16 Jul.	7	1.59	Continental
18	09 Jul.	23 Jul.	14	2.63	Atlantic
19	20 Jul.	28 Jul.	8	2.78	Continental
20	24 Jul.	04 Aug.	11	2.43	Continental
21	03 Aug.	08 Aug.	5	1.84	Continental
22	19 Aug.	24 Aug.	5	2.96	Continental
23	26 Aug.	01 Sep.	6	1.81	Atlantic
24	08 Sep.	22 Sep.	14	2.00	Continental
25	23 Sep.	30 Sep.	7	2.27	Atlantic
26	04 Oct.	09 Oct.	5	3.31	Continental
27	15 Oct.	25 Oct.	10	3.33	Atlantic
28	23 Nov.	29 Nov.	6	3.95	Continental
29	26 Nov.	01 Dec.	5	3.12	Continental
30	08 Dec.	27 Dec.	19	4.02	Atlantic
31	23 Dec.	03 Jan.	11	3.88	Pacific

Table B.1c. Same as Table B.1a except for NH 2003

EVENT NO.	START DATE	END DATE	DURATION (DAYS)	BI	GEOGRAPHIC LOCATION
1	02 Jan.	10 Jan.	8	5.30	Pacific
2	12 Jan.	18 Jan.	6	2.24	Pacific
3	14 Jan.	20 Jan.	6	3.07	Continental
4	23 Jan.	06 Feb.	14.5	2.76	Continental
5	25 Jan.	01 Feb.	7	3.40	Atlantic
6	09 Feb.	15 Feb.	6	3.67	Pacific
7	09 Feb.	22 Feb.	13	4.65	Atlantic
8	20 Feb.	02 Mar.	11	3.39	Atlantic
9	20 Feb.	26 Feb.	6	2.47	Pacific
10	07 Mar.	18 Mar.	10.5	4.21	Atlantic
11	19 Mar.	25 Mar.	6	5.39	Pacific
12	29 Mar.	08 Apr.	9.5	3.11	Atlantic
13	04 Apr.	13 Apr.	9	2.99	Atlantic
14	14 Apr.	22 Apr.	8.5	2.31	Atlantic
15	26 Apr.	06 May	10	2.70	Atlantic
16	01 May	22 May	21	2.52	Pacific
17	12 May	23 May	11	3.13	Continental
18	13 May	28 May	15	2.22	Atlantic
19	25 May	12 Jun.	17	2.01	Continental
20	03 Jun.	12 Jun.	9	1.50	Atlantic
21	04 Jun.	22 Jun.	18.5	3.20	Pacific
22	13 Jun.	24 Jun.	11	2.99	Atlantic
23	24 Jun.	05 Jul.	11	3.20	Pacific
24	28 Jun.	07 Jul.	9	1.23	Pacific
25	09 Jul.	10 Aug.	32	1.77	Continental
26	11 Jul.	19 Jul.	7.5	1.75	Pacific
27	18 Jul.	05 Aug.	18	2.23	Continental
28	06 Aug.	13 Aug.	7	1.96	Atlantic
29	12 Aug.	26 Aug.	14	2.15	Continental
30	24 Aug.	13 Sep.	21.5	2.52	Atlantic
31	01 Sep.	10 Sep.	9	1.96	Continental
32	10 Sep.	20 Sep.	10	2.15	Continental
33	11 Sep.	20 Sep.	9	2.31	Pacific
34	13 Sep.	25 Sep.	12	2.12	Atlantic
35	24 Sep.	10 Oct.	16	3.37	Atlantic
36	25 Aug.	07 Sep.	12	4.38	Pacific
37	28 Sep.	05 Oct.	7	1.62	Continental
38	28 Sep.	05 Oct.	7	0.91	Pacific
39	13 Oct.	24 Oct.	11	3.12	Atlantic
40	29 Oct.	08 Nov.	9.5	4.32	Pacific

41	01 Nov.	06 Nov.	5	2.95	Continental
42	05 Nov.	16 Nov.	11	4.21	Atlantic
43	27 Oct.	04 Nov.	7	3.51	Atlantic
44	04 Dec.	10 Dec.	6.5	4.32	Atlantic
45	16 Dec.	21 Dec.	5	2.15	Continental
46	19 Dec.	26 Dec.	7	3.33	Atlantic
47	28 Nov.	05 Dec.	8	2.20	Atlantic
48	29 Nov.	04 Dec.	6	3.17	Atlantic

Table B.2a. Same as Table B.1a except for SH 2000. For explanation of asterisk (*), see Chapter 2.

EVENT NO.	START DATE	END DATE	DURATION (DAYS)	BI	GEOGRAPHIC LOCATION
1	08 Mar.	14 Mar.	5.5	2.54	Atlantic
2	20 May	25 May	5	2.80	Indian
3	23 May	03 Jun.	11	4.71	Pacific
4	22 Jun.	27 Jun.	5	3.92	Pacific
*5	27 Jun.	25 Jun.	5	1.93	Pacific
6	11 Jul.	17 Jul.	6	2.44	Pacific
7	20 Aug.	28 Aug.	8	4.38	Indian
*8	11 Sep.	14 Sep.	10.5	2.99	Pacific

Table B.2b. Same as Table B.1a except for SH 2001.

EVENT NO.	START DATE	END DATE	DURATION (DAYS)	BI	GEOGRAPHIC LOCATION
1	28 Apr.	07 May	9	1.37	Pacific
2	09 May	16 May	6.5	4.60	Pacific
3	25 May	01 Jun.	7	3.11	Pacific
4	03 Jul.	11 Jul.	8.5	2.72	Pacific
5	13 Jul.	24 Jul.	11	3.33	Pacific

6	15 Aug.	30 Aug.	15.5	4.00	Pacific
7	26 Aug.	02 Sep.	7	1.38	Pacific
8	08 Sep.	14 Sep.	6.5	1.80	Pacific
9	11 Sep.	16 Sep.	5	2.31	Atlantic
10	30 Sep.	06 Oct.	5.5	2.21	Pacific

Table B.2c. Same as Table B.1a except for SH 2003. For explanation of asterisk (*), see Chapter 2.

EVENT NO.	START DATE	END DATE	DURATION (DAYS)	BI	GEOGRAPHIC LOCATION
1	07 Jan.	12 Jan.	5	1.95	Pacific
2	19 Feb.	23 Feb.	6	3.35	Pacific
3	26 Feb.	09 Mar.	11	2.92	Pacific
4	18 Mar.	26 Mar.	8	2.32	Pacific
5	07 Apr.	14 Apr.	7	2.01	Indian
6	01 May	07 May	6	1.33	Indian
7	25 May	02 Jun.	8	2.31	Indian
8	14 Jun.	19 Jun.	5	2.68	Pacific
9	26 Jun.	02 Jul.	6	3.10	Indian
10	20 Jul.	29 Jul.	9	2.36	Pacific
*11	25 Aug.	10 Sep.	5	2.20	Pacific
12	13 Aug.	19 Aug.	6	3.58	Pacific
13	21 Aug.	08 Sep.	18	3.42	Pacific
*14	27 Sep.	20 Oct.	5	3.01	Atlantic
15	30 Sep.	10 Oct.	7	3.51	Pacific
16	13 Oct.	26 Oct.	13.5	1.78	Pacific
17	13 Nov.	18 Nov.	5	2.00	Pacific
18	19 Nov.	24 Nov.	5	2.51	Pacific

Table B.3a. Planetary- and synoptic-scale dominance results for all the blocking events during NH 2000. See Chapter 2 for details.

EVENT NO.	START DATE	END DATE	DURATION (DAYS)	PLANETARY SCALE DOMINENCE	SYNOPTIC SCALE DOMINENCE
1	09 Jan.	23 Jan.	14	Positive	Negative
2	29 Jan.	07 Feb.	10	Positive	Negative
3	11 Feb.	23 Feb.	12	Positive	Negative
4	23 Feb.	05 Mar.	10	Positive	Negative
5	12 Mar.	20 Mar.	8	Positive	Negative
6	18 Mar.	31 Mar.	13	Positive	Negative
7	11 Apr.	20 Apr.	9	Negative	Positive
8	11 Apr.	17 Apr.	6	Positive	Negative
9	24 Apr.	06 May	12	Negative	Positive
10	03 May	13 May	10	Negative	Positive
11	17 May	28 May	11	Positive	Negative
12	22 May	30 May	8	Positive	Negative
13	06 Jun.	13 Jun.	7	Negative	Positive
14	10 Jun.	18 Jun.	8	Negative	Positive
15	15 Jun.	29 Jun.	14	Positive	Negative
16	22 Jun.	28 Jun.	6	Positive	Negative
17	30 Jun.	07 Jul.	8	Alternating	Alternating
18	11 Jul.	25 Jul.	14	Alternating	Alternating
19	14 Jul.	20 Jul.	6	Positive	Negative
20	17 Aug.	24 Aug.	7	Negative	Positive
21	18 Sep.	03 Oct.	15	Alternating	Alternating
22	06 Oct.	14 Oct.	8	Negative	Positive
23	16 Oct.	21 Oct.	5	Positive	Negative
24	06 Nov.	11 Nov.	5	Positive	Negative
25	19 Nov.	24 Nov.	5	Negative	Positive
26	09 Dec.	16 Dec.	7	Positive	Negative
27	20 Dec.	25 Dec.	5	Negative	Positive
28	22 Dec.	29 Dec.	7	Negative	Positive

Table B.3b. Same as Table B.3a except for NH 2001.

EVENT NO.	START DATE	END DATE	DURATION (DAYS)	PLANETARY SCALE DOMINENCE	SYNOPTIC SCALE DOMINENCE
1	02 Jan.	11 Jan.	9	Alternating	Alternating
2	10 Feb.	15 Feb.	5	Negative	Positive
3	23 Feb.	03 Mar.	8	Negative	Positive
4	26 Feb.	06 Mar.	8	Positive	Negative
5	04 Mar.	10 Mar.	6	Negative	Positive
6	15 Mar.	23 Mar.	8	Positive	Negative
7	21 Mar.	30 Mar.	9	Positive	Negative
8	29 Mar.	07 Apr.	9	Positive	Negative
9	02 Apr.	08 Apr.	6	Negative	Positive
10	25 Apr.	05 May	10	Positive	Negative
11	10 May	19 May	9	Negative	Positive
12	15 May	21 May	6	Negative	Positive
13	18 May	26 May	8	Positive	Negative
14	23 May	01 Jun.	9	Negative	Positive
15	03 Jun.	13 Jun.	10	Negative	Positive
16	17 Jun.	22 Jun.	5	Positive	Negative
17	09 Jul.	16 Jul.	7	Negative	Positive
18	09 Jul.	23 Jul.	14	Alternating	Alternating
19	20 Jul.	28 Jul.	8	Negative	Positive
20	24 Jul.	04 Aug.	11	Positive	Negative
21	03 Aug.	08 Aug.	5	Positive	Negative
22	19 Aug.	24 Aug.	5	Negative	Positive
23	26 Aug.	01 Sep.	6	Negative	Positive
24	08 Sep.	22 Sep.	14	Positive	Negative
25	23 Sep.	30 Sep.	7	Negative	Positive
26	04 Oct.	09 Oct.	5	Positive	Negative
27	15 Oct.	25 Oct.	10	Negative	Positive
28	23 Nov.	29 Nov.	6	Negative	Positive
29	26 Nov.	01 Dec.	5	Alternating	Alternating
30	08 Dec.	27 Dec.	19	Positive	Negative
31	23 Dec.	03 Jan.	11	Positive	Negative

Table B.3c. Same as Table B.3a except for NH 2003.

EVENT NO.	START DATE	END DATE	DURATION (DAYS)	PLANETARY SCALE DOMINENCE	SYNOPTIC SCALE DOMINENCE
1	02 Jan.	10 Jan.	8	Negative	Positive
2	12 Jan.	18 Jan.	6	Positive	Negative
3	14 Jan.	20 Jan.	6	Positive	Negative
4	23 Jan.	06 Feb.	14.5	Alternating	Alternating
5	25 Jan.	01 Feb.	7	Positive	Negative
6	09 Feb.	15 Feb.	6	Alternating	Alternating
7	09 Feb.	22 Feb.	13	Positive	Negative
8	20 Feb.	02 Mar.	11	Negative	Positive
9	20 Feb.	26 Feb.	6	Negative	Positive
10	07 Mar.	18 Mar.	10.5	Positive	Negative
11	19 Mar.	25 Mar.	6	Negative	Positive
12	29 Mar.	08 Apr.	9.5	Negative	Positive
13	04 Apr.	13 Apr.	9	Negative	Positive
14	14 Apr.	22 Apr.	8.5	Positive	Negative
15	26 Apr.	06 May	10	Negative	Positive
16	01 May	22 May	21	Alternating	Alternating
17	12 May	23 May	11	Positive	Negative
18	13 May	28 May	15	Alternating	Alternating
19	25 May	12 Jun.	17	Positive	Negative
20	03 Jun.	12 Jun.	9	Negative	Positive
21	04 Jun.	22 Jun.	18.5	Negative	Positive
22	13 Jun.	24 Jun.	11	Positive	Negative
23	24 Jun.	05 Jul.	11	Positive	Negative
24	28 Jun.	07 Jul.	9	Alternating	Alternating
25	09 Jul.	10 Aug.	32	Positive	Negative
26	11 Jul.	19 Jul.	7.5	Alternating	Alternating
27	18 Jul.	05 Aug.	18	Positive	Negative
28	06 Aug.	13 Aug.	7	Alternating	Alternating
29	12 Aug.	26 Aug.	14	Alternating	Alternating
30	24 Aug.	13 Sep.	21.5	Alternating	Alternating
31	01 Sep.	10 Sep.	9	Positive	Negative
32	10 Sep.	20 Sep.	10	Positive	Negative
33	11 Sep.	20 Sep.	9	Positive	Negative
34	13 Sep.	25 Sep.	12	Negative	Positive
35	24 Sep.	10 Oct.	16	Alternating	Alternating
36	25 Aug.	07 Sep.	12	Alternating	Alternating
37	28 Sep.	05 Oct.	7	Positive	Negative
38	28 Sep.	05 Oct.	7	Alternating	Alternating
39	13 Oct.	24 Oct.	11	Negative	Positive

40	29 Oct.	08 Nov.	9.5	Positive	Negative
41	01 Nov.	06 Nov.	5	Positive	Negative
42	05 Nov.	16 Nov.	11	Positive	Negative
43	27 Oct.	04 Nov.	7	Alternating	Alternating
44	04 Dec.	10 Dec.	6.5	Alternating	Alternating
45	16 Dec.	21 Dec.	5	Positive	Negative
46	19 Dec.	26 Dec.	7	Positive	Negative
47	28 Nov.	05 Dec.	8	Positive	Negative
48	29 Nov.	04 Dec.	6	Alternating	Alternating

Table B.4a. Same as Table B.3a except for SH 2000. For explanation of asterisk (*), see Chapter 2.

EVENT NO.	START DATE	END DATE	DURATION (DAYS)	PLANETARY SCALE DOMINENCE	SYNOPTIC SCALE DOMINENCE
1	08 Mar.	14 Mar.	5.5	Positive	Negative
2	20 May	25 May	5	Negative	Positive
3	23 May	03 Jun.	11	Positive	Negative
4	22 Jun.	27 Jun.	5	Positive	Negative
*5	27 Jun.	25 Jun.	5		
6	11 Jul.	17 Jul.	6	Positive	Negative
7	20 Aug.	28 Aug.	8	Positive	Negative
*8	11 Sep.	14 Sep.	10.5		

Table B.4b. Same as Table B.3a except for SH 2001.

EVENT NO.	START DATE	END DATE	DURATION (DAYS)	PLANETARY SCALE DOMINENCE	SYNOPTIC SCALE DOMINENCE
1	28 Apr.	07 May	9	Positive	Negative
2	09 May	16 May	6.5	Positive	Negative

3	25 May	01 Jun.	7	Positive	Negative
4	03 Jul.	11 Jul.	8.5	Alternating	Alternating
5	13 Jul.	24 Jul.	11	Alternating	Alternating
6	15 Aug.	30 Aug.	15.5	Positive	Negative
7	26 Aug.	02 Sep.	7	Positive	Negative
8	08 Sep.	14 Sep.	6.5	Positive	Negative
9	11 Sep.	16 Sep.	5	Negative	Positive
10	30 Sep.	06 Oct.	5.5	Alternating	Alternating

Table B.4c. Same as Table B.3a except for SH 2003. For explanation of asterisk (*), see Chapter 2.

EVENT NO.	START DATE	END DATE	DURATION (DAYS)	PLANETARY SCALE DOMINENCE	SYNOPTIC SCALE DOMINENCE
1	07 Jan.	12 Jan.	5	Positive	Negative
2	19 Feb.	23 Feb.	6	Positive	Negative
3	26 Feb.	09 Mar.	11	Positive	Negative
4	18 Mar.	26 Mar.	8	Negative	Positive
5	07 Apr.	14 Apr.	7	Negative	Positive
6	01 May	07 May	6	Positive	Negative
7	25 May	02 Jun.	8	Positive	Negative
8	14 Jun.	19 Jun.	5	Positive	Negative
9	26 Jun.	02 Jul.	6	Positive	Negative
10	20 Jul.	29 Jul.	9	Positive	Negative
*11	25 Aug.	10 Sep.	5		
12	13 Aug.	19 Aug.	6	Positive	Negative
13	21 Aug.	08 Sep.	18	Alternating	Alternating
*14	27 Sep.	20 Sep.	5		
15	30 Sep.	10 Oct.	7	Positive	Negative
16	13 Oct.	26 Oct.	13.5	Negative	Positive
17	13 Nov.	18 Nov.	5	Positive	Negative
18	19 Nov.	24 Nov.	5	Alternating	Alternating

REFERENCES

Alaskan Climate Record Center, 2004: Record breaking summer of 2004. http://climate.gi.alaska.edu/News/summer04.html.

Athar, H., A. R. Lupo, and S. Dostoglou 2007a: A calculation of Lyapunov exponents for atmospheric blocking. *Preprint of the talk given at 16th Conference on Atmospheric and Oceanic Fluid Dynamics (16th FLUID), 25–29 June, 2007, Santa Fe, NM.*

Athar, H., A. R. Lupo, C. Strong, and S. Dostoglou, 2007b: A diagnostic study of atmospheric blocking using Lyapunov exponents over a 50 year period. *Preprint of the talk at 19th Conference on Climate Variability and Change (19th CVC), 14–18 January, 2007, San Antonio, TX.*

Austin, J. F., 1980: The blocking of middle latitude westerly winds by planetary waves. *Quart. J. Roy. Meteor. Soc.*, **106,** 327–350.

Baldwin, M. P., and T. J. Dunkerton, 2001: Stratospheric harbingers of anomalous weather regimes. *Science,* **294,** 581–584.

Barriopedro, D., R. Garcia-Herrera, A. R. Lupo, and E. Hernandez, 2006: A climatology of northern hemisphere blocking, *J. Clim.*, **19,** 1042–1063.

Benzi, R., B. Saltzman, and A. C. Wiin-Nielsen, 1986: *Anomalous Atmospheric Flows and Blocking (Adv. in Geophys.* **29***)*: Academic Press, 459 pp.

Burkhardt, J. P., and A. R. Lupo, 2005: The planetary- and synoptic-scale interactions in a southeast Pacific blocking episode using PV Diagnostics. *J. Atmos . Sci.*, **62,** 1901–1916.

Carrera, M. L., R. W. Higgins, V. E. Kousky, 2004: Downstream weather impacts associated with atmospheric blocking over the northern Pacific. *J. Clim.* **17,** 4823–4838.

Charney, J. G., and J. G. De Vore, 1979: Multiple flow equilibria in the atmosphere and blocking. *J. Atmos . Sci.*, **36,** 1205–1216.

Cohen, R. A., and D. M. Schultz, 2005: Contraction rate and its relationship to frontogenesis, the Lyapunov exponent, fluid trapping, and airstream boundaries. *Mon. Wea. Rev.*, **133**, 1353–1369.

Colucci, S. J., 2001: Planetary-scale preconditioning for the onset of blocking. *J. Atmos. Sci.*, **58,** 933–942.

Colucci, S. J., and D. P. Baumhefner, 1998: Numerical prediction of the onset of blocking: A case study with forecast ensembles. *Mon. Wea. Rev.*, **126**, 773–784.

De Swart, H. E., 1988: Low-order spectral models of the atmospheric circulation: A survey. *Acta Appl. Math*., **11,** 49–96.

Dong, L., and S. J. Colucci, 2005: The role of deformation and potential vorticity in southern hemisphere blocking onsets. *J. Atmos. Sci.*, **62,** 4043–4056.

Dong, L., and S. J. Colucci, 2007: Interpreting the opposition between two block-onset forcing mechanisms. *J. Atmos. Sci.,* **64,** 2091–2104.

Dymnikov, V. P., and A. N. Filatov, 1995: On several problems of mathematical theory of climate. *Izv. Acad. Sci. USSR, Atmos. Oceanic Phys.,* **31,** 293–303.

Dymnikov, V. P., Ye. V. Kazantsev, V. V. Kharin, 1992: Information entropy and local Lyapunov exponents of barotropic atmospheric circulation. *Izv. Acad. Sci. USSR, Atmos. Oceanic Phys.,* **28,** 425–432.

Federov, A. V., S. L. Harper, S. G. Philander, B. Winter, and W. Wittenberg, 2003: How predictable is El Niño? *Bull. Amer. Meteor. Soc.*, **84,** 911–919.

Frederiksen, J. S., 1982: A unified three-dimensional instability theory of the onset of blocking and cyclogenesis. *J. Atmos. Sci*., **39,** 969–982.

Ghil, M., and S. Childress, 1987: *Topics in Geophysical Fluid Dynamics: Atmospheric Dynamics, Dynamo Theory, and Climate Dynamics*. Springer-Verlag, 485 pp.

Glisan, J. M., 2007: *Two Extreme Cases of Atmospheric Blocking Over Europe and North America*. M.S. Thesis. University of Missouri, Columbia, MO, 125 pp.

Haines, K., and A. J. Holland, 1998: Vacillation cycles and blocking in a channel. *Quart. J. Roy. Meteor. Soc.*, **124**, 873–897.

Hansen, A. R., 1986: Observational characteristics of atmospheric planetary waves with bimodal amplitude distributions. *Adv. Geophys.*, **29**, 101–133.

Hansen, A. R., and A. Sutera, 1988: Planetary wave amplitude bimodality in the southern hemisphere. *J. Atmos. Sci.*, **45**, 3771–3783.

Kalnay–Rivas, E., and L. O. Merkine, 1981: A simple mechanism for blocking. *J. Atmos. Sci.*, **38**, 2077–2091.

Kalnay, E., and Co-authors, 1996: The NCEP/NCAR 40-year reanalysis project. *Bull. Amer. Meteor. Soc.*, **77,** 437–471.

Kistler, R. and Co-authors, 2001: The NCEP-NCAR 50-year reanalysis: monthly means CD-ROM and documentation. *Bull. Amer. Meteor. Soc.*, **82**, 247–267.

Legras, B., and M. Ghil, 1985: Persistent anomalies, blocking and variations in atmospheric predictability. *J. Atmos. Sci*., **42,** 433**–**471.

Lejenäs, H., and H. Øakland, 1983: Characteristics of northern hemisphere blocking as determined from long time series of observational data. *Tellus,* **35A**, 350–362.

Lorenz, E. N., 1963: Deterministic nonperiodic flow. *J. Atmos. Sci.*, **20**, 130–141.

Lupo, A. R., and P. J. Smith, 1995a: Climatological features of blocking anticyclones in the northern hemisphere. *Tellus*, **47A,** 439–456.

Lupo, A. R., and P. J. Smith, 1995b: Planetary and synoptic-scale interactions during the life cycle of a mid-latitude blocking anticyclone over the north Atlantic. *Tellus,* **47A**: *Tellus Special Issue: The life cycles of extratropical cyclones*, 575–596.

Lupo, A. R., and L. F. Bosart, 1999: An analysis of a relatively rare case of continental blocking. *Quart. J. Roy. Meteor. Soc.*, **125,** 107–138.

Lupo, A. R., et al., 2007: Assessment of the impact of the planetary scale on the decay of blocking and the use of phase diagrams and enstrophy as a diagnostic. *Izv. Acad. Sci. USSR, Atmos. Oceanic Phys.*, **43,** 45–51.

Lynch, P., 2003: Resonant Rossby wave triads and the swinging spring. *Bull. Amer. Meteor. Soc.*, **84,** 605–616.

Marques, R. F. C., and V. B. Rao, 1999: A diagnosis of a long-lasting blocking event over the southeast Pacific ocean. *Mon. Wea. Rev.*, **127,** 1761–1776.

Mokhov, I. I., A. V. Eliseev, and D. V. Khvorostyanov, 2000: Evolution of characteristics of the climate variability related to the El Nino and La Nina phenomena. *Izv. Acad. Sci. USSR, Atmos. Oceanic Phys.*, **36,** 741–751.

Mokhov, I. I., D. V. Khvorostyanov, and A. V. Eliseev, 2004: Decadal and longer-term changes in ENSO characteristics. *I. J. Climatol.*, **24,** 401–414.

Mullen, S. L., 1986: The local balances of vorticity and heat for blocking anticyclones in a spectral general circulation model. *J. Atmos. Sci*., **43,** 1406–1441.

Mullen, S. L., 1987: Transient eddy forcing and blocking flows. *J. Atmos. Sci.,* **44,** 3–22.

Nakamura, H., and J. M. Wallance, 1990: Observed changes in baroclinic wave activity during the life cycles of low-frequency circulation anomalies. *J. Atmos. Sci.,* **47,** 1100–1116.

Nakamura, H., M. Nakamura, and J. L. Anderson, 1997: The role of high- and low-frequency in blocking formation. *Mon. Wea. Rev.*, **125,** 2074–2093.

Nese, J. M., J. A. Dutton, and R. Wells, 1987: Calculated attractor dimensions for low-order spectral models. *J. Atmos. Sci.*, **44,** 1950–1972.

O' Neill, A. and B. F. Taylor, 1979: A study of the major stratospheric warming of 1976/77. *Quart. J. Roy. Meteor. Soc.*, **105,** 71–92.

Rex, D., 1950a: Blocking action in the middle troposphere and its effect upon regional climate I. An aerological study of blocking action. *Tellus* **2,** 196–211.

Rex, D., 1950b: Blocking action in the middle troposphere and its effect upon regional climate II. The climatology of blocking action. *Tellus* **2,** 275–301.

Shapiro, R., 1970: Smoothing, filtering, and boundary effects. *Rev. Geophys. Space Phys.*, **8,** 359–387.

Shutts, G. J., 1983: The propagation of eddies in diffluent jet streams: Eddy vorticity forcing of blocking flow fields. *Quart. J. Roy. Met. Soc.*, **109,** 737–761.

Skiba, Y. N., 2002: On the spectral problem in the linear stability study of flows on a sphere. *J. Math. Anal. Appl.*, **270,** 165–180.

Tracton, M. S., 1990: Predictability and its relationship to scale interaction processes in blocking. *Mon. Wea. Rev.*, **118,** 1666–1695.

Tsou, C. H., and P. J. Smith, 1990: The role of synoptic/planetary-scale interactions during the development of a blocking anticyclone. *Tellus*, **42A,** 174–193.

Wiedenmann, J. M., A. R. Lupo, I. I. Mokhov, and E. Tikhonova, 2002: The climatology of blocking anticyclones for the northern and southern hemispheres: Block intensity as a diagnostic. *J. Climate*, **15**, 3459–3474.

VITA

Athar Hussain, was born in Rawalpindi, Pakistan. He obtained his M.Sc., M. Phil. and Ph.D. degrees in Physics in 1990, 1992 and 1996 respectively from Quaid-i-Azam University, Islamabad, Pakistan. He also completed a one year diploma course in High Energy Physics from The Abdus Salam Centre for Theoretical Physics, Trieste, Italy, during 1992-1993. He was married to Sara Hashmi in 2000, while he was a post-doctoral fellow under JSPS fellowship at Tokyo Metropolitan University, Tokyo, Japan. Subsequently, he served as a visiting assistant professor at Physics Division of National Center for Theoretical Sciences, Taiwan until 2005.

Dr. Athar has authored or coauthored 18 refereed papers on various topics in Physics ranging from the magnetic properties of high T_c superconductors to neutrino mixing effects on astrophysical neutrinos. These include a well-known paper on the neutrino mixing effects with 50+ citations and a very well-known paper with 100+ citations according to Stanford Linear Accelerator Center Library, Stanford, USA (SLAC-Spires) as of 2008.

Physics provided him an excellent opportunity to visit institutes and deliver talks on topics in Astroparticle Physics in 24 countries. The institutes include FermiLab (USA), Aspen Center for Physics (USA), CERN (Switzerland), DESY (Germany), The Abdus Salam Centre for Theoretical Physics (Italy), LAPP (France), Institute for Theoretical Physics (Austria), JINR (Russia), KEK (Japan), KAIS (Korea) and Academia Sinica (Taiwan).

After obtaining a Ph.D. in Atmospheric Science from University of Missouri, Columbia, USA in 2008, he is planning to engage in research and teaching in Atmospheric Science.